July 2016

Synthesis and Applications of Non-migratory Metal Chelating Active Packaging

Maxine J. Roman
University of Massachusetts Amherst

SYNTHESIS AND APPLICATIONS OF NON-MIGRATORY METAL CHELATING ACTIVE PACKAGING

A Dissertation Presented

By

MAXINE JASMINE ROMAN

Submitted to the Graduate School of the

University of Massachusetts Amherst in partial fulfillment

of the requirements of the degree of

DOCTOR OF PHILOSOPHY

May 2016

Food Science

SYNTHESIS AND APPLICATIONS OF

NON-MIGRATORY METAL CHELATING ACTIVE PACKAGING

A Dissertation Presented

By

MAXINE JASMINE ROMAN

Approved as to style and content by:

_____

Julie M. Goddard, Chair

_____

Eric A. Decker, Member

_____

Sankaran Thayumanavan, Member

_____

Eric A. Decker, Department Head

Food Science

DEDICATION

To my family for their constant support, laughter & love.

ACKNOWLEDGEMENTS

Completing a PhD is not something that can be done alone---many wonderful people have supported me in this endeavor. First and foremost, I would like to thank my advisor, Dr. Julie Goddard, for being an exceptional manager, mentor and friend throughout this process. Her technical curiosity, positive attitude, and work ethic have inspired me in so many ways. Many thanks as well to my coadvisor, Dr. Eric Decker, and committee member, Dr. Sankaran Thayumanavan, for challenging me and providing me with their vast knowledge, guidance, and support.

It has been a pleasure and privilege to complete my doctoral studies in the Department of Food Science at UMass Amherst. My studies were supported by two generous fellowships, the Northeast Alliance for Graduate Education and the Professoriate (NEAGEP) Fellowship and the Peter Salmon Fellowship. Thank you to both committees for investing in my work. I am very grateful to the Food Science department staff, without whom nothing would get done--- Fran, Deby, Stacy, Dan, Dave, Jean, Ruth, and Cindy. I would like to thank all of the members (past and present) of the Bioeng Research Group, who over the past four years have become a second family to me, including, Joey, Jeff, Fei, Luis, Dana, Vivian, Minhui, Charmaine, Sam, Juhong, Ziyuan, Stephanie, Anna, Danhui, Kang, Angelica, and Anne. I would especially like to thank those who worked on the metal chelating active packaging project: Fang Tian, Yoshiko Ogiwara, David Johnson, Jason Lin, Rachael Lyons and Paul Castrale. In addition, I would like to extend my gratitude to everyone in the labs of Dr. Lynne McLandsborough, Dr. Julian McClements and Dr. Eric Decker for letting me use all of their equipment and welcoming me as an 'honorary' lab member. I am also thankful to have received overwhelming technical support from the

Polymer Science, Chemistry, and Environmental Engineering departments, especially from the students and staff in the labs of Dr. Julian Tyson and Dr. David Reckhow.

My interest in food science began when I attended the Research Apprentice Program at the University of Illinois at Urbana-Champaign after my freshman year of high school. I am deeply grateful to the program director, Dr. Jesse Thompson, who has always provided me with opportunities and tools for success. Through this program, I met another valuable mentor, Dr. Elvira de Mejia, who taught me how to be a researcher and provided me the opportunity to work in her lab during my high school and undergraduate studies. She advised me to apply to UMass for graduate school and for that I am forever grateful. I would also like to thank my master's advisor, Dr. R. Paul Singh, who taught me the value of becoming an effective mentor and teacher.

Finally, I would like to express my love and gratitude to all of my closest friends and family. They are all unique and intelligent individuals whose drive and talent inspire me to be my best self. Many thanks to my amazing family for their unconditional love and support, especially my sister Jackie who has been my best friend and biggest cheerleader. Last but not least, I would like to thank my parents without whose sacrifices I would not have been able to get this far. This achievement is as much theirs as it is mine.

ABSTRACT

SYNTHESIS AND APPLICATIONS OF
NON-MIGRATORY METAL CHELATING ACTIVE PACKAGING

MAY 2016

MAXINE J. ROMAN
B.S., UNIVERSITY OF ILLINOIS AT URBANA-CHAMPAIGN
M.S., UNIVERSITY OF CALIFORNIA, DAVIS
PH.D., UNIVERSITY OF MASSACHUSETTS, AMHERST
Directed by: Professor Julie M. Goddard

Many packaged foods use synthetic chelators (e.g. ethylenediaminetetraacetic acid, EDTA) to inhibit metal promoted oxidation and/or microbial growth that may cause food spoilage. Consumer demand for foods without synthetic additives has prompted growing interest in alternative preservation methods. Our research group has previously developed non-migratory metal chelating active packaging materials by surface immobilization of polymeric chelators and demonstrated their ability to inhibit lipid oxidation in model food emulsions. The work presented in this dissertation investigates the synthesis, performance stability, and practical application of metal chelating surface modifications to optimize design of non-migratory metal chelating active packaging materials.

Metal chelating active packaging materials were synthesized by grafting of metal chelating polymers from the surface of polypropylene (PP). Three metal chelating ligand chemistries were investigated for their known affinity for iron: carboxylic acids, hydroxamic acids, and catechols. Iron was chosen a target metal ion because it is a strong prooxidant and essential nutrient for spoilage bacteria. When utilizing photoinitiated graft polymerization to surface graft poly(acrylic acid) that contained carboxylic acid ligands, it

was demonstrated metal chelating polymer chain length and density may be manipulated to tailor both overall material iron chelating capacity (chain length) and ligand to metal binding ratio (chain density on food contact surface). Carboxylic acid functionalized PP (PP-*g*-PAA) enhanced the antimicrobial activity of lysozyme against *Listeria monocytogenes* under conditions that minimized protein fouling onto the charged food contact surface (PP-*g*-PAA, pKa^{bulk} 6.45). Compared to PP-*g*-PAA, hydroxamic acid functionalized PP (PP-*g*-PHA) was hypothesized to have a higher performance stability due to its low effective charge (pKa^{bulk} 9.65) and high specific affinity for iron. PP-*g*-PHA retained iron chelating capacity over a wide range of pH (3.0-5.0) and viscosity (~1 to 10^5 mPa·s) conditions as well as in presence of competing ions (Na^+, Mg^{2+}, Ca^{2+}) and hydrocolloids typically found in foods.

In order to investigate the efficacy of catechol based surface modifications, a metal chelating material inspired by polyphenol chemistry was developed. Polyphenol coatings were fabricated by oxidative polymerization of catechol and catechin from the surface of PP. Application of coating onto chitosan functionalized PP prevented coating delamination in food simulants under standard migration test conditions. Polyphenol coated PP exhibited both iron chelating and radical scavenging capacity for dual antioxidant functionality. In accelerated storage studies, polyphenol coated PP extended the lag phase of lipid oxidation and inhibited lycopene degradation in oil-in-water emulsions (pH 4.0). This work demonstrates the synthesis of non-migratory metal chelating active packaging materials and their antimicrobial and antioxidant applications. Such technology may allow for the removal of synthetic additives from product formulations, while maintaining food safety, quality, and shelf life.

TABLE OF CONTENTS

PAGE

APPENDICES

LIST OF TABLES

LIST OF FIGURES

LIST OF ABBREVIATIONS

AA	acrylic acid
AAPH	2,2-Azobis(2-methylpropionamidine) dihydrochloride
ABTS	2,2'-azino-bis(3-ethylbenzothiazoline-6-sulphonic acid)
ANOVA	analysis of variance
ATR-FTIR	attenuated total reflectance/Fourier transform infrared spectroscopy
AUC	area under the curve
BC	β-carotene
BCA	bicinchoninic acid
BHA	butylated hydroxyanisole
BHT	butylated hydroxytoluene
BP	benzophenone
COOH	carboxylic acid
DFO	deferoxamine
EDC	1-ethyl-3-(-3-dimethylaminopropyl) carbodiimide hydrochloride
EDTA	ethylenediaminetetraacetic acid
EU	European Union
Fe^{2+}	ferrous ion
Fe^{3+}	ferric ion
FDA	Food and Drug Administration
FTIR	Fourier transformed infrared
GAE	gallic acid equivalents
HA	hydroxamic acid
HCl	hydrochloric acid
HEPES	4-(2-hyddroxyethyl)-1-piperazineethane-sulfonic acid
HPLC	high performance liquid chromatography
ICP-MS	inductively coupled plasma-mass spectrometry
ICP-OES	inductively coupled plasma-optical emission spectrometry
L·	alkyl radical

LDPE	low-density polyethylene
LH	unsaturated lipid
LM	*Listeria monocytogenes*
LO·	alkoxyl radical
LOO·	peroxyl radical
LOOH	lipid hydroperoxide
LRV	log reduction value
MA	methyl acrylate
MC	methyl cellulose
MCT	medium chain triacyglycerols
MIC	minimum inhibitory concentration
Mn^{n+}	reduced transition metal
Mn^{n+1}	oxidized transition metal
NHS	n-hydroxysuccinimide
NTA	nitrilotriacetic acid
ORAC	oxygen radical absorbance capacity
PAA	poly(acrylic acid)
PHA	poly(hydroxamic acid)
PMA	poly(methyl acrylate)
PMAA	poly(methacrylic acid)
PP	polypropylene
SEM	scanning electron microscopy
TBO	toluidine blue O
TCA	trichloroacetic acid
TEAC	Trolox equivalent antioxidant capacity
Trolox	6-hydroxy-2,5,7,8-tetramethylchroman-2-carboxylic acid
TSA	tryptic soy agar
TSB	tryptic soy broth
UV	ultraviolet

CHAPTER 1

INTRODUCTION

1.1 Introduction

Metal chelators are used throughout product formulations in the packaged food industry to maintain overall food quality and safety in order to extend shelf life and minimize food waste.[1] The most effective and most commonly used metal chelator is the synthetic food additive, ethylenediaminetetraacetic acid (EDTA). Recently, the use of synthetic additives in food products has been overwhelmingly criticized by consumers. In fact, a 2013 Gallup Study of Clean Food & Beverage Labels found that 23% of U.S. adults are clean label advocates.[2] Major retail chains, such as Whole Foods and Panera Bread, have responded by banning synthetic additives from their product formulations.[3, 4] In order to maintain food quality and enable removal of synthetic additives (e.g. EDTA) from product formulations, it is imperative to develop effective alternative preservation strategies. For this work, metal chelating surface modifications for the development of non-migratory metal chelating active packaging materials are explored for application in packaged food preservation.

1.2 Role of Metal Chelators in Food Industry

Trace amounts of transition metals, especially iron, accelerate chemical and microbial degradation reactions that reduce food quality and safety.[5] Since metal contaminants are ubiquitous in food ingredients as well as the food processing and packaging environment, the most effective means of inhibiting such degradation is the use of metal chelators. Metal chelators bind free metals to hinder their reactivity. Extensive research has demonstrated that metal chelators can contribute to food preservation by

inhibiting oxidative degradation (ie: lipid rancidity, color loss, vitamin degradation) and improving antimicrobial efficacy.

1.2.1 Inhibiting Oxidative Degradation

Many food products undergo quality deterioration during transport and storage due to oxidative reactions that cause lipid rancidity, color loss, and vitamin degradation. In the food industry, lipids are considered one of the most chemically unstable ingredients due to their susceptibility to oxidative degradation. Typically, unsaturated lipids, which contain conjugated dienes, are the most chemically unstable. Lipid oxidation proceeds via a free radical chain reaction wherein radicals (e.g. alkyl radicals (L·), peroxyl radicals (LOO·), alkoxyl radicals (LO·)) react with unsaturated lipids (LH) to propagate the production of lipid hydroperoxides (LOOH) (**Figure 1.1**).[5] Lipid hydroperoxides are known as primary oxidation products. Although they have little impact on overall food quality, they are an important marker to indicate the early stages of lipid oxidation and play a key role in metal-promoted oxidation. Transition metals (Mn), especially ferrous iron, primarily catalyze lipid oxidation by promoting the decomposition of lipid hydroperoxides to propagate free radicals. The decomposition of lipid hydroperoxides may result in β-scission reaction that promote the formation of secondary oxidation products (e.g. aldehydes, ketones, alcohols, hydrocarbons, organic acids, epoxy compounds), which are responsible for sensory characteristics associated with lipid rancidity.[6, 7]

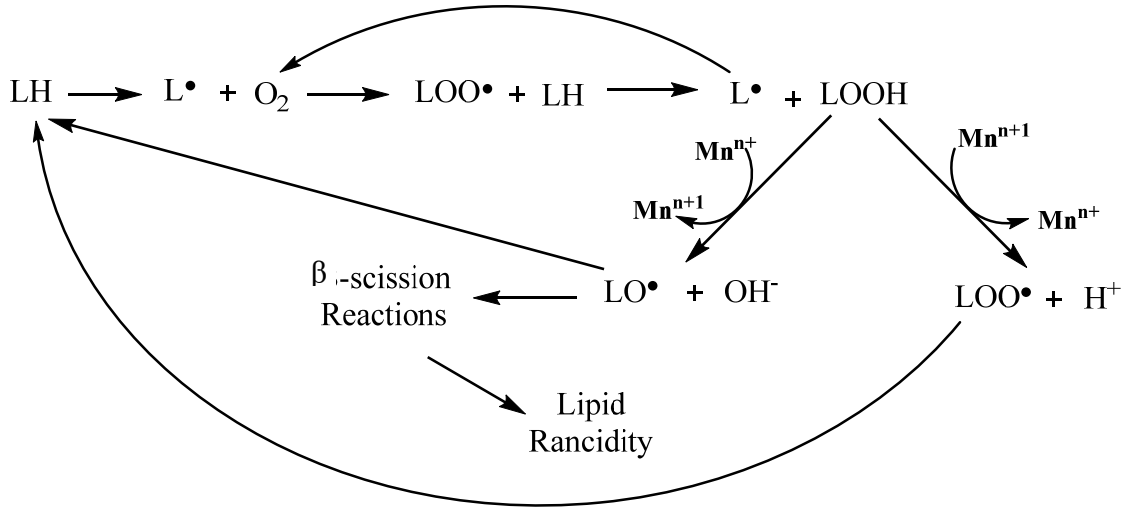

Figure 1.1. Mechanism of metal-promoted lipid oxidation. Adapted from Decker and McClements [8]

Metal-promoted oxidation may also contribute to degradation of colors, especially naturally occurring colors. Common natural food colors, such as carotenoids, chlorophyll, and betanins, contain conjugated dienes that, similar to unsaturated lipids, are prone to oxidation degradation via free radical chain reaction that causes color loss.[9-11] Similar to natural colors, vitamins that contain conjugated dienes are degraded by oxidation reactions. These include vitamin C (ascorbic acid), vitamin E (tocopherols and tocotrienol), vitamin A and its precursors (carotenoids), vitamin D, and vitamin B (e.g. riboflavin, thiamin).[12]

The influence of transition metal reactivity on the acceleration of oxidative degradation is often evaluated by screening the efficacy of different types of antioxidants in a particular food system. The major types of antioxidant ingredients used in food systems are as follows: free radical scavengers (e.g. BHT, BHA), singlet oxygen quenchers (e.g. carotenoids), and metal chelators (e.g. EDTA, citric acid, polyphosphates).[13, 14] Many research groups have demonstrated that metal chelators have the highest efficacy in inhibiting metal-promoted oxidation in aqueous systems, such as food emulsions.[15-17] It is hypothesized transition metals are most reactive in food emulsions due to the high surface

area of the interfacial layer between oil phase and aqueous phase that favors the accessibility of metal prooxidants to react with lipids.[6, 7] For this reason, metal chelators are most effective as antioxidants in food emulsions such as beverages, salad dressings, mayonnaise, sauces, and spreads.[18]

1.2.2 Improving Antimicrobial Efficacy

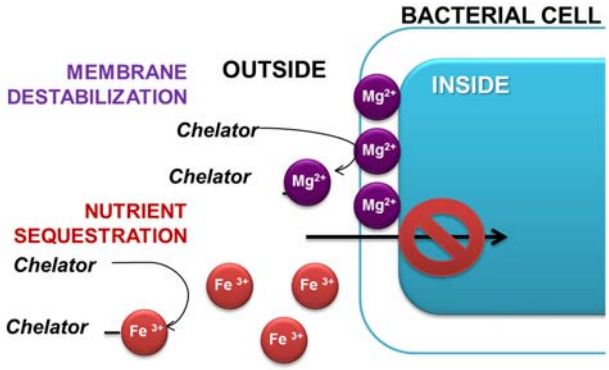

Figure 1.2. Possible mechanisms of chelator antimicrobial activity. Adapted from Rufian-Henares et al.[19]

Metal chelators, typically EDTA, play a key role in food product formulations by enhancing the efficacy of food grade antimicrobials. Metal chelators may acts as antimicrobials by chelating metal ions that stabilize the outer membrane of a bacterial cell (e.g. calcium and magnesium) and/or sequestering essential bacterial nutrients (e.g. iron) (**Figure 1.2**).[19] Although the chelator concentration necessary for antimicrobial efficacy exceeds the limit of use in foods (e.g. FDA limit for beverages 33 ppm EDTA[20]; minimum inhibitory concentration for *Listeria monocytogenes* Scott A 250 ppm EDTA[21]), lower concentrations of chelators have demonstrated potent synergy with food grade antimicrobials. Branen and Davidson [22] reported that 31.3 μg ml^{-1} EDTA reduced the minimum inhibitory concentration (MIC) of lysozyme against *Listeria monocytogenes* Scott A by ten-fold, from 250 μg ml^{-1} to 25 μg ml^{-1}. Antimicrobial synergy of chelators and membrane-disrupting antimicrobials (ie: lysozyme, nisin, monolaurin) was also

observed against *E. coli* O157:H7.[22-24] Therefore, removal of metal chelators from a food system may have a significant impact on antimicrobial performance and subsequent product shelf life.

1.3 Strategies to Prevent Metal-Promoted Degradation

Metal-promoted degradation in packaged foods is most widely inhibited by the addition of EDTA. EDTA is a potent synthetic metal chelator that requires only small amounts to be effective and therefore has minimal impact on sensory qualities of food. The efficacy of EDTA is most likely due to its high binding affinity for reactive metals, such as iron (log $\beta^{Fe(III)}$ 25.7[25]). Natural metal chelators, such as citric acid, may also be used to inhibit metal-promoted oxidation. The structures of EDTA and citric acid are shown in **Figure 1.3**. A challenge of replacing EDTA with natural chelators is that they are not nearly as effective due to their lower affinity for reactive metals like iron (e.g. citric acid log $\beta^{Fe(III)}$ 11.85[25]), and therefore may need to be added in larger amounts that may alter the flavor, color, viscosity, and cost of a food.[26] Also, in some cases, natural chelators may act as prooxidants by solubilizing transition metals without occupying all of the coordination sites to prevent reactivity.[27]

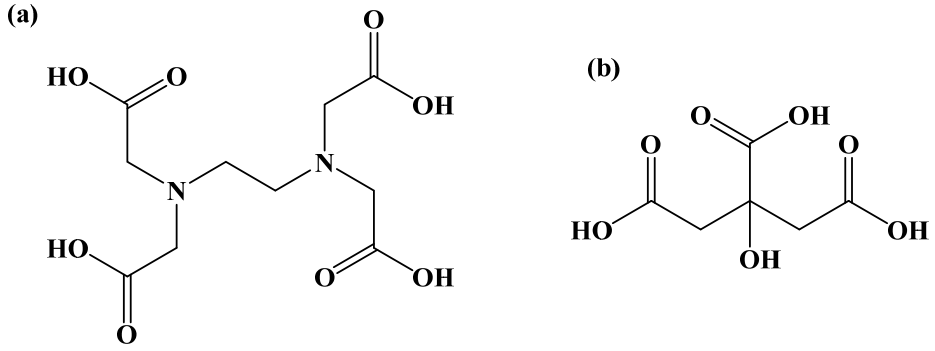

Figure 1.3. Chemical structures of FDA approved metal chelators (a) EDTA and (b) citric acid.

An alternative preservation strategy for packaged foods is active packaging. Active packaging is a packaging material wherein an active compound has been deliberately incorporated to improve performance,[28] in this case food preservation. Active compounds may be incorporated into packaging materials in many ways including coating, extrusion, and surface immobilization.[29, 30] The majority of research on the synthesis of active packaging materials that contain metal chelators has focused on coating and extrusion,[31-34] which may rely on migration of the active compound to the food products to function. These approaches pose many limitations including possible alteration of material bulk properties and/or necessity to label active compounds as *direct additives* due to migration.

Surface immobilization is an emerging field of active packaging research that investigates direct attachment or tethering of active compounds to the surface of a packaging material.[35, 36] This type of active packaging material is designed to be non-migratory so that it would require *food contact notification* rather than *direct additive* approval,[37, 38] which precludes a label claim and may allow for application with all natural and organic foods. In addition, such modifications techniques have minimal impact on bulk material properties.[39] Although active packaging synthesized by surface immobilization is theoretically possible,[40-42] research on the synthesis and application of such materials has thus far been limited. Our research group has developed non-migratory metal chelating active packaging materials by surface immobilization of polymeric chelators to enable removal of EDTA from food product formulations and demonstrated their ability to inhibit lipid oxidation.[43, 44] However, there is further research to be done to optimize the surface chemistry of such materials and to demonstrate their ability to function in a wide variety of applications.

1.4 Research Objectives

The overall objective for this work is to explore the synthesis and applications of non-migratory metal chelating active packaging materials, along with these specific objectives:

1. Synthesize and characterize non-migratory metal chelating active packaging materials.
2. Determine the performance stability of non-migratory metal chelating active packaging materials under conditions typically found in packaged food products (ie: pH, competing ions, competitive chelating ingredients, viscosity).
3. Demonstrate antimicrobial and antioxidant application of non-migratory metal chelating active packaging materials.

CHAPTER 2

IRON CHELATING POLYPROPYLENE FILMS: MANIPULATING PHOTOINITIATED GRAFT POLYMERIZATION TO TAILOR CHELATING ACTIVITY[1]

2.1 Abstract

Transition metals, especially iron, enhance the oxidative degradation of lipids. Non-migratory metal chelating active packaging can inhibit lipid oxidation and meet consumer demand for 'cleaner' labels. Recently, the development of iron chelating films prepared by photoinitiated graft polymerization of acrylic acid on polypropylene (PP-*g*-PAA) was reported. The objective of this study was to tailor the chelating activity of PP-*g*-PAA by manipulating graft conditions. Carboxylic acids graft density and PAA graft thickness increased with graft time and acrylic acid concentration, with carboxylic acids density of up to 143 ± 32 nmol cm^{-2}, PAA graft thickness of ~6-18 μm, and ligand (carboxylic acid) to metal (Fe^{2+}) binding ratio of ~4-5. Reducing photoinitiator graft density decreased this ratio to ~2-2.5, suggesting that graft chain density influences chelating activity. This work demonstrates the ability to tailor chelating activity of PP-*g*-PAA with potential applications in active packaging, chelation therapy, and water purification.

2.2 Introduction

The presence of trace amounts of transition metals, especially iron, promotes deterioration of food quality via lipid oxidation. Metal-promoted lipid oxidation is

[1] The contents of this chapter have been published: Roman, M. J.; Tian, F.; Decker, E. A.; Goddard, J. M. Iron chelating polypropylene films: Manipulating photoinitiated graft polymerization to tailor chelating activity. *Journal of Applied Polymer Science* **2014**, *131*, 39948.

primarily initiated by the reduced state of iron, ferrous iron (Fe^{2+}), which reacts with hydroperoxides to create radicals that propagate oxidation and contribute to the formation of off flavors, loss of nutrients, and degradation of color.[45] Since it is difficult to completely remove trace amounts of iron from foods and the processing environment, the principal method of inhibiting metal-promoted lipid oxidation is the addition of metal chelators that bind iron to hinder its reactivity.[7] The most effective (and most widely used) metal chelator is a synthetic compound ethylenediaminetetraacetic acid (EDTA). In an effort to produce products with less synthetic additives, there has been increasing interest in alternative methods of inhibiting metal-promoted lipid oxidation. These methods include the replacement of synthetic additives with natural antioxidants and/or active packaging. Natural antioxidants tend to be less potent than their synthetic counterparts and therefore must be added to food products in excessive quantities that have yet to be evaluated for safety and may have adverse impacts on sensory perception.[26] Active packaging is a promising area of research that investigates the incorporation of active compounds, such as antioxidants, into the food packaging rather than directly into the food product.[30] However, most of the research in this area has been dedicated to the development of active packaging where functionality relies on the migration of active compounds from the packaging into the food, thus requiring labeling as an additive. Recently, non-migratory iron chelating active packaging was developed with the intended use of inhibiting lipid oxidation in liquid and semi-liquid foods.[43, 46] Compared with traditional active packaging, in which the active agent would require approval as a *direct additive*, the active agent in non-migratory active packaging would require *food contact notification*.[37]

Non-migratory active packaging can be synthesized by direct covalent binding or tethering of active compounds to the surface of common packaging materials.[35, 36] This concept has been used to modify surfaces for immobilization of enzymes and inhibition of microbial growth.[40, 47, 48] In order to bind active compounds to packaging, their inert surfaces must be pretreated to create active sites. Some techniques for surface activation include wet chemical, silanization, ionized gas treatments (i.e. plasma, corona discharge, flame treatment), and UV irradiation.[36, 49-52] UV radiation is a low cost and easy to control method that yields uniform, high density surface modifications with minimal damage to bulk material properties, which makes it advantageous compared to other surface modification techniques.[51]

The current generation of iron chelating active packaging relies on the chelating activity of polymers covalently bound to the surface of films by photoinitiated living graft polymerization.[43] The basic principle of photoinitiated living graft polymerization relies on using a photoinitiator in the presence of UV light to abstract a hydrogen to create surface radicals that can bind the photoinitiator to the film's surface.[53, 54] Then, a vinyl or acrylic monomer in the presence of UV light replaces the photoinitiator and polymerizes onto the surface to form polymer chains. Extensive research on photoinitiated graft polymerization of acrylic acid has been conducted in the field of membrane technology for the purpose of reducing protein fouling and tailoring membrane permeability. Successful grafting of poly(acrylic acid) to polypropylene,[53, 55-59] polyamide,[59, 60] polyethersulfone,[61, 62] cellulose acetate,[58] and polyvinylidene fluoride[58] membranes by photoinitiated graft polymerization has been previously reported. Poly(acrylic acid) surface grafts onto polyolefin films, such as polyethylene[63] and polypropylene,[64, 65] have been shown to reduce gas permeability.

The iron chelating capacity of poly(acrylic acid) chains bound to polypropylene films (PP-*g*-PAA) by photoinitiated graft polymerization has been demonstrated.[43] A basic schematic of this surface modification method is shown in **Figure 2.1**. This surface modification utilizes a sequential surface application of the photoinitiator and the monomer, which allows for controlled grafting of polymer chains with minimal homopolymer and cross-linking reactions.[53] The active functional group on acrylic acid that binds metal ions is carboxylic acid. Carboxylic acids are found in many common food grade chelators, including EDTA and citric acid.[30] The theoretical ligand (carboxylic acid) to metal (Fe^{2+}) binding ratio of poly(acrylic acid) chains is 2 as depicted in **Figure 2.2**. This ratio may be observed to be different experimentally due to steric restriction of polymer grafting and/or environmental conditions (i.e. pH, ionic strength). It was previously reported that PP-*g*-PAA extended the lag phase of lipid oxidation in a soybean oil-in-water emulsion from 2 to 9 days compared with native polypropylene (PP).[43]

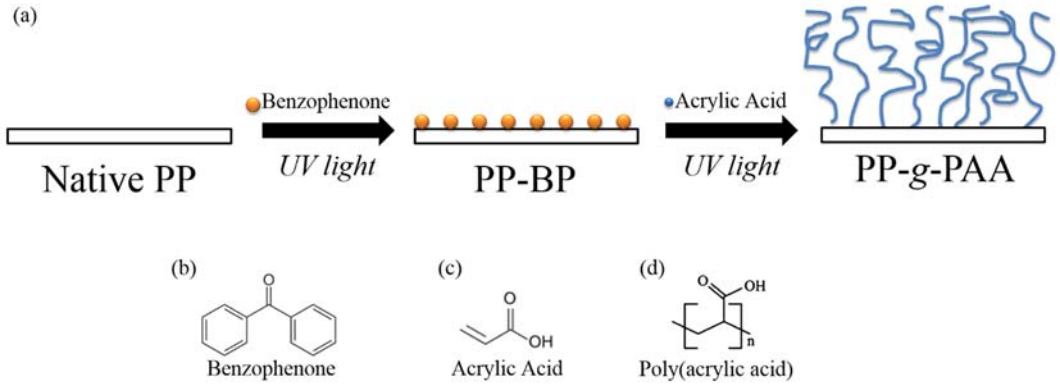

Figure 2.1. Two step photoinitiated graft polymerization of acrylic acid onto polypropylene – PP-*g*-PAA (a) and the chemical structures of (b) photoinitiator, (c) monomer, and (d) grafted polymer.

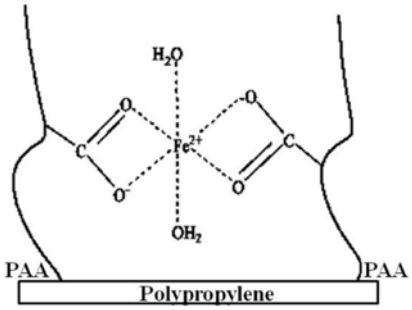

Figure 2.2. Theoretical binding of ferrous iron by PP-*g*-PAA. Adapted from Tian, et al. [43]

Inhibiting metal-promoted oxidative degradation by such non-migratory iron chelating films has application in an array of food, beverage, and consumer products applications, however individual applications may have different chelation needs as determined by factors such as iron concentration, pH and ionic strength. As such, it is important to optimize photoinitiated graft polymerization in order to tailor its iron chelating activity. The objective of this study was therefore to optimize the production of PP-*g*-PAA non-migratory metal chelating active packaging films by manipulating graft conditions of photoinitiator (benzophenone) and acrylic acid. Increasing acrylic acid concentration resulted in an exponential increase in iron chelating activity and manipulating the graft of benzophenone altered the ligand to metal binding ratio. These data suggest that the length of the polymer chains as well as the density of polymer chain graft have a significant impact on the chelating activity of iron chelating films.

2.3 Materials and Methods

2.3.1 Materials

Polypropylene (isotactic, pellets) was purchased from Scientific Polymer Products (Ontario, NY). Hydroxylamine hydrochloride, ferrous sulfate heptahydrate (99+%), imidazole (99%), 3-(2-pyridyl)-5,6-diphenyl-1,2,4-triazine-*p,p'*-disulfonic acid disodium

salt hydrate (ferrozine, 98+%), toluidine blue O (TBO), and ethanol (99.5+%) were purchased from Acros Organics (Morris Plains, NJ). Acrylic acid (anhydrous) and benzophenone (99%) were purchased from Sigma-Aldrich (St. Louis, MO). All other chemicals were purchased from Fisher Scientific (Fair Lawn, NJ).

2.3.2 Polypropylene Film Preparation

Polypropylene (PP) films were prepared as previously reported.[43] PP pellets were cleaned by sequentially sonicating in the following solvents twice for 10 min each rinse: isopropanol, acetone, and deionized water, and then dried over anhydrous calcium sulfate. Clean PP film was prepared on a Carver Laboratory Press (Carver, Inc., NJ). The press was set to 160°C, PP pellets were heated on the press for 1 min, and then 9000 lbs of pressure was applied. PP films, average thickness of 387 ± 35 μm, were cut into 2 x 2 cm^2 pieces and washed using the same method as the PP pellets.

2.3.3 Photoinitiated Graft Surface Modification of Polypropylene

Sequential photoinitiated graft polymerization was used to attach poly(acrylic acid) (PAA) to the surface of polypropylene (PP). This method is adapted from previously reported work.[43, 53] For this research, concentration and UV exposure time for both the photoinitiator graft and monomer graft and polymerization were examined variables (**Table 2.1**). The photoinitiator tested was benzophenone and the monomer tested was acrylic acid. Control parameters refer to the grafting conditions for film previously tested for inhibition of lipid oxidation.[43]

Table 2.1. Photoinitiated graft polymerization of acrylic acid on polypropylene (PP-*g*-PAA) reaction parameters tested for study. Asterisks (*) indicate control parameters held constant in optimization experiments.

Role	Compound	Graft Condition	Test Parameters
Photoinitiator	Benzophenone	Benzophenone Concentration (w/w)	5%*, 3%, 1%
		Benzophenone Graft Time	1.5 min*, 1 min, 0.5 min
Monomer	Acrylic Acid	Acrylic Acid Concentration (w/w)	30%, 25%*, 20%, 15%, 10%
		Acrylic Acid Graft Time	6 min*, 4.5 min, 3 min, 1.5 min

Thirty µl benzophenone in heptanes was spin coated (WS-400-6NPP, Laurell Technologies, North Wales, PA) onto each side of 2 x 2 cm^2 polypropylene at 2000 rpm for 10 sec. During the spin coating, the spin coater chamber was purged with clean dry air and heptanes were evaporated from the film surface leaving a dried thin layer of benzophenone. The 2 x 2 cm^2 benzophenone coated PP films were cut into 1 x 2 cm^2 pieces and then each 1 x 2 cm^2 piece was placed into a screw top vial and sealed with a septum fitted aluminum cap. The vials were flushed with nitrogen for 5 min and then exposed to UV light (Dymax 5000-EC Series, Torrington, CT) at 365 nm with an average light intensity of 209 ± 4.3 mW cm^{-2}. After benzophenone grafting was completed, the films were washed 3 times with acetone to remove unreacted benzophenone and then dried at room temperature.

Benzophenone activated PP (PP-BP) films were placed into a screw top vial and 6 ml of acrylic acid in ethanol was added before the vials were sealed with septum fitted aluminum caps. The acrylic acid in ethanol solution in the sealed vials was flushed with nitrogen for 15 min. Nitrogen flushed vials were exposed to UV light to graft and polymerize acrylic acid onto PP-BP. PP-*g*-PAA was rinsed in deionized water for 30 min

at room temperature, 60 min at 60°C and then 30 min at room temperature to remove unattached monomer and homopolymer. PP-*g*-PAA was dried overnight over anhydrous calcium sulfate.

2.3.4 Attenuated total reflectance/ Fourier transform infrared spectroscopy (ATR-FTIR)

Attenuated total reflectance Fourier transform infrared spectroscopy (ATR-FTIR) was used to confirm the grafting of functional groups on the surface of PP-*g*-PAA. An IRPrestige FTIR Spectrometer (Shimadzu Scientific Instruments, Inc., Kyoto, Japan) with a diamond ATR crystal was used to measure the spectrum. Each spectrum was collected under the following parameters: Happ-Genzel function, 32 scans, and 4 cm^{-1} resolution. Spectrum analysis was performed on KnowItAll(R) Informatics System 9.5 (Bio-Rad Laboratories, Inc., Informatics Division, Philadelphia, PA) and Sigma Plot 12 (Systat Software, Inc., San Jose, CA).

2.3.5 Scanning Electron Microscopy (SEM)

Surface and cross sectional images of PP-*g*-PAA were taken with JCM-5000 NeoScope (JEOL, Japan) at 10 kV. Cross sectional samples were prepared by freeze fracturing films under liquid nitrogen. Prior to imaging, samples were mounted on a small aluminum platform with double sided carbon tape and then sputter coated with gold under nitrogen for 3 min. For each treatment, measurements were collected from images taken of two independently prepared replicates.

2.3.6 Contact Angle

Water (HPLC grade deionized water, Fisher Scientific, Fair Lawn, NJ) contact angles of PP-*g*-PAA were measured using a Kruss DSA100 (Hamburg, Germany)

equipped with a software controlled direct dosing system (DO3210, Hamburg, Germany) to determine film surface hydrophilicity. Advancing and receding angles were recorded every 0.10 sec and calculated using tangent method 2 on DSA software (Hamburg, Germany).

2.3.7 Available Carboxylic Acids Density

Toluidine blue O (TBO) dye assay, in which each molecule of dye reversibly binds with carboxylic acids at a 1:1 stoichiometric ratio, was used to quantify surface carboxylic acids as previously described.[46, 66, 67] Each 1 x 2 cm^2 film was submerged in 5 ml TBO (0.5mM TBO, pH 10), incubated while shaking at room temperature for 2 h and then rinsed 3 times in pH 10 deionized water. TBO dye was desorbed from each film in 8 ml 50% acetic acid while shaking at room temperature for 15 min. The absorbance of TBO dye in 50% acetic acid was measured at 633 nm to quantify surface carboxylic acids by comparison to a standard curve of TBO in 50% acetic acid.

2.3.8 Ferrous Iron Chelating Activity

Iron chelating activity of PP-*g*-PAA was determined by measuring the density of ferrous iron bound to PP-*g*-PAA at pH 5.0 (pH value at which PP-*g*-PAA was previously shown to exhibit optimal ferrous iron chelation).[43, 46] In this method, the amount of chelated ferrous iron is released from the film and quantified by colorimetric reaction with ferrozine reagent. Each treatment was submerged in 20 ml of ferrous iron solution (1 mM ferrous sulfate heptahydrate in 0.05 M sodium acetate/imidazole, pH 5.0) and rotated at room temperature for 30 min to attach iron to films and then rinsed 3 times in deionized water. Ferrous iron was released from the films by incubating each 1 x 2 cm^2 film with 3 ml of releasing agent (0.1 g ml^{-1} hydroxylamine hydrochloride and 0.05 g mL^{-1} trichloroacetic

acid) while shaking for 2.5 h. After ferrous iron was released from the film, 0.5 ml releasing agent (containing released ferrous iron) was added to 0.5 ml ferrozine solution (9.0 mM ferrozine in 50 mM HEPES, pH 7.0) and incubated while shaking for 1 h at room temperature. The absorbance of ferrozine reacted releasing agent was measured at 562 nm to quantify ferrous iron chelating activity by comparison to a standard curve of ferrous iron in releasing agent.

2.3.9 Statistical Analysis

All measurements were conducted in at least quadruplicate. Results are expressed at mean ± standard deviation. For each graft condition examined, a one way ANOVA and Pearson correlation coefficient were calculated using GraphPad Prism 6.0 (La Jolla, CA). Means were separated using a Tukey's post hoc test ($p<0.05$).

2.4 Results and Discussion

2.4.1 Surface Chemistry

The ATR-FTIR spectra of native PP and PP-*g*-PAA films as affected by acrylic acid concentration, acrylic acid graft time, benzophenone concentration, and benzophenone graft time are shown in **Figure 2.3**. ATR-FTIR is a rapid technique for surface chemistry characterization that quantifies specific bonds within a few microns of a substrates surface.[68] In the spectra shown, the narrow absorbance at 1700-1725 cm^{-1} and the broad absorbance at 1211-1320 cm^{-1} illustrate the C=O bond and the C-O bond,

respectively, of the carboxylic acids in the PAA graft. Absorbance characteristics of carboxylic acids are not present in the spectra of native PP.

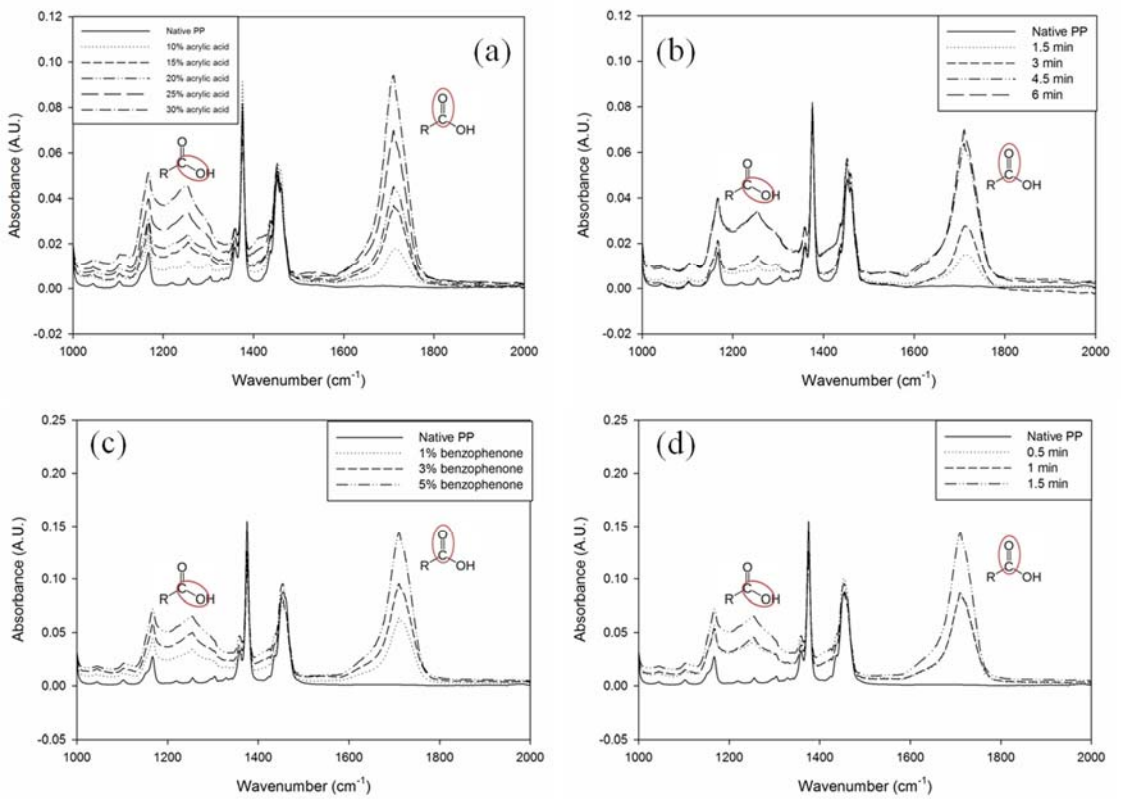

Figure 2.3. ATR-FTIR of PP-*g*-PAA as affected by (a) acrylic acid concentration, (b) acrylic acid graft time, (c) benzophenone concentration and (d) benzophenone graft time.

As the acrylic acid concentration and acrylic acid graft time increases, the intensity of absorbance characteristics of carboxylic acid, 1211-1320 cm^{-1} and 1700-1725 cm^{-1}, increases (**Figure 2.3a** and **2.3b**). The acrylic acid graft times of 4.5 and 6 min have similar absorbance intensities, indicating that the graft of PAA may not significantly increase at graft times higher than 4.5 min. As the benzophenone concentration and benzophenone graft time increases, the intensity of carboxylic acid absorbance increases as well (**Figure 2.3c** and **2.3d**). However, it is important to note that contrary to the acrylic acid concentration and graft time treatments, this increase in carboxylic acid absorbance intensity does not correlate with the available carboxylic acids surface density (see **2.4.4.**

Ligand to Metal Binding). None of the treatments contained significantly less available carboxylic acids than the highest benzophenone concentration and graft time tested. Given that ATR-FTIR only measures the first few microns of a substrate's surface and the thickness of the graft layer is >6 μm as measured by SEM (see **2.4.2. Surface and Cross Section Morphology**), the decrease peak intensity at lower benzophenone concentrations and graft times suggests a decreased PAA chain graft density. Since PAA chains may only polymerize from benzophenone grafted on PP, lower benzophenone graft would theoretically yield a lower PAA chain graft density.

2.4.2 Surface and Cross Section Morphology

In order to determine the effect of PAA graft on the morphology of PP films, surface and cross section SEM images of the following representative treatments were taken: native PP, 10% acrylic acid (low PAA graft), 25% acrylic acid (control parameters), and 30% acrylic acid (high PAA graft) (**Figure 2.4**). Native PP exhibited a relatively smooth surface with a uniform cross section. Under low PAA graft conditions (10% acrylic acid), there were no noticeable changes in the surface morphology compared with native PP, however a small layer of PAA (6.23 ± 0.94 μm) was present in the cross section image. Control (25% acrylic acid) and high PAA graft (30% acrylic acid) films exhibited surface cracking and thicker PAA graft layers of 11.2 ± 0.83 μm and 17.6 ± 2.3 μm, respectively. Grafting of poly(acrylic acid) to polypropylene has been previously reported to increase surface cracking and roughness and may be caused by shrinkage of grafted PAA chains under dry conditions.[43, 65] Although the interface between the PAA graft layer and polypropylene is not well defined, it is clear that an increase in PAA graft yielded an increased thickness of the PAA graft layer.

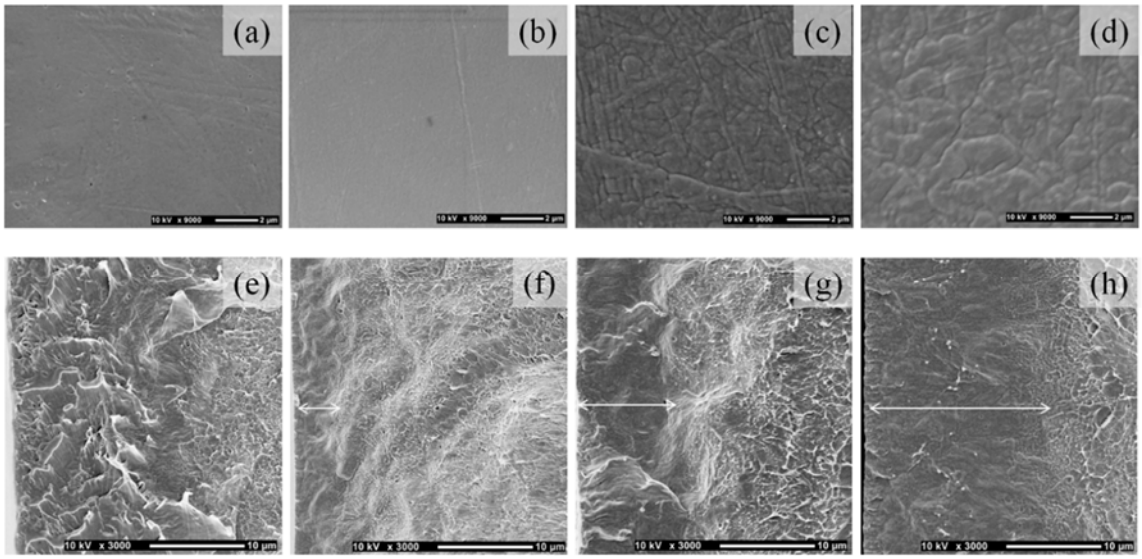

Figure 2.4. SEM analysis of surface of (a) native PP, (b) PP-*g*-PAA (10% AA), (c) PP-*g*-PAA (control parameters), (d) PP-*g*-PAA (30% AA) and cross section of (e) native PP, (f) PP-*g*-PAA (10% AA), (g) PP-*g*-PAA (control parameters), (h) PP-*g*-PAA (30% AA).

2.4.3 Surface Hydrophilicity

Surface hydrophilicity of native PP and PP-*g*-PAA films was determined by measuring advancing and receding angles via water contact angle analysis. Grafting of benzophenone alone (no subsequent PAA grafting) had no significant impact on the advancing and receding angles of native PP. It has been previously reported that surface modification of polypropylene with poly(acrylic acid) improved its surface wettability due to the introduction of hydrophilic carboxylic acids functional groups.[65] All of the PP-*g*-PAA modified films were hydrophilic (advancing and receding contact angle < 80°) (see **Table B.1.** in **Appendix B**). Although decreasing the graft of acrylic acid and benzophenone resulted in decreased surface wettability (ie: higher advancing water contact angle) of PP-*g*-PAA when compared to control parameters (25% acrylic acid, 6 min acrylic acid graft, 5% benzophenone, 1.5 min benzophenone graft), PP-*g*-PAA films remained hydrophilic compared with native PP films.

2.4.4 Ligand to Metal Binding

The influence of manipulating grafting parameters on the functional properties of the resulting PP-*g*-PAA films was quantified by measuring the number of available carboxylic acids on the films surface using the TBO dye assay and the ferrous iron chelating activity as quantified by the ferrozine assay, described above. The ratio of available carboxylic acids density to iron chelating activity was calculated as the ligand to metal binding ratio. The influence of acrylic acid and benzophenone graft conditions on ligand to metal binding ratio are described below.

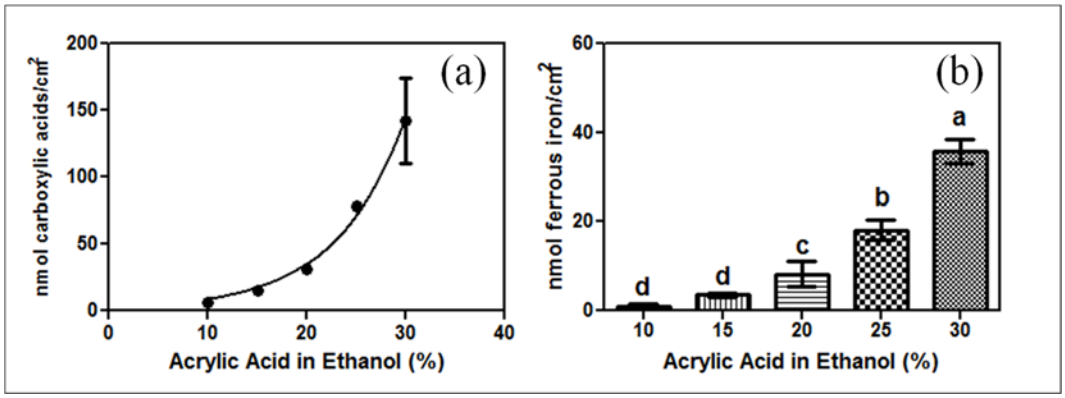

Figure 2.5. Effect of AA concentration on (a) available carboxylic acids density and (b) ferrous iron chelating activity. Values are means ± standard deviations (n=4). Letters denote significant differences ($p<0.05$).

Acrylic Acid Graft Conditions. The effect of acrylic acid concentration on available carboxylic acids density and iron chelating activity is reported in **Figure 2.5**. Standard deviations for acrylic acid concentrations ranging from 10 to 25% were less than ± 3.5 and therefore are not visible on **Figure 2.5a**. Increasing acrylic acid concentration produced an exponential-like increase in available carboxylic acids on PP-*g*-PAA surface. This increase in carboxylic acids was proportional to the increase in iron chelating activity, with a maximum carboxylic acids density of 143 ± 32 nmol cm^{-2} and iron chelating activity of 35.8 ± 2.8 nmol Fe^{2+} cm^{-2} at 30% AA. For every 5% increase in acrylic acid concentration,

the available carboxylic acids and iron chelating capacity roughly doubled. However, at acrylic acid concentrations above 25%, limited solubility and increases in solution polymerization impacted the consistency of graft polymerization, as noted by the larger standard deviation at 30% acrylic acid; therefore, concentrations higher than 30% were not investigated.

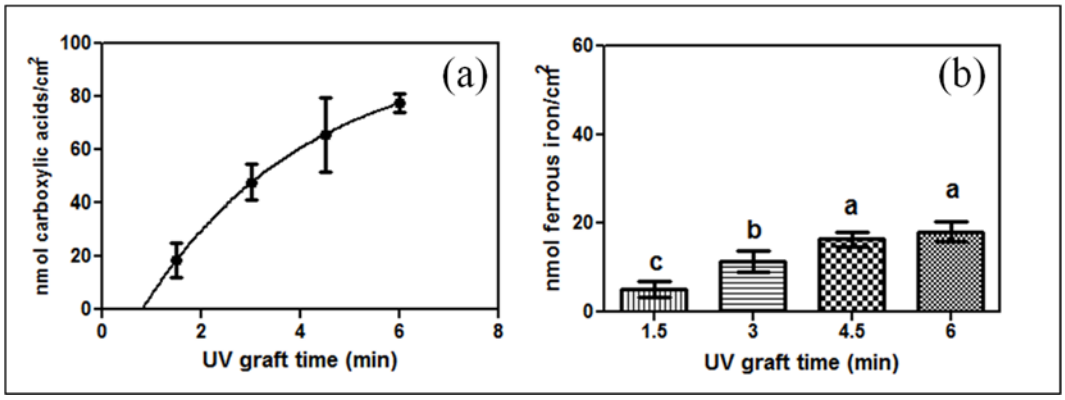

Figure 2.6. Effect of AA graft time on (a) available carboxylic acids density and (b) ferrous iron chelating activity. Values are means ± standard deviations (n=4). Letters denote significant differences ($p<0.05$).

Figure 2.6 shows the effect of acrylic acid graft time on available carboxylic acids density and iron chelating activity. As the acrylic acid graft time increased, the available carboxylic acids density increased, approaching a plateau of 77.7 ± 3.5 nmol cm^{-2} at 6 min. Acrylic acid graft times longer than 6 min caused acrylic acid in ethanol solution to leak out of vials due to pressure build up, therefore longer graft times were not investigated. In agreement with the acrylic acid concentration data, the increase in carboxylic acids was proportional to the increase in iron chelating activity. The Pearson correlation coefficient of available carboxylic acids and iron chelating activity for all acrylic acid graft conditions was 0.996 ($p<0.05$), suggesting that these two measurements are highly correlated. The 4.5 and 6 min graft times did not have significantly different iron chelating activities,16.4 ± 1.8 nmol Fe^{2+} cm^{-2} at 4.5 min and 18.1 ± 2.2 nmol Fe^{2+} cm^{-2} at 6 min. This observation

corresponds with the similarities in the ATR-FTIR spectra of 4.5 and 6 min graft time (**Figure 2.3b**).

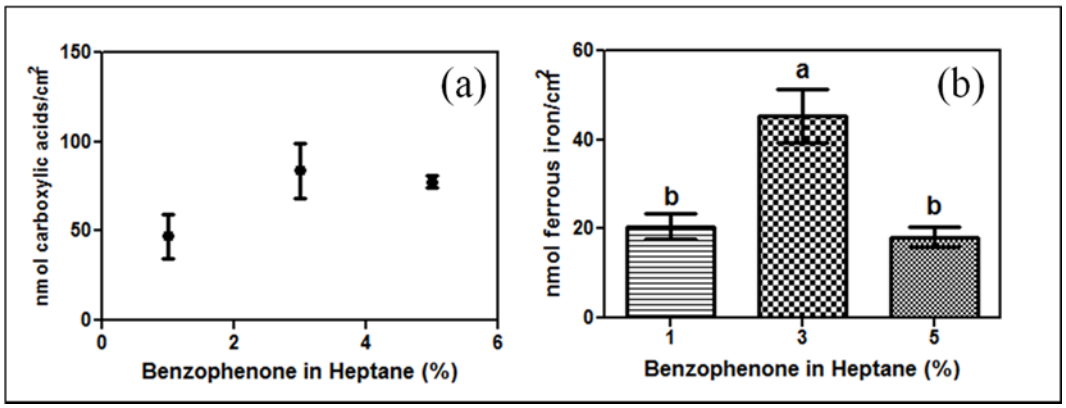

Figure 2.7. Effect of BP concentration on (a) available carboxylic acids density and (b) ferrous iron chelating activity. Values are means ± standard deviations (n=4). Letters denote significant differences ($p<0.05$).

Benzophenone Graft Conditions. The effect of benzophenone concentration on available carboxylic acids density and iron chelating activity is shown in **Figure 2.7**. There is no distinct trend that correlates benzophenone concentration with available carboxylic acids, but rather it appears that an optimum amount of carboxylic acids, 84.0 ± 15 nmol cm^{-2}, was grafted at 3% benzophenone. The control parameter (5% benzophenone) exhibited the lowest iron chelating capacity, while decreasing the benzophenone concentration to 3% more than doubled the iron chelating capacity (45.4 ± 5.9 nmol Fe^{2+} cm^{-2} at 3% benzophenone). **Figure 2.8** shows the effect of benzophenone graft time on available carboxylic acids density and iron chelating activity. Again, there was no clear trend that correlates benzophenone concentration with available carboxylic acids, but rather that an optimum carboxylic acids density of 103 ± 11 nmol cm^{-2} was grafted at 1.0 min benzophenone graft. The control parameter (1.5 min benzophenone graft) exhibited the lowest iron chelating capacity, while lower benzophenone graft times exhibited up to almost double of the iron chelating capacity, 41.6 ± 2.9 nmol Fe^{2+} cm^{-2} at 1.0 min and 29.1

± 4.7 nmol Fe^{2+} cm^{-2} at 0.5 min. Unlike changes to the acrylic acid graft parameters, adjusting the benzophenone graft parameters did not yield proportional increases in the available carboxylic acids and iron chelating capacity. The Pearson correlation coefficient of available carboxylic acids and iron chelating activity for all benzophenone graft conditions was 0.625 (p = 0.185), suggesting that these two measurements are not highly correlated.

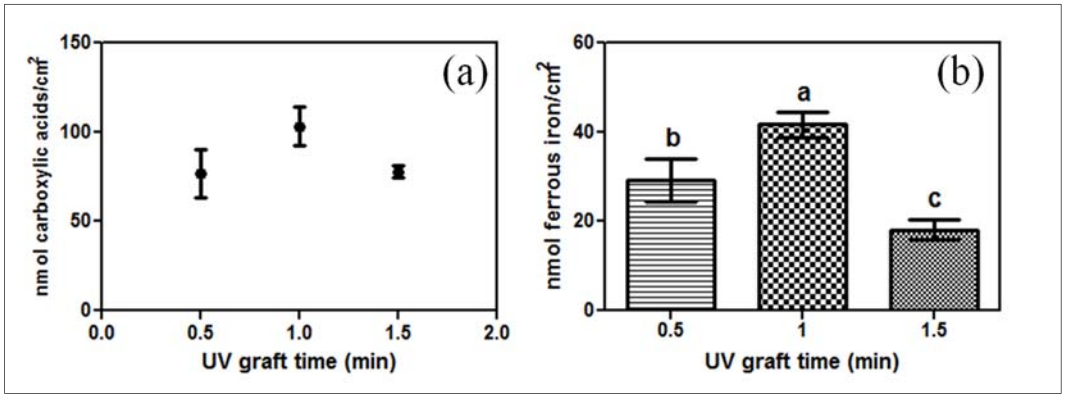

Figure 2.8. Effect of BP graft time on (a) available carboxylic acids density and (b) ferrous iron chelating activity. Values are means ± standard deviations (n=4). Letters denote significant differences ($p<0.05$).

In order to demonstrate the effect of benzophenone graft conditions on iron chelating capacity, the ligand to metal binding ratio for all treatments was calculated and reported in **Table 2.2**. Reducing benzophenone graft density below control parameter (5% benzophenone and 1.5 min graft time) decreased ligand (carboxylic acid) to metal (Fe^{2+}) ratio from approximately 4 – 5 to approximately 2- 2.5. Given that acrylic acid will only polymerize from benzophenone grafted on PP, these data suggest that the density of PAA grafted chains may impact the ligand to metal binding ratio of PP-*g*-PAA. It is hypothesized that higher density PAA grafted chains may exhibit increased apparent ligand to metal binding ratio due to reduced chain flexibility caused by chain cross-linking. PAA chain cross-linking may be initiated by chain transfer reactions or tertiary carbon radicals induced

by UV light exposure.[64] More closely packed PAA chains may be more susceptible to these types of reactions.

Table 2.2. Ligand (COOH) to metal (Fe^{2+}) binding ratio for all experimental treatments. Letters denote significant differences ($p<0.05$).

Graft Condition	Test Parameters	Ligand to Metal Binding Ratio
Control Parameters		$4.30 \pm 0.56^{a,b}$
Benzophenone Concentration	3%	1.85 ± 0.42^{b}
	1%	2.30 ± 0.68^{b}
Benzophenone Graft Time	1 min	$2.48 \pm 0.32^{a,b}$
	0.5 min	$2.63 \pm 0.63^{a,b}$
Acrylic Acid Concentration	30%	$3.98 \pm 0.94^{a,b}$
	20%	$3.93 \pm 1.4^{a,b}$
	15%	$4.38 \pm 0.81^{a,b}$
	10%	5.42 ± 1.6^{a}
Acrylic Acid Graft Time	4.5 min	$3.99 \pm 0.95^{a,b}$
	3 min	$5.12 \pm 2.3^{a,b}$
	1.5 min	$3.65 \pm 1.8^{a,b}$

2.4.5 Optimization of PP-*g*-PAA

The preceding data on the effect of PP-*g*-PAA graft parameters suggest that adjusting control parameters to increase acrylic acid concentration and decreasing graft of benzophenone should yield PP-*g*-PAA with high iron chelating capacity. In order to test this hypothesis, PP-*g*-PAA films were produced under the following parameters 5% benzophenone, 1.0 min benzophenone graft , 30% acrylic acid, and 6.0 min acrylic acid graft. The concentration of BP in solution was not adjusted to optimum conditions (3% BP) because of the effect of reduced solution viscosity of the homogeneity of spin coating. This

set of parameters yielded a PP-*g*-PAA film with a carboxylic acids density of 167 ± 31 nmol cm^{-2} and iron chelating activity of 76.8 ± 10 nmol Fe^{2+} cm^{-2}. As predicted by grafting trends, increasing the acrylic acid concentration of the 1.0 min benzophenone graft parameter by 5% roughly doubled available carboxylic acids density and iron chelating activity.

2.5 Conclusions

Herein, we report the effect of adjusting photoinitiated graft polymerization conditions on the surface chemistry and iron chelating activity of PP-*g*-PAA films that have previously demonstrated inhibition of lipid oxidation in an oil-in-water emulsion.[43] Graft chain length and density, manipulated by changing acrylic acid and benzophenone graft conditions, significantly influenced the chelating activity of PP-*g*-PAA both in terms of overall iron binding capacity as well as ligand to metal binding ratio. High chelating capacity may be obtained with longer graft chain length (higher acrylic acid graft) and lower graft chain density (lower benzophenone graft) to ensure high amounts of available carboxylic acids and adequate chain flexibility. Such ability to tailor the iron chelating capacity of PP-*g*-PAA enables the ability to adapt functional characteristics of chelating polymer materials for specific applications in active packaging for food and consumer products as well as water purification.

CHAPTER 3

METAL CHELATING ACTIVE PACKAGING FILM ENHANCES LYSOZYME INHIBITION OF *LISTERIA MONOCYTOGENES*[2]

3.1 Abstract

Several studies have demonstrated that metal chelators enhance the antimicrobial activity of lysozyme. This study examined the effect of metal chelating active packaging film on the antimicrobial activity of lysozyme against *Listeria monocytogenes*. Polypropylene films were surface modified by photoinitiated graft polymerization of acrylic acid (PP-*g*-PAA) from the food contact surface of the films to impart chelating activity based on charge interactions. PP-*g*-PAA exhibited a carboxylic acid density of 113 ± 5.4 nmol cm^{-2} and an iron chelating activity of 53.7 ± 9.8 nmol cm^{-2}. The antimicrobial interaction of lysozyme and PP-*g*-PAA depended on growth media composition. PP-*g*-PAA hindered lysozyme activity at low ionic strength (2.48 log increase at 64.4 mM total ionic strength) and enhanced lysozyme activity at moderate ionic strength (5.22 log reduction at 120 mM total ionic strength). These data support the hypothesis that, at neutral pH, synergy between carboxylate metal chelating films (pKa^{bulk} 6.45) and lysozyme (pI 11.35) is optimal in solutions of moderate to high ionic strength to minimize undesirable charge interactions, such as lysozyme absorption onto film. These findings suggest that active packaging that chelates metal ions based on ligand-specific interactions, in contrast to electrostatic interactions, may improve antimicrobial synergy. This work demonstrates

[2] The contents of this chapter have been published: Roman, M. J.; Decker, E. A.; Goddard, J. M. Metal-Chelating Active Packaging Film Enhances Lysozyme Inhibition of *Listeria monocytogenes*. *Journal of Food Protection*® **2014**, *77*, 1153-1160.

the potential application of metal chelating active packaging films to enhance the antimicrobial activity of membrane-disrupting antimicrobials, such as lysozyme.

3.2 Introduction

Food antimicrobials are important to prevent the growth of microorganisms that decrease food shelf life and threaten food safety. Most traditional food antimicrobials, such as organic acids and nitrites, are produced by synthetic means.[69] Increasing consumer demand for foods without synthetic additives has given rise to increasing interest in food antimicrobials that are derived from natural sources. Egg white lysozyme (E.C. 3.2.1.17) is an antimicrobial enzyme approved for use in organic foods that hydrolyzes 1,4 glycosidic bonds to damage the peptidoglycan layer of bacteria.[70, 71] The application of lysozyme in foods has been limited by the high concentrations needed for antimicrobial activity and the resistance of gram negative bacteria to its antimicrobial action.[72]

Ethylenediaminetetraacetic acid (EDTA) is a synthetic metal chelator that is often added to food to inhibit oxidative degradation and to enhance the efficacy of food antimicrobials, such as lysozyme.[22-24, 73-75] Metal chelators may enhance food antimicrobial activity by sequestering essential nutrients (e.g. iron) and/or removing membrane stabilizing cations (e.g. magnesium, calcium).[19] Branen et al. reported that 31.3 μg/ml EDTA reduced the minimum inhibitory concentration (MIC) of lysozyme against *Listeria monocytogenes* Scott A by ten-fold, from 250 μg ml^{-1} to 25 μg ml^{-1}.[22] Synergy between lysozyme and EDTA against *Escherichia coli* 0157:H7 was reported at lysozyme concentration of 200-600 μg ml^{-1} and EDTA concentrations of 300-1500 μg ml^{-1}.[24] In a study examining the effect of cations on lysozyme synergy with EDTA, it was proposed that chelation of multivalent cations by EDTA was inherent to antimicrobial synergy.[23]

Recently, non-migratory metal chelating active packaging was developed as a promising alternative to synthetic metal chelators.[43, 46, 76] Since the chelator is covalently attached to the packaging, this type of packaging would require *food contact notification* rather than *direct additive* approval, which may make it suitable for use with natural and organic foods.[37] Metal chelating polypropylene films were synthesized by photoinitiated graft polymerization of acrylic acid onto polypropylene (PP-*g*-PAA).[43] Tian et al.[43] reported that metal chelating film with a ferrous iron chelating activity of 71.07 ± 12.95 nmol cm^{-2} extended the lag phase of lipid oxidation in a soybean oil-in-water emulsion from 2 to 9 days (using accelerated storage conditions). There has yet to be any investigation of the antimicrobial activity of such non-migratory metal chelating active packaging films.

The objective of this study was to evaluate the antimicrobial activity of metal chelating active packaging films when used in combination with lysozyme. We further examined the influence of ionic strength on the synergy between metal chelating films and lysozyme. *Listeria monocytogenes* Scott A was chosen as the test food pathogen because of its importance in food safety, and because it does not produce siderophores (microbial produced iron chelators that, if produced, may compete with the metal chelating film and may complicate the interpretation of our results).

3.3 Materials and Methods

3.3.1 Materials

Polypropylene (isotactic pellets, catalog number 130) was purchased from Scientific Polymer Products (Ontario, NY). Hydroxylamine hydrochloride, ferrous sulfate heptahydrate (99+%), imidazole (99%), 3-(2-pyridyl)-5,6-diphenyl-1,2,4-triazine-*p,p'*-

disulfonic acid disodium salt hydrate (ferrozine, 98+%), toluidine blue O (TBO), and ethanol (99.5+%) were purchased from Acros Organics (Morris Plains, NJ). Acrylic acid (anhydrous), benzophenone (99%), and lysozyme from chicken egg white (lyophilized powder, protein ≥98 %, ≥40,000 units mg^{-1} protein) were purchased from Sigma-Aldrich (St. Louis, MO). Bicinchoninic acid (BCA) protein assay kit was purchased from Thermo Scientific (Rockford, IL). All other chemicals were purchased from Fisher Scientific (Fair Lawn, NJ). *Listeria monocytogenes* Scott A (FSL-J1-225) was obtained from M. Weidmann, Cornell University. EDTA solutions were autoclaved and lysozyme solutions were filter sterilized prior to use in antimicrobial assays.

3.3.2 Preparation of Metal Chelating Film

Metal chelating polypropylene films were prepared using a modification of previously reported work.[43, 76] Polypropylene (PP) pellets were cleaned by sequentially sonicating in isopropanol, acetone, and deionized water (each solvent twice for 10 min each rinse), and then dried over anhydrous calcium sulfate. Clean PP film was prepared from PP pellets on a Carver Laboratory Press (Carver, Inc., NJ) set to 160°C. PP films, average thickness of 387 ± 35 μm, were cut into 7.5 x 7.5 cm^2 pieces and washed using the same method as the PP pellets.

Benzophenone in heptanes (5% w/w) was spin coated (WS-400-6NPP, Laurell Technologies, North Wales, PA) onto each side of 7.5 x 7.5 cm^2 polypropylene at 500 rpm for 5 sec and then, 2000 rpm for 30 sec. Each 7.5 x 7.5 cm^2 benzophenone coated PP film was cut into 2.5 x 7.5 cm^2 pieces and then each 2.5 x 7.5 cm^2 piece was placed into a screw top 250 ml square borosilicate glass bottle and sealed with a polytetraflouroethylene faced silicon septum fitted polybutylene terephthalate cap (Corning Inc., Corning, NY). The vials

were flushed with nitrogen for 5 min and then exposed to UV light (Dymax 5000-EC Series, Torrington, CT) at 365 nm with an average light intensity of 209 ± 4.3 mW cm^{-2} for 60 sec. Films were washed three times with acetone after benzophenone-surface activation to remove unreacted benzophenone and then dried at room temperature.

Benzophenone-activated PP (PP-BP) films were placed into a screw top 250 ml square borosilicate glass bottle and 56.25 ml of acrylic acid in ethanol (30% w/w) was added before the bottles were sealed with polytetraflouroethylene faced silicon septum fitted polybutylene terephthalate cap and then flushed with nitrogen for 20 min. Nitrogen flushed vials were exposed to UV light for 6 min to graft and polymerize acrylic acid. PP films with grafted poly(acrylic acid) (PP-*g*-PAA) were rinsed in deionized water for 30 min at room temperature, 60 min at 60°C and then 30 min at room temperature to remove unattached monomer and homopolymer. PP-*g*-PAA was dried overnight over anhydrous calcium sulfate.

3.3.3 Scanning Electron Microscopy (SEM) of Metal Chelating Film

Cross sectional images of PP-*g*-PAA were taken with JCM-5000 NeoScope (JEOL, Japan) at 10 kV. Cross sectional samples were prepared by freeze fracturing films under liquid nitrogen. Prior to imaging, samples were mounted on a small aluminum platform with double sided carbon tape and then sputter coated with gold under nitrogen for 3 min.

3.3.4 Attenuated total reflectance/ Fourier transform infrared spectroscopy (ATR-FTIR) of Metal Chelating Film

Attenuated total reflectance Fourier transform infrared spectroscopy (ATR-FTIR) was used to confirm the grafting of functional groups on the surface of PP-*g*-PAA. An

IRPrestige FTIR Spectrometer (Shimadzu Scientific Instruments, Inc., Kyoto, Japan) with a diamond ATR crystal was used to measure the spectrum. Each spectrum was collected under the following parameters: Happ-Genzel function, 32 scans, and 4 cm^{-1} resolution. Spectrum analysis was performed on KnowItAll(R) Informatics System 9.5 (Bio-Rad Laboratories, Inc., Informatics Division, Philadelphia, PA) and Sigma Plot 12 (Systat Software, Inc., San Jose, CA).

3.3.5 Available Carboxylic Acids Density of Metal Chelating Film

Toluidine blue O (TBO) dye assay, in which each molecule of dye reversibly binds with carboxylic acids at a 1:1 stoichiometric ratio, was used to quantify surface carboxylic acids as previously described.[46, 66, 67] Each 2.5 x 7.5 cm^2 film was cut into 1 x 2.5 cm^2 pieces for the assay. Each piece of film was incubated in 5 ml TBO (0.5mM TBO, pH 10) while shaking at room temperature for 2 h and then rinsed three times in deionized water, adjusted to pH 10 by sodium hydroxide. TBO dye was desorbed from each piece of film in 8 ml 50% acetic acid while shaking at room temperature for 15 min. The absorbance of TBO dye in 50% acetic acid was measured at 633 nm to quantify surface carboxylic acids by comparison to a standard curve of TBO in 50% acetic acid.

3.3.6 Ferrous Iron Chelating Activity of Metal Chelating Film

Iron chelating activity of PP-*g*-PAA was determined by measuring the density of ferrous iron bound to PP-*g*-PAA at pH 5.0 (pH value at which PP-*g*-PAA was previously shown to exhibit optimal ferrous iron chelation and have good iron solubility).[43, 46] In this method, the amount of chelated ferrous iron is released from the film and quantified by colorimetric reaction with ferrozine reagent. Each 2.5 x 7.5 cm^2 film was cut into 1 x 2.5 cm^2 pieces for the assay. Films were submerged in 20 ml ferrous iron solution (1mM

ferrous sulfate heptahydrate in 0.05M sodium acetate/imidazole, pH 5.0) and rotated at room temperature for 30 min followed by rinsing 3 times in deionized water to remove loosely adsorbed iron. Each 1 x 2.5 cm^2 film was incubated with 3 ml releasing agent (0.1 g ml^{-1} hydroxylamine hydrochloride and 0.05 g ml^{-1} trichloroacetic acid) while shaking for 2.5 h to release ferrous iron. After ferrous iron was released from the film, 0.5 ml releasing agent (containing released ferrous iron) was added to 0.5 ml ferrozine solution (9.0 mM ferrozine in 50mM HEPES, pH 7.0) and incubated while shaking for 1 h at room temperature. The absorbance of ferrozine reacted releasing agent was measured at 562 nm to quantify ferrous iron chelating activity by comparison to a standard curve of ferrous iron in releasing agent.

3.3.7 Microtiter Plate Assay of Antimicrobial Activity of Lysozyme and EDTA

L. monocytogenes Scott A was chosen as a model gram positive microorganism to test the synergistic antimicrobial activity of PP-*g*-PAA and lysozyme. PP-*g*-PAA was designed to mimic the chelating mechanism of EDTA, therefore EDTA was chosen as the positive control for antimicrobial experiments. A checkerboard microtiter plate assay was used as a rapid screening test for the antimicrobial activity of lysozyme, EDTA, and combinations of lysozyme and EDTA against *L. monocytogenes* in tryptic soy broth (TSB). All treatments were tested in triplicates. Concentrations tested were as follows (in µg ml^{-1}): EDTA, 500, 250, 125, 62.5, 31.3, 15.6; lysozyme, 2000, 1000, 500, 250, 125, 62.5, 31.3. Ninety-six well microtiter plates with a well capacity of 300 µl were used for this experiment. For each well, 100 µl of lysozyme or EDTA (or 50 µl of each lysozyme and EDTA) and 100 µl of inoculum diluted in TSB (~10^5 cfu/ml) were added. Microtiter plates were incubated at 37°C for 24 h. Minimum inhibitory concentrations (MIC) of lysozyme

or EDTA were defined at the lowest concentrations for which growth was inhibited after overnight incubation. Antimicrobial inhibition was confirmed by plating onto tryptic soy agar (TSA) with an automated spiral plater Autoplater 4000 (Spiral Biotech Inc., Norwood, MA). Colonies were counted with a plate reader Scan 500 (Interscience, Saint-Non-la-Brèteche, France) in a range of 30–300 colonies using the instrument's software.

3.3.8 Microarray Microtiter Plate Assay of Antimicrobial Activity of Metal Chelating Film and Lysozyme

To quantify synergistic antimicrobial activity between lysozyme and metal chelating active packaging film, a microtiter assay was developed using a 96-well microarray microtiter plate (AHC4x24, ArrayIt Corporation, Sunnyvale, CA), in which swatches of film (4 – 2.5 x 7.5 cm^2 pieces) are assembled at the bottom of the plate and function as the bottom of each well (**Figure 3.1**). Native PP film was used as a control film. Each microarray microtiter plate was placed in a polypropylene box (Sterilite 0.3-Gallon (1.2-Quart) Modular Latch Storage Box, Ennis, TX) and autoclaved to sterilize.

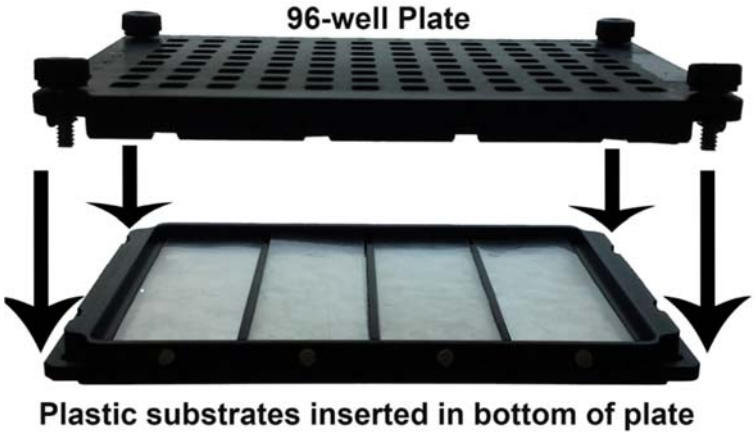

Figure 3.1. Microarray plate adapted for use in film microbiological assays. Each plate can hold 4 -2.5 x 7.5 cm^2 films for testing of up to 24 samples per film (96-well plate). Each well exposes 48.75 mm^2 of film.

In order to increase surface area to volume ratio, the volume in the antimicrobial assay was reduced to 100 µl total: 50 µl lysozyme and 50 µl inoculum diluted in TSB (~10^5 cfu/ml). Each well exposes samples to a film surface area of 7.5 x 6.5 mm^2 for a surface area to volume ratio of approximately 5 cm^2 ml^{-1}. Microarray microtiter plates were covered with sterile SealPlate Film (Excel Scientific, Victorville, CA), incubated at 37°C for 24 h and then MIC was quantified by plating on TSA as described in the previous section.

Additional experiments were performed to assess the effect of ionic strength on the MIC of lysozyme in the presence of control film and on combinatory effect of metal chelating film and lysozyme. To vary the overall ionic strength of the assay, lysozyme was prepared in sodium chloride or potassium phosphate buffer, pH 7 (0 mM, 33.3 mM, 66.7 mM, and 100 mM) instead of TSB. As in the previous experiment, inocula were prepared in TSB to ensure proper nutrient and neutral pH conditions for bacterial growth. Since ionic strength had a significant influence on the lysozyme MIC, the lysozyme MIC for each ionic strength condition was determined. At the lysozyme MIC for each ionic strength condition, combinatory effect of metal chelating film and lysozyme on antimicrobial activity was assessed and compared to control film by calculating the log reduction value. Log reduction value (LRV) was defined as the log number of microorganisms inactivated after exposure to both lysozyme and metal chelating film compared with those inactivated by lysozyme and control film and calculated using the following equation:

$$LRV = \log_{10}\left(\frac{N_{PAA}}{N_{PP}}\right) \quad (1)$$

where N_{PAA} is the number of microorganisms after exposure to lysozyme and metal chelating films and N_{PP} is the number of microorganisms after exposure to lysozyme and control film.

3.3.9 Lysozyme Adsorption onto Metal Chelating Films

Adsorption of lysozyme onto the metal chelating films as a function of ionic strength was quantified using native PP as a control film. Films were fixed to the bottom of the microarray microtiter plate as described previously. Each 7.5 x 6.5 mm^2 well was exposed to 100 µl of lysozyme (~800 µg ml^{-1}) in phosphate buffer, pH 7.0 (0, 33.3, 66.7, 100, 200 mM) for 24 h at 37°C. Lysozyme binding was quantified by comparing the protein content of lysozyme solutions before and after incubation with metal chelating film. Protein content was measured by BCA Protein Assay Kit (Thermo Scientific, Rockford, IL) using the standard test tube protocol. Briefly, 0.1 ml lysozyme in phosphate buffer was added to 2.0 ml BCA working reagent, incubated at 37°C for 30 min, cooled to room temperature. Absorbances were measured at 562 nm and protein content was quantified by comparison to a standard curve of bovine serum albumin in phosphate buffer.

3.4 Results and Discussion

3.4.1 Characterization of Metal Chelating Active Packaging Films

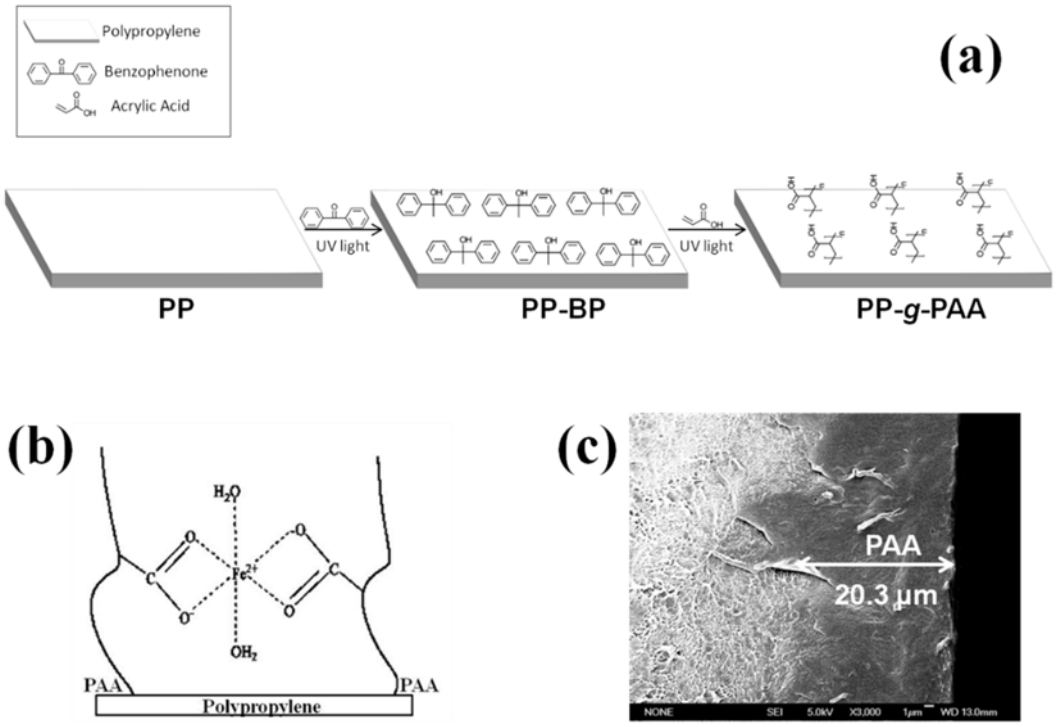

Figure 3.2. (a) Synthesis of metal chelating films (PP-*g*-PAA) by photoinitiated graft polymerization, (b) theoretical ligand to metal binding structure (ligand:metal binding ratio = 2) adapted from Tian, et al. [43]and (c) SEM cross sectional image of metal chelating films (arrow indicates approximate thickness of PAA graft layer).

Metal chelating active packaging films were synthesized by two-step photoinitiated graft polymerization to graft poly(acrylic acid) from the surface of polypropylene (PP-*g*-PAA), imparting carboxylic acid based metal chelating moieties (**Figure 3.2a**).[43, 76] Under pH conditions for which the carboxylic acids are deprotonated, the theoretical ligand (carboxylic acid) to metal (ferrous iron) binding ratio is 2 (**Figure 3.2b**). Poly(acrylic acid) surface modification yielded a uniform surface grafted polymer layer approximately 20 µm thick (**Figure 3.2c**), in agreement with previously published work.[43, 76]

The surface chemistry of native, photoinitiator-activated, and metal chelating PP films was characterized by ATR-FTIR (**Figure 3.3**). Unlike native PP film, the FTIR

spectrum of photoinitiator-activated PP (PP-BP) film exhibited absorbance at around 700 cm^{-1} that was attributed to the aromatic ring in benzophenone. After acrylic acid polymerization on the surface of the film (PP-*g*-PAA), the absorbance of the aromatic ring of benzophenone decreased and new absorbances indicative of carboxylic acid groups at 1700-1725 cm^{-1} and 1211-1320 cm^{-1}, representing the C=O bond and the C-O bond, respectively, were present in the IR spectrum. Changes in the spectrum suggest that benzophenone was partially displaced by acrylic acid, which was subsequently polymerized from the film's surface. This IR spectrum confirmed successful covalent grafting of poly(acrylic acid) from the surface of PP.

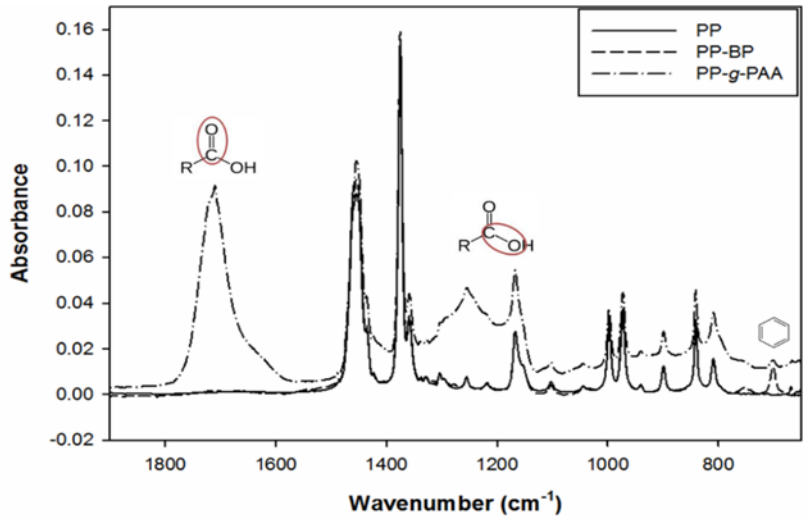

Figure 3.3. ATR-FTIR of native polypropylene (PP), photoinitiator-activated polypropylene (PP-BP), and metal chelating polypropylene (PP-*g*-PAA).

The density of available carboxylic acids density and the ferrous iron chelating activity of native PP, photoinitiator-activated PP (PP-BP) and metal chelating film (PP-*g*-PAA) were further quantified (**Figure 3.4**). PP and PP-BP exhibited minimal surface carboxylic acids and iron chelating activity (<2.5 nmol cm^{-2}, below the value of standard deviation). After grafting of poly(acrylic acid), films exhibited a carboxylic acid density of

113 ± 5.4 nmol cm^{-2} and a ferrous iron chelating activity of 53.7 ± 9.8 nmol cm^{-2} for a ligand to metal binding ratio of approximately 2 to 1. The experimental ligand to metal binding ratio was very similar to the theoretical ligand to metal binding for deprotonated carboxylic acids (**Figure 3.2b**).

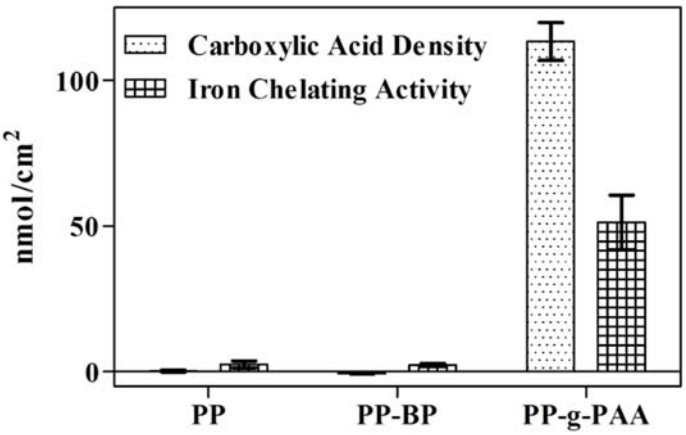

Figure 3.4. Carboxylic acid density and ferrous iron chelating activity of native polypropylene (PP), photoinitiator-activated polypropylene (PP-BP), and metal chelating polypropylene (PP-*g*-PAA).

Metal chelating activity of poly(acrylic acid) is highly dependent on charge interactions that require deprotonation of carboxylic acid chelating moieties In order to understand the influence of bulk solution pH on the disassociation behavior of metal chelating active packaging film, an FTIR titration was performed to determine the pKa^{bulk} of surface grafted poly(acrylic acid) (PP-*g*-PAA), calculated to be 6.45.[77] The pKa of poly(acrylic acid) in solution has been previously reported to be ~4.7.[78] The pKa^{bulk} of surface-grafted poly(acrylic acid) was higher than the pKa of poly(acrylic acid) in solution due to the influence of the surface and surrounding grafted chains on charge distribution within the surface modification.[79, 80] The antimicrobial studies were conducted at a neutral pH (7.0) that was higher than the pKa^{bulk} of metal chelating active packaging films, which favors deprotonation of metal chelating moieties.

3.4.2 Antimicrobial Activity of Metal Chelating Film in Combination with Lysozyme in TSB

The objective of the first antimicrobial study was to demonstrate the antimicrobial activity of metal chelating films, from which chelating moieties had been surface-grafted, in comparison to the antimicrobial activity of EDTA in solution against *L. monocytogenes* Scott A. Chelating film and EDTA tested alone and in combination with lysozyme using TSB as the media for both the inocula and the antimicrobial stock solutions. Recently it was reported that the MIC of EDTA against *L. monocytogenes* Scott A in TSB was 250 μg/ml and that low concentrations of EDTA (≤ 31.3 μg/ml) exhibit potent synergy with lysozyme against *L. monocytogenes* Scott A.[22] An approximate EDTA equivalent concentration was calculated so that the film chelating activity would be greater than or equal to reported EDTA MIC. In each well of the microarray microtiter plates (surface area= 48.75 mm^2), at a total volume of 50 μl, metal chelating film yielded an approximate EDTA equivalent concentration of 305 μg ml^{-1}. For assays in which the total volume was 100 μl, metal chelating film yielded an approximate EDTA equivalent concentration of 153 μg ml^{-1}. These calculations do not take into account possible differences in the binding affinity of the metal chelating films as compared to EDTA.

Table 3.1. Minimum inhibitory concentrations (MIC) against *L. monocytogenes* Scott A in tryptic soy broth (TSB).

Antimicrobial	**MIC (μg/ml)**	
Lysozyme	2000	
EDTA	250	
	Lysozyme	*EDTA*
	31.3	62.5
Lysozyme + EDTA	125	31.3
	250	15.6
Lysozyme + PP-*g*-PAA	1000	~153 *(equivalence)*

The MICs for lysozyme, EDTA, lysozyme + EDTA, and lysozyme + metal chelating films in TSB are reported in **Table 3.1**. Metal chelating films alone (EDTA equivalent ~ 305 μg ml^{-1}) were unable to inhibit the growth of *L. monocytogenes*. The MICs of the lysozyme, EDTA, and lysozyme + EDTA in TSB against *L. monocytogenes* were in agreement with previously published research.[22, 81] In the presence of metal chelating films (EDTA equivalent ~ 153 μg ml^{-1}), the MIC of lysozyme decreased from 2000 to 1000 μg ml^{-1}. Although metal chelating films demonstrated synergy with lysozyme against *L. monocytogenes*, the synergy was not as potent as the synergy between EDTA and lysozyme, wherein as little as 31.25 μg ml^{-1} EDTA decreased the lysozyme MIC by greater than ten-fold. EDTA has a known affinity for binding of multivalent cations, especially Fe^{2+} and Fe^{3+}.[23] Since the metal chelating activity of surface poly(acrylic acid) chains is by electrostatic interactions rather than ligand-specific binding of high affinity metals, it was hypothesized that the decreased synergistic impact of lysozyme with metal chelating films may be due to competitive binding of positively charged large molecules, such as proteins present in TSB or the lysozyme itself, by the negatively charged metal chelating films. Since protein-polyelectrolyte interactions can be influenced by ionic strength, additional antimicrobial activity assays were performed in which ionic strength of the growth media was varied to assess the influence of electrostatic screening on protein-material interactions and subsequent antimicrobial activity.

3.4.3 Antimicrobial Activity of Metal Chelating Film in Combination with Lysozyme in Solutions of Varying Ionic Strength

As in the previous antimicrobial activity assays, ionic strength experiments were performed by blending lysozyme stock solution with inocula prepared in TSB, and

exposing the resulting inocula to control or chelator modified films in the modified microarray plate. Ionic strength of antimicrobial assays was controlled by changing the composition of the lysozyme stock solution. Lysozyme was prepared in potassium phosphate buffer, pH 7 or sodium chloride of concentrations ranging from 0 to 100 mM. Ionic strength was calculated for each antimicrobial assay using the following equation:

$$I = \frac{1}{2}\sum_{i=1}^{n} c_i z_i^2 \quad (2)$$

in which I is ionic strength, c is ion concentration, and z is the ion charge number (**Table 3.2**). TSB, which contains 5 g l^{-1} sodium chloride and 2.5 g l^{-1} dipotassium hydrogen phosphate, contributed 64.4 mM ionic strength to each antimicrobial assay.

Table 3.2. Influence of ionic strength on lysozyme MIC (in contact with native PP). Total ionic strength of each antimicrobial assay with contribution from TSB and lysozyme stock solution (sodium chloride or phosphate buffer) is reported in adjacent columns.

Salt or Buffer Concentration of Lysozyme Stock Solution (mM)	Sodium Chloride		Phosphate Buffer	
	Lysozyme MIC (μg/ml)	Total Ionic Strength (mM)	Lysozyme MIC (μg/ml)	Total Ionic Strength (mM)
0	31.3	64.4	31.3	64.4
33.3	62.5	81.1	125	92.3
66.7	250	97.7	250	120
100	500	114	1000	176

Preliminary antimicrobial activity assays demonstrated that the MIC of lysozyme alone (in the presence of control film) was affected by ionic strength. **Table 3.2** shows the effect of ion concentration on lysozyme MIC. Ionic strength had a significant impact on lysozyme MIC, with lysozyme MIC for *L. monocytogenes* increasing from 31.3 to 1000

μg ml^{-1} with increasing ionic strength. These data suggest that high ion concentration may have reduced the antimicrobial effectiveness of lysozyme against *L. monocytogenes* when in contact with control film. Kihm, et al. [82] conducted a study where they investigated the impact of Ca and Mg ions on resistance of *L. monocytogenes* against egg white lysozyme in whole milk and MES buffer. They found that removal of Ca and Mg ions improved the antimicrobial efficacy of lysozyme against *L. monocytogenes* and suggested that the mineral content of media can significantly influence the sensitivity of *L. monocytogenes* to lysozyme. Ion-induced resistance of *L. monocytogenes* to lysozyme is possibly due to the ability of excess cations to stabilize the peptidoglycan layer of the cell membrane against hydrolysis by lysozyme as well as electrostatic screening of lysozyme-microbial membrane interactions.

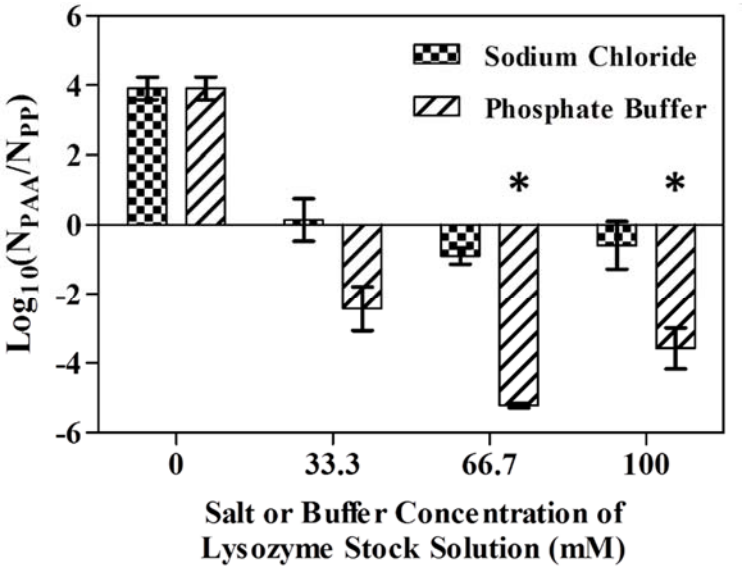

Figure 3.5. Effect of salt or buffer concentration of lysozyme stock solution on log reduction value of lysozyme in the presence of PP-*g*-PAA compared with native PP. Bacteriocidal treatments are marked with an asterisk (*).

In order to assess the influence of ionic strength on the synergistic antimicrobial activity of lysozyme + metal chelating film, the effect of metal chelating films on lysozyme

activity for each ionic strength condition was quantified at their respective lysozyme MIC by log reduction value (**Figure 3.5**). Data are reported as log reduction values (LRV), in which lysozyme with metal chelating film was the test and lysozyme with control film (native PP) was the control. Positive values represent antagonistic interactions between lysozyme and metal chelating films and negative values represent synergistic interactions between lysozyme and metal chelating films. Under conditions of low ionic strength (0 mM ion in lysozyme stock solution), lysozyme and metal chelating film worked antagonistically compared with the control film, exhibiting an increase in microbial populations of ~4 log. As ionic strength increased (≥33.3 mM sodium chloride or phosphate buffer), the interactions between lysozyme and metal chelating film shifted from antagonistic to synergistic. An increasing presence of divalent ions (phosphate buffer) appeared to have a greater influence on antimicrobial synergy than monovalent ions alone (sodium chloride), possibly due the greater contribution of divalent ions to ionic strength. When lysozyme was prepared in 66.7 and 100 mM phosphate buffer, lysozyme and metal chelating films exhibited a bactericidal effect (~3-5 log reduction). These data indicate that, at neutral pH, synergy between lysozyme and metal chelating films may only be observed under conditions of moderate to high ionic strength.

At the neutral pH conditions of the antimicrobial assay, poly(acrylic acid) grafted from metal chelating films (pKa^{bulk} 6.45) have a net negative charge and lysozyme (pI 11.35) has a net positive charge. It was hypothesized that under conditions of low ionic strength, surface-grafted poly(acrylic acid) may bind lysozyme or other media proteins and reduce the antimicrobial activity of the enzyme. In order to test this hypothesis, the binding of lysozyme was examined in phosphate buffers of varying ion concentrations under the

same conditions as the antimicrobial assay (**Figure 3.6**). As hypothesized, the maximum adsorption of lysozyme onto PP-*g*-PAA films occurred under conditions of low ion concentration (33.3 mM phosphate buffer), exhibiting up to 41.7 μg cm^{-2} of bound protein. As buffer concentration increased, the amount of lysozyme bound by the film decreased and at 200 mM phosphate buffer, there was no observable lysozyme bound to the film. The observed relationship between ion concentration and lysozyme binding onto PP-*g*-PAA supports that of other published data for lysozyme-polyelectrolyte interactions, in which maximum protein binding is observed in solutions of low ionic strength (~5-60 mM).[83]

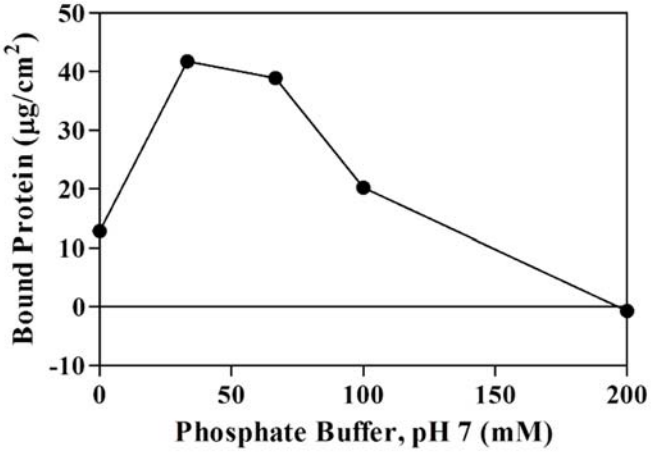

Figure 3.6. Adsorption of lysozyme onto PP-*g*-PAA at different concentrations of phosphate buffer, pH 7.

Lysozyme binding to PP-*g*-PAA is hypothesized to be mediated by electrostatic screening (**Figure 3.7**). Under low ionic strength conditions, electrostatic screening is minimal and the adsorption of lysozyme onto poly(acrylic acid) grafts may be favored. Binding of lysozyme as well as other proteins under low ionic strength conditions may also hinder synergy by compressing poly(acrylic acid) chains to interfere with metal chelation. Halperin [84] previously reported that that large proteins may only approach polymer chain modified surfaces by compressing the surface grafted polymer chains. Under moderate to high ionic strength conditions, there may be sufficient electrostatic screening to hinder

lysozyme – poly(acrylic acid) interactions and favor metal chelation. The presented data demonstrate the importance of solution conditions (e.g. pH and ionic strength) on metal chelating films antimicrobial activity and synergy with lysozyme as well as other charged antimicrobials.

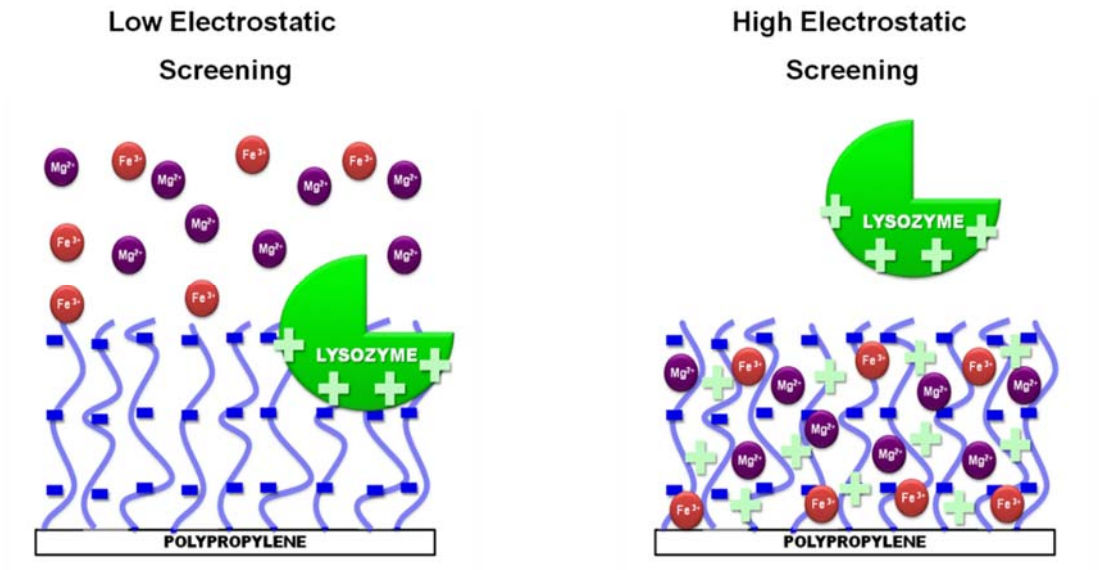

Figure 3.7. Proposed metal chelating film-lysozyme interactions under conditions of low and high electrostatic screening.

3.5 Conclusions

In this work, metal chelating active packaging films were prepared by grafting metal chelating poly(acrylic acid) grafts from the surface of polypropylene films. The resulting metal chelating films enhanced antimicrobial activity of lysozyme to inhibit growth of *L. monocytogenes* under condition of moderate to high ionic strengths, enabling up to 5.22 log reductions in microbial growth under optimal conditions. The charged nature of the chelating material evaluated herein resulted in protein adsorption onto the material surface under low ionic strength. Our ongoing research in metal chelating active packaging materials that are net neutral and chelate metal ions based on specific ligand-metal

interactions rather than charge may be more effective as synergistic antimicrobials across a wider range of pH values and ionic strength.[44, 85] Finally, understanding the potential interactions between food matrix components (e.g. ions, proteins, bioactive molecules, antimicrobials) and packaging materials (active or traditional) is critical when considering commercial application. This work demonstrates the potential application of metal chelating active packaging to enhance the efficacy of lysozyme, a natural food antimicrobial, and possibly enable removal of synthetic chelators from product formulations.

CHAPTER 4

FOURIER TRANSFORMED INFRARED STUDIES ON THE DISSOCIATION BEHAVIOR OF METAL CHELATING POLYELECTROLYTE BRUSHES[3]

4.1 Abstract

The dissociation behavior of surface-grafted polyelectrolytes is of interest for the development of stimuli-responsive materials. Metal chelating polyelectrolyte brushes containing acrylic acid (PAA) or hydroxamic acid (PHA) chelating moieties were grafted from the surface of polypropylene (PP). Fourier transformed infrared spectroscopy (FTIR) was used to determine the effective bulk pKa of the polyelectrolyte brushes (pKa^{bulk}) and to characterize metal chelating behavior. The pKa^{bulk} of PP-*g*-PAA and PP-*g*-PHA were 6.45 and 9.65, respectively. Both PP-*g*-PAA and PP-*g*-PHA exhibited bridging bidentate and chelating bidentate iron chelation complexes. This is the first reported determination of pKa^{bulk} of surface-grafted poly(hydroxamic) acid.

4.2 Introduction

The attachment of polyelectrolytes onto solid supports enables synthesis of stimuli-responsive functional surfaces that have numerous applications in water treatment,[60] colloidal stabilization,[86] protein immobilization,[87] drug delivery,[88] and biosensors.[89, 90] The functionality of these surfaces, which often relies on charge and ligand-specific interactions, depends on the microenvironment at the interface. The microenvironment of surface-grafted polyelectrolytes is not only influenced by solvent conditions, such as pH and ionic strength, as is the case with their solution-based analogs, but is also influenced by the

[3] The contents of this chapter have been published: Roman, M. J.; Decker, E. A.; Goddard, J. M. Fourier Transform Infrared studies on the dissociation behavior of metal-chelating polyelectrolyte brushes. *ACS Applied Materials & Interfaces* **2014**, *6*, 5383-5387.

properties of the surface and surrounding grafted polymers. Due to the steric restrictions associated with attachment of polyelectrolytes to a surface, the dissociation behavior of surface-grafted polyelectrolytes may be very different from that corresponding to polyelectrolytes in solution.[36] For example, Dong et al. reported a pKa^{bulk}, which characterizes the dissociation behavior of the surface-grafted polyelectrolytes, of poly(acrylic acid) (PAA) brushes that was *two units higher* than previously reported pKa values of PAA in solution.[78, 80]

Dissociation behavior of polyelectrolytes in solution as a function of pH, salt concentration or metal chelation is quantifiable by well-established titration techniques. However, these methods are not applicable to polymers grafted onto a solid support due to the inability of the equipment used to collect data, such as pH meters and isothermal titration calorimeters, to directly monitor charge fraction within the surface-grafted polyelectrolyte layer. There have been studies that generate titration curves of surface-grafted polyelectrolytes, mainly carboxylate-containing polymers such as PAA and poly(methacrylic acid) (PMAA), from data collected by contact angle,[80, 91] reflectometry,[92, 93] ellipsometry,[90, 91, 94, 95] and Fourier transformed infrared spectroscopy (FTIR)[80, 90, 96, 97] techniques. Titration curves generated by contact angle measurements reflect the ionization properties of only the top few nanometers of surface grafted polyelectrolytes ($pKa^{surface}$), while titration curves generated by reflectometry, ellipsometry, and FTIR measurements can be used to examine dissociation behavior of the entire surface-grafted polyelectrolyte layer (pKa^{bulk}).[80] Of the techniques that characterize pKa^{bulk}, FTIR is the only technique which enables direct quantification of the charged fraction to characterize dissociation behavior by measuring absorbance bands of specific bonds. FTIR may also be used to

characterize the absorption of charged species, such as proteins and metal ions, to polyelectrolyte-modified surfaces.

We recently developed metal chelating polymer films for antioxidant packaging applications, wherein either PAA or poly(hydroxamic acid) (PHA) brushes were grafted from the surface of polypropylene (PP) via photoinitiated graft polymerization.[43] Herein, we report the characterization of the dissociation and iron chelation behavior of these surface-grafted polyelectrolytes brushes using FTIR-based characterization techniques. Particularly, pKa^{bulk} and possible metal coordination complexes were determined. This is the first reported determination of pKa^{bulk} of surface-grafted PHA.

4.3 Materials and Methods

4.3.1 Materials

Polypropylene (isotactic, pellets) was purchased from Scientific Polymer Products (Ontario, NY). Hydroxylamine hydrochloride, imidazole (99%), 3-(2-pyridyl)-5,6-diphenyl-1,2,4-triazine-*p,p'*-disulfonic acid disodium salt hydrate (ferrozine, 98+%), and ethanol (99.5+%) were purchased from Acros Organics (Morris Plains, NJ). Acrylic acid (anhydrous), methyl acrylate (99%), and benzophenone (99%) were purchased from Sigma-Aldrich (St. Louis, MO). All other chemicals were purchased from Fisher Scientific (Fair Lawn, NJ).

4.3.2 Photoinitiated Graft Polymerization of Poly(acrylic acid) and Poly(methyl acrylate) onto Polypropylene

Poly(acrylic acid) grafted onto polypropylene **(**PP-*g*-PAA) and poly(methyl acrylate) onto polypropylene (PP-*g*-PMA) were prepared using a modification of previously reported work .[43, 44, 76] Polypropylene (PP) pellets were cleaned by sequentially

sonicating in isopropanol, acetone, and deionized water (each solvent twice for 10 min each rinse), and then dried over anhydrous calcium sulfate. Clean PP film was prepared from PP pellets on a Carver Laboratory Press (Carver, Inc., NJ) set to 160°C. PP films, average thickness of 387 ± 35 μm, were cut into 8 x 8 cm^2 pieces and washed using the same method as the PP pellets.

Benzophenone in heptanes (5% w/w) was spin coated (WS-400-6NPP, Laurell Technologies, North Wales, PA) onto each side of 8 x 8 cm^2 polypropylene at 500 rpm for 5 sec and then, 2000 rpm for 30 sec. Each 8 x 8 cm^2 benzophenone coated PP film was cut into 2 x 8 cm^2 pieces and then each 2 x 8 cm^2 piece was placed into a screw top 250 ml square borosilicate glass bottle and sealed with a polytetraflouroethylene faced silicon septum fitted polybutylene terephthalate cap (Corning Inc., Corning, NY). The vials were flushed with nitrogen for 5 min and then exposed to UV light (Dymax 5000-EC Series, Torrington, CT) at 365 nm for 90 sec. For PP-*g*-PAA, a low brush density film was synthesized by decreasing the benzophenone graft time to 60 sec.[76] Films were washed with acetone after benzophenone-surface activation to remove unreacted benzophenone and then dried at room temperature.

For the preparation of PP-*g*-PAA, benzophenone-activated PP (PP-BP) films were placed into a screw top 250 ml square borosilicate glass bottle and acrylic acid in ethanol (25% w/w) was added before the bottles were sealed and then flushed with nitrogen for 20 min. Nitrogen flushed bottles were exposed to UV light for 6 min to graft and polymerize acrylic acid. PP films with grafted poly(acrylic acid) (PP-*g*-PAA) were rinsed in deionized water for 30 min at room temperature, 60 min at 60°C and then 30 min at room temperature

to remove unattached monomer and homopolymer. PP-*g*-PAA was dried overnight over anhydrous calcium sulfate.

For the preparation of PP-*g*-PMA, benzophenone-activated PP (PP-BP) films were cut into 1 x 2 cm^2 pieces, placed into a screw top vial, methyl acrylate in acetone (70% w/w) was added before the vials were sealed with septum fitted aluminum caps and flushed with nitrogen for 5 min. Nitrogen flushed vials were exposed to UV light for 3 min to graft and polymerize methyl acrylate onto PP-BP. Overnight Soxhlet extraction was performed to remove any unattached monomer and homopolymers from the surface of poly(methyl acrylate)-grafted PP (PP-*g*-PMA) films.

4.3.4 Conversion of Surface Grafted Poly(methyl acrylate) to Poly(hydroxamic acid)

Ester groups on the surface of PP-*g*-PMA were converted to hydroxamic acid by reaction with hydroxylamine, as previously described.[85, 98, 99] A basic hydroxylamine solution was prepared by dissolving hydroxylamine hydrochloride (0.1 g ml^{-1}) in methanol/water (5:1) solution (0.1 g ml^{-1}), adjusting the pH of the solution to 13 by sodium hydroxide, and finally removing sodium chloride precipitate by filtration for a final methanol/water ratio of 4:1. PP-*g*-PMA films were submerged in the basic hydroxylamine solution, and the conversion reaction was conducted under reflux while stirring at 73 °C for 4 h to produce poly(hydroxamic acid) grafted onto polypropylene (PP-*g*-PHA). Then, films were washed methanol/water (5:1) solution, treated with acidic (0.2 M HCl) methanol/water (5:1) solution, rinsed in methanol/water (5:1) solution, and finally rinsed in deionized water. PP-*g*-PHA films were dried and stored over anhydrous calcium sulfate until further use.

4.3.5 FTIR Titration of PAA and PHA Brushes

An ATR-FTIR titration of PP-*g*-PAA was adapted from previously reported work to determine pKa^{bulk} of carboxylate and hydroxamate ligands of PP-*g*-PAA and PP-*g*-PHA, respectively.[80] A 1 M sodium hydroxide solution and 1 M hydrochloric acid solution was used to adjust the pH of buffer solutions. PP-*g*-PAA was incubated in 0.1M MES buffers of different pH, ranging from 3 to 10, for 1 h shaking, rinsed with anhydrous ethanol, and then dried with nitrogen gas. PP-*g*-PHA was incubated in buffers of different pH values: 0.1M MES buffer ranging from pH values 5 to 7 and 0.1M sodium carbonate buffer ranging from pH values 8 to 13, for 1 h shaking, rinsed with anhydrous ethanol, and then dried with nitrogen gas. A FTIR spectrum of each sample was collected on an IRPrestige FTIR Spectrometer (Shimadzu Scientific Instruments, Inc., Kyoto, Japan) with a diamond ATR crystal. Each spectrum was collected under the following parameters: Happ-Genzel function, 32 scans, and 4 cm^{-1} resolution. Spectral analysis was performed on KnowItAll(R) Informatics System 9.5 (Bio-Rad Laboratories, Inc., Informatics Division, Philadelphia, PA).

4.3.6 Iron Binding of PP-*g*-PAA and PP-*g*-PHA Films

PP-*g*-PAA and PP-*g*-PHA films were incubated in 0.08mM ferric chloride in 0.05M sodium acetate/imidazole, pH 5.0 for 24 h and then rinsed with copious amounts of deionized water. Iron binding was confirmed by ferrozine assay and ICP-MS. The FTIR spectrum of each sample was measured as described in **4.3.5. FTIR titration of PAA and PHA brushes**. The FTIR spectra before and after iron binding were compared and interpreted based on previously published research on metal binding by polyelectrolyte brushes.[100]

4.4 Results and Discussion

The synthesis of poly(acrylic acid) grafted from PP (PP-*g*-PAA) and poly(hydroxamic acid) grafted from PP (PP-*g*-PHA) by the described techniques for iron chelation applications has been confirmed by FTIR, contact angle, SEM, AFM, and colorimetric assays.[43, 44] For this study, ATR-FTIR spectra of PP-*g*-PAA and PP-*g*-PHA films were used to characterize chemistry of surface-grafted polyelectrolytes. Spectra were collected at wavenumbers ranging from 4000-600 cm^{-1}. At wavenumbers above 1800, the only absorbance bands attributed the surface-grafted poly(acrylic acid) and poly(hydroxamic acid) brushes were broad absorbance bands corresponding to O-H and N-H bonds that were easily influenced by the presence of water. Therefore, the FTIR analysis was restricted to absorbance bands present in the range of 1800-600 cm^{-1}. Absorbance bands were assigned based on analysis by KnowItAll(R) Informatics System 9.5 (Bio-Rad Laboratories, Inc., Informatics Division, Philadelphia, PA) and comparison to previously published research.[43, 44, 80, 100-105] **Tables C.1** and **C.2** show the absorbance band assignments for PP-*g*-PAA and PP-*g*-PHA, respectively (see **Appendix C**).

FTIR studies on the dissociation behavior of surface-grafted polymers with carboxylate ligands, such as PAA and PMAA, have been previously conducted by monitoring the C=O absorbance band.[80, 90, 96, 97] Deprotonated and protonated carboxylate ligands absorb at different wavelengths. Representative FTIR spectra of PP-*g*-PAA after incubation in buffers of different pH values are shown in **Figure 4.1a**. C=O absorbance bands at ~1710 cm^{-1} and ~1564 cm^{-1} corresponded to protonated carboxylic acid and deprotonated carboxylic acid, respectively. As pH increased, the intensity of the deprotonated C=O band increased and the intensity of the protonated C=O band decreased,

which illustrated the dissociation of carboxylate groups as a function of solution pH. Degree of dissociation, α, was calculated using the following equation:

$$\alpha = \frac{[COOH]}{[COO-] + [COOH]*\frac{\varepsilon(COO-)}{\varepsilon(COOH)}} \quad (1)$$

where [COO-] and [COOH] correspond to the integrated area of deprotonated and protonated carboxylic acid absorbance bands and ε(COO-) and ε(COOH) are the extinction coefficients of deprotonated and protonated carboxylic acid.[80] A previously determined $\frac{\varepsilon(COO-)}{\varepsilon(COOH)}$ value of 1.8 was used in the calculations.[100]

Degree of dissociation and their corresponding pH values were fitted to a sigmoid dose-response function (GraphPad Prism 6.0, La Jolla, CA) to generate a titration curve that was used to determine pKa^{bulk} (**Figure 4.1b**). The pKa^{bulk} was defined as the solution pH value corresponding to the midpoint of the titration curve and calculated to be 6.45 for PP-*g*-PAA. This value is in agreement with a previous FTIR study of dissociation behavior of poly(acrylic acid) brushes on gold substrates.[80] The pKa of poly(acrylic acid) in solution has been reported to be ~4.7, which is approximately 2 units lower than the pKa^{bulk} of poly(acrylic acid) brushes.[78] The pKa^{bulk} values of poly(acrylic acid) brushes is hypothesized to be greater than the pKa values of poly(acrylic acid) in solution due to the influence of the surface and surrounding grafted poly(acrylic acid) on charge distribution within the modified surface.[79, 80] Electrostatic interactions between surface-grafted carboxylate ligands dictate the distribution of charges within the grafted layer, wherein it is energetically unfavorable to ionize ligands closer to the surface due to the energy cost of repulsion between surface-grafted poly(acrylic acid) that occurs upon deionization.[80, 97] Therefore, it is hypothesized that the solution pH may be higher than the local pH within the grafted poly(acrylic acid) layer as the surface is approached. This phenomenon would

have brought about the increase in the pKa^{bulk} of the surface-grafted poly(acrylic acid) compared to poly(acrylic acid) in solution. This shift of the pKa^{bulk} of surface-grafted carboxylate polyelectrolytes approximately 2 pH units higher has been reported many times in literature.[79, 80, 94, 97] The pKa^{bulk} of polyelectrolyte brushes as a function of solution pH are important when determining applications of such surface-modified materials.

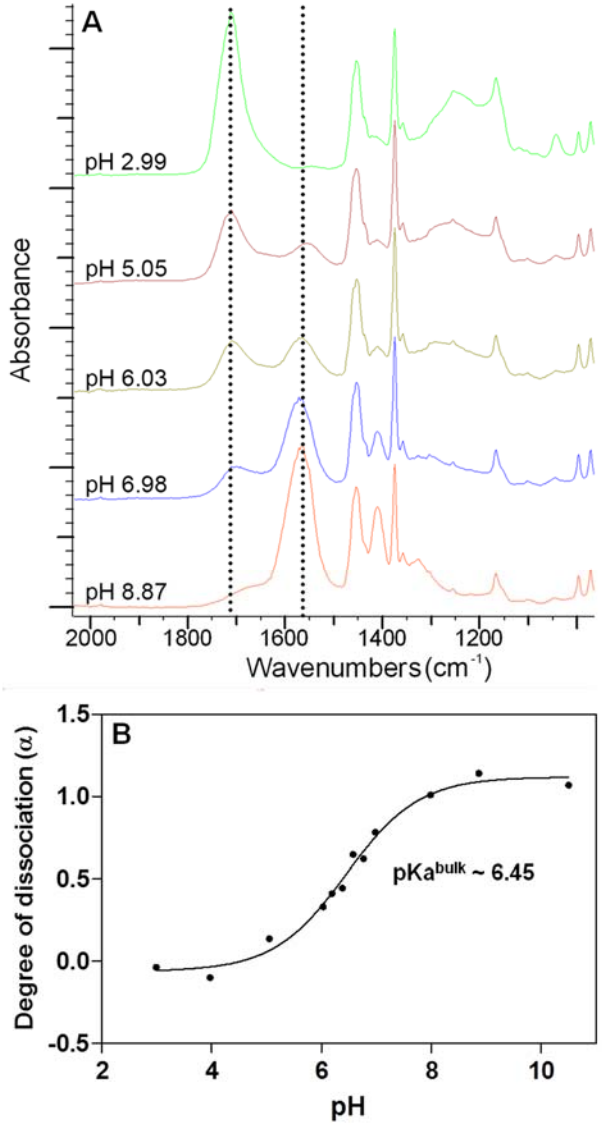

Figure 4.1. (a) ATR-FTIR spectra of PP-*g*-PAA treated with buffer solutions of varying pH. Protonated and deprotonated IR bands are marked at 1710 and 1566 cm^{-1}, respectively. (b) FTIR titration curve for PP-*g*-PAA. The pKa_{bulk} calculated at the midpoint of the titration curve is 6.45.

FTIR spectroscopy investigations on the dissociation behavior of hydroxamate-containing compounds in solution have demonstrated that deprotonation of hydroxamic acids most notably results in a downshift of the C=O absorbance band that is likely attributed to the weakened C=O bond strength of deprotonated hydroxamic acids due to the delocalization of π electrons to C-N and N-O bonds.[101-103] Therefore, for this study, deprotonation of the hydroxyl group of poly(hydroxamic acid) brushes grafted from PP was monitored by quantifying the shift in the C=O absorbance band from ~1650 (protonated) to ~1612 cm^{-1} (deprotonated) as dependent on pH (**Figure 4.2a**).The shift of the C=O absorbance band as a function of solution pH was fitted to a sigmoid function to generate a titration curve from which the pKa^{bulk} could be estimated (**Figure 4.2b**). As with PP-*g*-PAA, the pKa^{bulk} was defined as the solution pH value corresponding to the midpoint of the titration curve. The pKa^{bulk} of poly(hydroxamic acid) brushes grafted from PP estimated from the titration curve, 9.65, was in the range for pKa of hydroxamic acids in solution. Deferoxamine B, a chelator that contains three hydroxamate ligands, has three pKa's ranging from 8.35 to 9.71.[106] Unlike PAA brushes, the pKa^{bulk} of hydroxamate ligands of PHA brushes was not strongly affected by attachment to a solid support. It is hypothesized that since hydroxamate ligands are much weaker acids than carboxylates, as indicated by their high pKa values, electrostatic interactions between grafted PHA chains may not be strong enough to have a significant effect on the charge distribution of the microenvironment close to the surface. Therefore, the PHA grafted layer, especially closer to the surface, may not greatly influence local pH as was suggested in the case with carboxylate ligands. However, further investigations on the effect of polyelectrolyte acidity on pKa shifts caused by solid support attachment are necessary to confirm the proposed

hypothesis. For the case of surface-grafted PHA, the reduced impact of the surface microenvironment on the dissociation behavior of hydroxamate ligands as well as the specificity of its reactivity with certain metals, such as iron, may be useful for broadening the working pH range of stimuli-responsive surface applications.

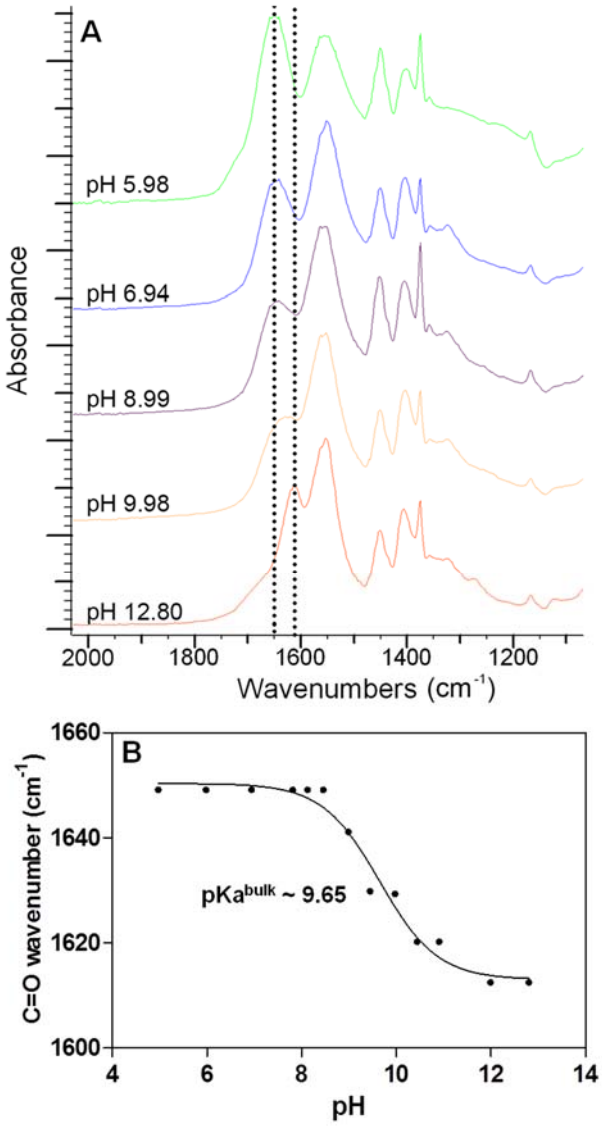

Figure 4.2. (a)ATR-FTIR spectra of PP-*g*-PHA treated with buffer solutions of varying pH. Absorbance band C=O shift caused by deprotonation, from 1649 and 1612 cm^{-1}, is marked. (b) FTIR titration curve for PP-*g*-PHA. The pKa_{bulk} calculated at the midpoint of the titration curve is 9.65.

Previous studies of metal chelation by polyelectrolyte brushes with carboxylate binding groups have demonstrated that the nature of the coordination complex influences

the wavelength at which the binding groups absorb.[100, 105] The two primary coordination complexes observed from carboxylate ligands are bridging bidentate and the chelating bidentate (**Figure 4.3b**). The C=O absorbance bands of bridging bidentate and chelating complexes have been previously observed at 1610 and 1552 cm^{-1}, respectively, for PMAA brushes.[100] Figure 4.3a shows the FTIR spectra of high and low brush density PP-*g*-PAA before and after iron chelation. A low graft density brush was synthesized by adjusting the parameters for attachment of the photoinitiator (see **4.3.2**). The FTIR spectra of the high and low brush density PP-*g*-PAA before chelation show C=O absorbance bands were present at 1710 cm^{-1}, the characteristic absorbance band for protonated carboxylate groups. After iron chelation at pH 5, the intensity of the absorbance band at 1710 cm^{-1} decreased and new bands were present at 1589 and 1547 cm^{-1}. It was hypothesized that these new bands corresponded to the bridging bidentate and chelating bidentate, respectively. Futhermore, the relative intensity of these absorbance bands may be indicative of which chelating coordination complex was favored under the given conditions. At low brush density, the absorbance band at 1589 cm^{-1} had a higher intensity than the absorbance band at 1547 cm^{-1}, which suggested that the bridging bidentate was favored. At high brush density, the absorbance band at 1589 cm^{-1} had a similar intensity as the absorbance band at 1547 cm^{-1}, which suggested that both bridging bidentate and chelating bidentate were equally favored. The lower brush density graft may have allowed for improved chain flexibility by minimizing cross-linking reactions during surface-initiated polymerization that allowed for more bridging bidentate coordination complexes.[64] Although the chelating and bridging complexes are both bidentate structures, the bridging complex may be thermodynamically favorable through additional stabilization that results from interaction

between metals in the complex. Konradi et al.[100] analyzed FTIR spectra of PMAA brushes of varying graft densities after incubation with 0.1M solutions of $Ca(NO_3)_2$, $Cu(NO_3)_2$, or $Al(NO^3)_3$ and noted that complex geometries can be influenced by brush density as well as the chelated metal ion. In order to corroborate the proposed hypothesis on the relationship between poly(acrylic acid) brush density and ferric iron coordination complex geometry, the study of coordination complex as a function of graft density may be the subject of future work. Additionally, a new absorbance band was observed at 631 cm^{-1} after the chelation of iron that was attributed to Fe-O stretching vibrations based on previous analysis of IR spectra of iron oxides.[107]

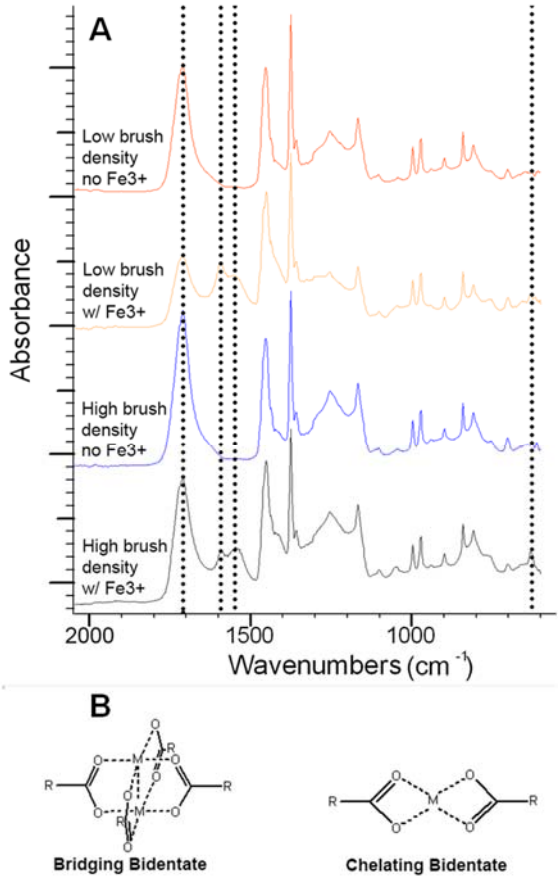

Figure 4.3. (a) ATR-FTIR spectra of PP-*g*-PAA before and after iron chelation performed at pH 5 at low and high brush density. Marked absorbance peaks were affected by iron chelation. Absorbance bands at 1589 and 1547 cm-1 correspond to bridging bidentate and chelating bidentate coordination complexes, respectively. (b) Known coordination complexes for carboxylate and metal ions.

Changes in the FTIR spectra of PHA grafted from PP before and after chelation resembled those observed in PP-*g*-PAA (**Figure 4.4a**). As with PP-*g*-PAA, an Fe-O absorbance band was observed at 631 cm^{-1} after chelation. The C-NH absorbance band split to 1587 and 1531 cm^{-1}. In addition, the C=O absorbance band split to 1720 and 1678 cm^{-1}, N-O absorbance band shifted to 1049 cm^{-1}, and a C-NH absorbance band shifted to 1207 cm^{-1}. FTIR spectra of deferoxamine B, a solution-based analog of poly(hydroxamic acid), have exhibited shifts of C=O and N-H absorbance bands after iron chelation and these band shifts were attributed to the formation of a chelating tridentate coordination complex (**Figure 4.4b**).[101, 108] The FTIR spectra collected in this study exhibited a combined shifting and splitting of the C=O and C-NH absorbances into two bands. Based on similarities between the absorbance band splitting observed in the FTIR spectra of PP-*g*-PAA and PP-*g*-PHA, it is suggested that after chelation of ferric iron at pH 5, two coordination complexes of the hydroxamate ligands may be present when PHA brushes chelate iron due to the steric restrictions of surface-grafted PHA. Further studies that examine the effect of graft density on the intensity of these bands could possibly clarify these findings.

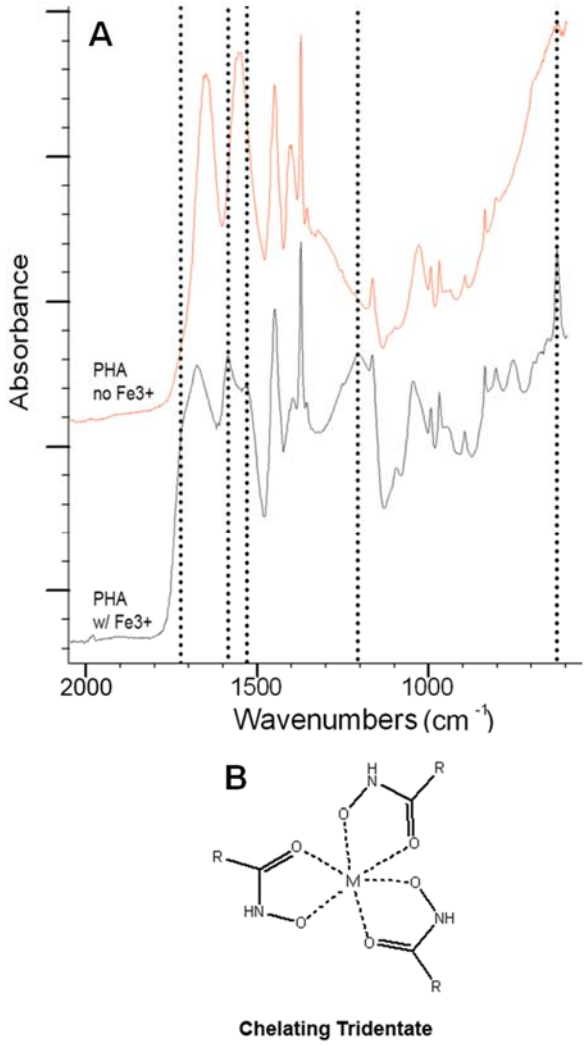

Figure 4.4. (a) ATR-FTIR spectra of PP-*g*-PHA before and after iron chelation performed at pH 5. Marked absorbance bands were affected by iron chelation.(b) Known coordination complex of hydroxamate and metal ions.

4.5 Conclusions

In summary, dissociation and metal chelating behavior of surface-grafted PAA and PHA brushes were characterized by simple and rapid FTIR-based analysis that directly monitored changes in absorbance bands of carboxylate and hydroxamate ligands responsible for metal chelation. This investigation of polyelectrolyte brushes has demonstrated the underlying importance of the steric restrictions of surface-grafted polyelectrolytes on electrostatic interactions that dictate local pH at the surface and its

impact on pKa^{bulk} as a function of solution pH. The effect of steric restrictions on the microenvironment within a grafted layer may be influenced by the chemical nature of the ionizable ligands as a weaker acid, poly(hydroxamic acid), did not exhibit significant differences between pKa^{bulk} and pKa of solution-based analogs as observed for poly(acrylic acid). Additional research to create a more complete understanding of the effect of pH, salt concentration and metal chelation on the dissociation behavior of surface-grafted polyelectrolytes may be useful in optimizing of the applications of these stimuli-responsive materials.

CHAPTER 5

PERFORMANCE OF NON-MIGRATORY IRON CHELATING ACTIVE PACKAGING MATERIALS IN VISCOUS MODEL FOOD SYSTEMS[4]

5.1 Abstract

Many packaged food products undergo quality deterioration due to iron promoted oxidative reactions. Recently, we have developed a non-migratory iron chelating active packaging material that represents a novel approach to inhibit oxidation of foods while addressing consumer demands for 'clean' labels. A challenge to the field of non-migratory active packaging is ensuring that surface-immobilized active agents retain activity in a true food system despite diffusional limitations. Yet, the relationship between food viscosity and non-migratory active packaging activity retention has never been characterized. The objective of this study was to investigate the influence of food viscosity on iron chelation by a non-migratory iron chelating active packaging material. Methyl cellulose was added to aqueous buffered iron solutions to yield model systems with viscosities ranging from ~1 to ~10^5 mPa·s, representing viscosities ranging from beverage to mayonnaise. Iron chelation was quantified by material-bound iron content using colorimetry and inductively coupled plasma-optical emission spectrometry (ICP-OES). Maximum iron chelation was reached in solutions up to viscosity ~10^2 mPa·s. In more viscous solutions (up to ~10^4 mPa·s), there was a significant decrease in iron chelating activity ($p<0.05$). However, materials still retained at least 76% iron chelating activity. Additionally, the effect of different food hydrocolloids on the performance of non-migratory iron chelating active

[4] The contents of this chapter have been published: Roman, M. J.; Decker, E. A.; Goddard, J. M. Performance of non-migratory iron chelating active packaging materials in viscous model food systems. *Journal of Food Science* **2015**, *80(9)*, E1965-E1973.

packaging was assessed. Methyl cellulose and carrageenan did not compete with the material for specific iron chelation ($p>0.05$). Materials retained 32-45% chelating activity when in contact with competitively chelating hydrocolloids guar gum, locust bean gum, and xanthan gum. This work demonstrates the potential application of non-migratory iron chelating active packaging in liquid and semi-liquid foods to allow for the removal of synthetic chelators, while maintaining food quality.

5.2 Introduction

Many food products undergo quality deterioration during transport and storage due to oxidative reactions that cause rancid off-flavors, nutrient loss and discoloration. In an effort to increase shelf life, it is common practice in the food industry to include synthetic additives, such as butylated hydroxytoluene (BHT) and ethylenediaminetetraacetic acid (EDTA), in food products. Consumer demand for packaged food products without synthetic additives has prompted growing interest in alternative preservation methods. Antioxidant active packaging is a promising alternate approach to protect foods against oxidative degradation. Several research groups have demonstrated the efficacy of active packaging materials with antioxidants incorporated by coating, extrusion, or covalent immobilization.[29, 30, 109] Garces, et al. [110] patented an antioxidant coating containing rosemary extract that improved the stability of fresh beef against discoloration and lipid oxidation.[111] Lopez de Dicastillo, et al. [112] developed an ethylene vinyl alcohol film containing green tea extract prepared by extrusion that demonstrated antioxidant activity in a variety of food simulants (i.e. aqueous, acid, alcoholic, fatty food). Arrua, et al. [113] showed that covalent immobilization of caffeic acid on the surface of polypropylene inhibited ascorbic acid degradation in orange juice. Whereas antioxidants of active

packaging materials prepared by coating or extrusion may migrate into liquid or semi-liquid foods during transport and storage, covalent immobilization ensures development of a non-migratory active packaging for these food types. Non-migratory active packaging presents a potential regulatory advantage, as it may be classified as a 'food contact material' rather than a 'direct additive.'[37]

Our research group has developed non-migratory iron chelating active packaging that is synthesized by polymerization of metal chelating ligands from the surface of packaging materials.[43, 76, 85] This active packaging functions by removing iron from a food to inhibit its reactivity. Trace amounts of transition metals, especially iron, are ubiquitous in the food processing environment (e.g. water, equipment) and promote the decomposition of lipid hydroperoxides to form free radicals that propagate oxidative reactions that accelerate food degradation.[6, 7] Potent iron chelators, such as EDTA, have demonstrated high efficacy in inhibiting metal-promoted oxidation in food emulsions.[15-17] The most recent generation of non-migratory iron chelating active packaging is a polypropylene film from which poly(hydroxamic acid) has been grafted (PP-*g*-PHA).[85] Hydroxamate-type chelators have high specificity for iron (e.g. deferoxamine B binding constant for ferric iron is 30.4) and maintain activity over a wide range of pH values.[114] Tian, et al. [44] observed that PP-*g*-PHA iron chelating active packaging materials prevented the formation of volatile oxidation products in model food emulsions at pH 3.0, even exceeding the antioxidant activity of EDTA. As trace metals, especially iron, are the primary pro-oxidant in food emulsions,[6] such non-migratory metal chelating active packaging would have application in liquid and semi-liquid food emulsions such as beverages, sauces, salad

dressings, and mayonnaise that are not a major source of nutritional iron, but for which trace iron influences oxidative degradation.

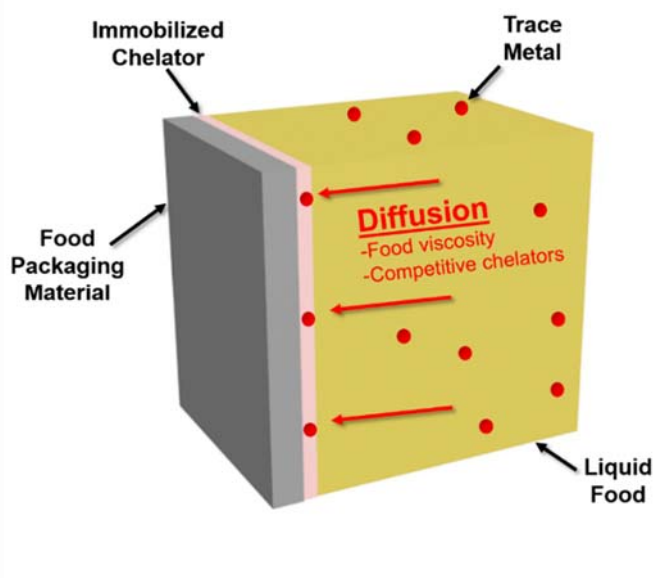

Figure 5.1. Schematic of non-migratory metal chelating active packaging materials in contact with a liquid food. Performance of such material is dependent on trace metal diffusion through food matrix.

The performance of such non-migratory active packaging material relies on the retained activity of the chelator following grafting to the packaging material surface, which is influenced by the diffusion behavior of iron through a food matrix to the packaging surface, where the chelator is immobilized (**Figure 5.1**). Diffusion behavior of small molecules through a food matrix has been extensively researched as it relates to flavor release.[115-120] Key studies have identified that such diffusion behavior is influenced primarily by viscosity and specific binding of small molecules by food matrix constituents (e.g. proteins, hydrocolloids). Complex liquid and semi-liquid food matrices may have a wide range of viscosities (**Table 5.1**). Although it is presumed that increasing viscosity of a liquid food will decrease the rate of diffusion from the food matrix to a non-migratory active packaging material, the relationship between food matrix viscosity and non-migratory active packaging activity retention has never been characterized. The objective

of this study was to investigate the influence of food matrix viscosity on iron chelation by non-migratory iron chelating active packaging material. Iron chelation was characterized by quantifying material-bound iron content of active packaging materials using colorimetry and inductively coupled plasma-optical emission spectrometry (ICP-OES). Additionally, the influence of hydrocolloid chemistry on the performance of non-migratory iron chelating active packaging was demonstrated.

Table 5.1. Approximate viscosities of typical liquid and semi-liquid food systems.

Food Product	Temperature	Shear rate (s^{-1})	Apparent Viscosity (mPa·s)	Reference
Raw Milk	20°C	Newtonian Fluid	84	Daubert and Foegeding [121]
Enchilada Sauce	24°C	5-40	1,960-480	Briggs and Steffe [122]
Catalina Salad Dressing	24°C	5-40	4,220-770	Briggs and Steffe [122]
Tomato Catsup	20°C	2.09-134.04	10,980-520	Daubert and Foegeding [121]
Mayonnaise	25°C	10-100	12,410-1,499	Maruyama, et al. [123]

5.3 Materials and Methods

5.3.1 Materials

Polypropylene (PP, isotactic, pellets) was purchased from Scientific Polymer Products (Ontario, NY); isopropanol, acetone, heptane, methanol, sodium acetate trihydrate, ferric chloride hexahydrate, hydrochloric acid, nitric acid (trace metal grade), and sodium hydroxide were purchased from Fisher Scientific (Fair Lawn, NJ); hydroxylamine hydrochloride and imidazole (99%) were purchased from Acros Organics (Morris Plains, NJ); benzophenone (BP, 99%) and methyl acrylate (MA, 99%) were purchased from Sigma-Aldrich (St. Louis, MO); all chemicals and solvents were used

without further purification. Methylcellulose (TICACEL HV Powder), guar gum (TIC Pretested Gum Guar 8/22 Powder), carrageenan (Ticaloid 780 Stabilizer), locust bean gum (TIC Pretested Locust Bean Por/A2), and xanthan gum (Pre-Hydrated Ticaxan Rapid-3) were kindly donated by TIC Gums (White Marsh, MD). All hydrocolloids were dissolved completely according to manufacturer's recommendations and were kept overnight in order to ensure full hydration.

5.3.2 Preparation of Iron Chelating Active Packaging Material

Iron chelating active packaging material was synthesized via photoinitiated graft polymerization of methyl acrylate onto polypropylene (PP) and conversion of grafted poly(methyl acrylate) (PMA) to poly(hydroxamic acid) (PHA) using a method previously reported by Tian, et al. [85]. A two-step grafting process was used to introduce PMA to the surface of PP films. In the first step, the photoinitiator benzophenone (BP; 5 wt% in heptane) was spin coated and then covalently grafted to the PP surface by exposure to ultraviolet (UV) irradiation (Dymax, Model 5000 flood, 320-395 nm, 200 mW/cm^2, Dymax Corporation, Torrington, CT) for 90 s under nitrogen. In the second step, the BP-functionalized PP (PP-BP) were submerged in methyl acrylate (70 wt% in acetone) and exposed to UV irradiation for 3 min under nitrogen. Soxhlet extraction (150 ml acetone under reflux for12 h) was used to remove any residual monomer and homopolymer from the surface of PMA-grafted PP (PP-*g*-PMA). Ester groups on the surface of PP-*g*-PMA were converted to hydroxamic acids by reaction with hydroxylamine. PP-*g*-PMA films were reacted with hydroxylamine solution (1.37M in methanol/water (4:1), pH 13) under reflux at 73 ºC for 4 h with stirring. After reaction, materials were rinsed in methanol/water (5:1), treated with hydrochloric acid solution (0.2M in methanol/water (5:1)), rinsed

methanol/water (5:1), and washed in deionized water. PHA grafted PP (PP-*g*-PHA) iron chelating active packaging materials were stored in a desiccator (25 ºC, 15% RH) until use.

5.3.3 Attenuated total reflectance/ Fourier transform infrared spectroscopy (ATR-FTIR)

Attenuated total reflectance Fourier transform infrared spectroscopy (ATR-FTIR) was used to confirm the grafting of iron chelating hydroxamate ligands on the surface of PP-*g*-PHA. An IRPrestige FTIR Spectrometer (Shimadzu Scientific Instruments, Inc., Kyoto, Japan) with a diamond ATR crystal was used to measure the spectrum. Each spectrum was collected under the following parameters: Happ-Genzel function, 32 scans, and 4 cm^{-1} resolution. Spectrum analysis was performed on KnowItAll(R) Informatics System 9.5 (Bio-Rad Laboratories, Inc., Informatics Division, Philadelphia, PA) and Sigma Plot 12 (Systat Software, Inc., San Jose, CA). All spectra presented are representative of three spectra taken at various points on each of three independently prepared materials.

5.3.4 Rheological Properties

The apparent shear viscosity of all aqueous buffered iron solutions thickened with food hydrocolloids was measured using a dynamic shear rheometer (Kinexus Rheometer, Malvern Instruments Ltd., MA, U.S.A.) with a cup-and-bob measurement cell. All measurements were performed using shear rates from 0.1 to 100 s^{-1} at 25 °C. Rheological measurements were collected using instrument software (Kinexus rSpace, version 1.30, Malvern Instruments Ltd., MA). The apparent shear viscosity data are reported at 10 s^{-1}, the approximate shear rate of the iron chelating assay (180 rpm) estimated by computational fluid dynamics.[124] The approximate shear rate of the iron chelating assay

(10 s^{-1}) was selected to be similar to that experienced by a food product during shipping (estimated to peak at 4 s^{-1} (Hz) for truck shipments and between 12-16 Hz for rail shipments).[125]

5.3.5 Iron Chelating Assay of Active Packaging Material

The influence of food matrix viscosity on iron chelating activity of PP-*g*-PHA iron chelating active packaging materials was determined by performing an iron chelation assay in model iron solutions. Briefly, materials (native PP or PP-*g*-PHA, 1 x 2 cm^2) were submerged in aqueous buffered iron solution (10 g of 0.08 mM ferric chloride in 50 mM sodium acetate/imidazole buffer, pH 5.0) of varying viscosity (0, 0.25, 0.5%, 1%, 2%, or 4% methyl cellulose) for up to 7 d to enable iron chelation by PP-*g*-PHA materials. The assay was conducted in the dark (to minimize precipitation of ferric iron) with shaking at 180 rpm at room temperature. At selected time points (12 h, 1 d, 2 d, 3 d, 5 d, and 7 d), the materials were removed from the aqueous buffered iron solution, washed with deionized water, and then dried in a desiccator for at least 24 h at room temperature until further analysis.

Additional experiments were conducted to compare activity of PP-*g*-PHA iron chelating materials in the presence of different food hydrocolloids. Preliminary test were used to determine the concentration of each food hydrocolloids necessary to match the viscosity of 1% methyl cellulose. Materials (native PP or PP-*g*-PHA, 1 x 2 cm^2) were reacted in ferric iron solution (10 g of 0.08 mM ferric chloride in 50 mM sodium acetate/imidazole buffer, pH 5.0) containing either methyl cellulose (1%), guar (0.5%), locust bean (0.5%), xanthan (0.3%), or carrageenan (1%) for 7 d, rinsed in deionized water and then dried in a desiccator for at least 24 h at room temperature.

Upon iron chelation, PP-*g*-PHA iron chelating active packaging materials develop a characteristic reddish-brown color due to the PHA/Fe^{3+} complex. Change in color of PP-*g*-PHA material was used to monitor iron chelation kinetics. A Hunter colorimeter (ColorFlez EZ, HunterLab, Reston, VA) was used to quantify material color by color coordinates (L^*, a^*, and b^*). L^* value is a measure of the lightness, and its value ranges from 0 to 100, corresponding to pure black to pure white. a^* refers to the color change from green to red, when its value changes from negative to positive. b^* value is a measure of the color from blue to yellow when it changes from negative to positive. Color difference (ΔE^*) of the material before (L_0^*, a_0^*, and b_0^*) and after chelating ferric iron (L_t^*, a_t^*, and b_t^*) was calculated using the following equation:

$$\Delta E^* = [(L_0^* - L_t^*)^2 + (a_0^* - a_t^*)^2 + (b_0^* - b_t^*)^2]^{1/2} \quad (1)$$

Additionally, selected treatments of PP and PP-*g*-PHA materials were analyzed for iron chelating activity by microwave acid digestion followed by quantification via inductively coupled plasma-optical emission spectroscopy (ICP-OES). Treatments were chosen as the first ΔE^* value that were not statistically different from the ΔE^* value at the next time point in the range of the plateau, except for native PP and high viscosity PP-*g*-PHA (2% MC and 4% MC) materials which did not achieve PP-*g*-PHA maximum color change capacity, therefore the last time point (7 d) was chosen. PP material samples were prepared for ICP-OES analysis using a standard method for analysis of lead in non-metal children's products.[126] Approximately 150 mg of the PP material (1 x 2 cm^2 pieces) were weighed directly into microwave digestion vessels (Mars Xpress 75 ml vessels, CEM, Matthews, NC) and nitric acid (5 ml) was added to each vessel. Calibration standards were prepared with iron solution (1,000 ppm Iron ICP-MS Standard, Ricca Chemical Company,

Arlington, TX) and clean PP. The microwave acid digestion was conducted in the Mars Xpress (CEM, Matthews, NC) and is as follows: ramp to 210°C for 20 min, hold at 210°C for 10 min, and cool for 10 min. Digested samples were transferred to 50 ml centrifuge tubes, diluted with deionized water, and held at 4°C until analysis. ICP-OES analysis was conducted on a Perkin Elmer Optima 4300 DV (Waltham, MA).

5.3.6 Statistical Analysis

All measurements were conducted in quadruplicate. Data are representative of at least two independent experiments. Non-linear regressions and one-way ANOVA ($p<0.05$) were calculated using GraphPad Prism 6.0 (La Jolla, CA).

5.4 Results and Discussion

5.4.1 Characterization of Iron Chelating Active Packaging Material

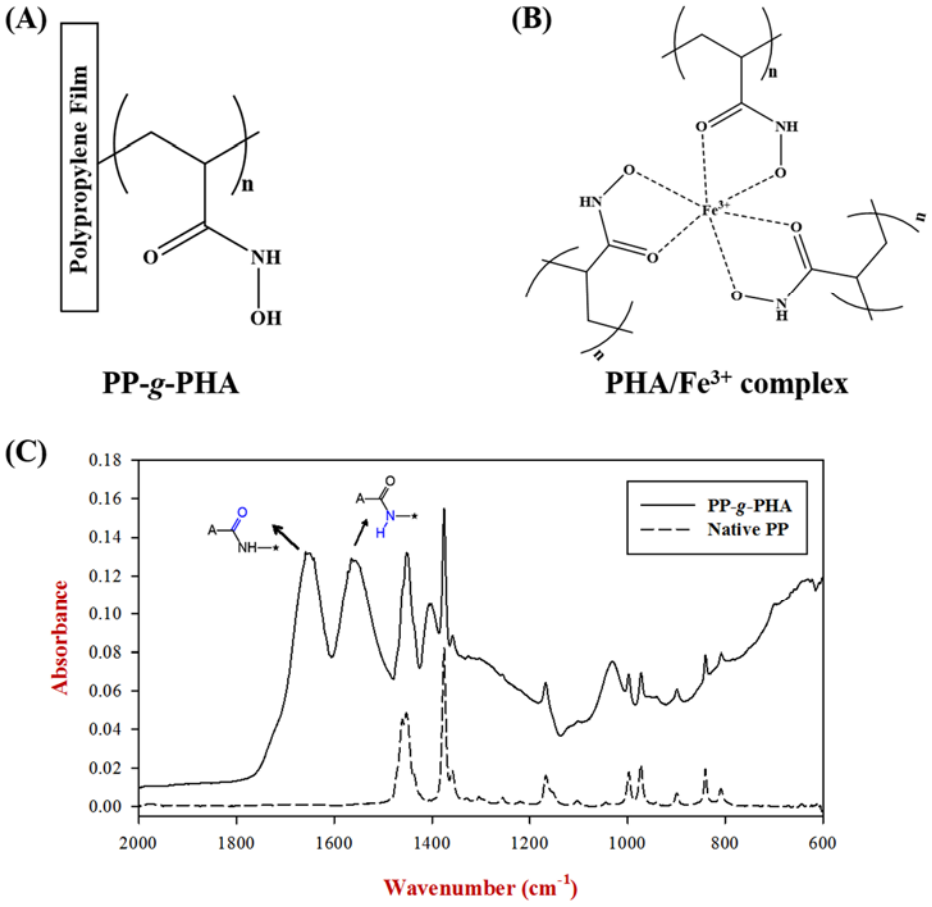

Figure 5.2. (A) Surface chemistry of non-migratory chelating packaging material and (B) theoretical tridentate binding of ferric iron by PHA as adapted from Tian, et al. [85] and (C) ATR-FTIR spectra of native PP and PP-*g*-PHA chelating packaging materials.

Photoinitiated graft polymerization represents a scalable method for covalent immobilization of active polymers that can be applied to a variety of surfaces and adapted to a continuous process.[39] Iron chelating active packaging materials synthesized for this study were prepared by photoinitiated graft polymerization of methyl acrylate from the surface of polypropylene (PP) materials and then subsequent conversion of poly(methyl acrylate) to poly(hydroxamic acid) (PHA), imparting hydroxamate-based metal chelating activity (**Figure 5.2**). The proposed hydroxamate-functionalized antioxidant active

packaging material uses low cost, widely available and highly stable polymers. The pKa of surface-grafted PHA was previously measured to be ~9.65, which indicates that the material may have a low effective charge in complex food systems that may have numerous charged ingredients.[77] Optimum iron chelation by PP-*g*-PHA iron chelating materials was demonstrated at pH 5.0.[85] The theoretical ligand (hydroxamic acid) to metal (ferric iron) binding ratio is 3 to 1 (**Figure 5.2b**). Hydroxamic acid content of the film may be estimated as up to 3 times the material-bound iron content in pH 5 buffer (~274 nmol cm^{-2}). The surface chemistry of native PP and PP-*g*-PHA iron chelating materials was confirmed by ATR-FTIR spectroscopy (**Figure 5.2c**). Unlike native PP material, PP-*g*-PHA exhibited spectral bands at 1649 cm^{-1} and 1554 cm^{-1}, corresponding to C=O and C-NH bonds of the grafted hydroxamic acid groups, respectively. This IR spectrum confirmed successful grafting of PHA from the surface of PP.

5.4.2 Influence of Food Matrix Viscosity on Iron Chelating Kinetics of Active Packaging Material

In order to characterize the influence of viscosity on the iron chelating kinetics of PP-*g*-PHA chelating active packaging materials, a common food hydrocolloid, methyl cellulose, was used to thicken an aqueous buffered iron solution (0.08 mM ferric chloride in 50 mM sodium acetate/imidazole buffer, pH 5.0). Methyl cellulose was chosen as the thickening agent because it is non-ionic and is not reported to have affinity for ferric iron,[127] as confirmed by preliminary experiments. It is important to note that for the purposes of this study, we sought to create simple models in which viscosity would be the only independent variable, and therefore the models do not fully reflect the complexity of real food systems. Methyl cellulose was added to aqueous buffered iron solutions at the

following concentrations: 0.25%, 0.5%, 1%, 2%, and 4%. All aqueous buffered iron solutions exhibited a shear thinning flow behavior (**Figure 5.3a**), which is the common flow behavior for liquid and semi-liquid food emulsion products.[128] The apparent viscosity of the iron solutions evaluated ranged from ~1 to ~10^5 mPa·s, which is comparable to example liquid and semi-liquid food viscosities listed in **Table 5.1**. Doubling the concentration of methyl cellulose in the aqueous buffered iron solution yielded approximately 1 log increase in viscosity (**Figure 5.3b**). Aqueous buffered iron solutions thickened with varying concentrations of methyl cellulose were used as viscous model food systems to characterize the influence of viscosity on the iron chelating kinetics of PP-*g*-PHA chelating active packaging materials.

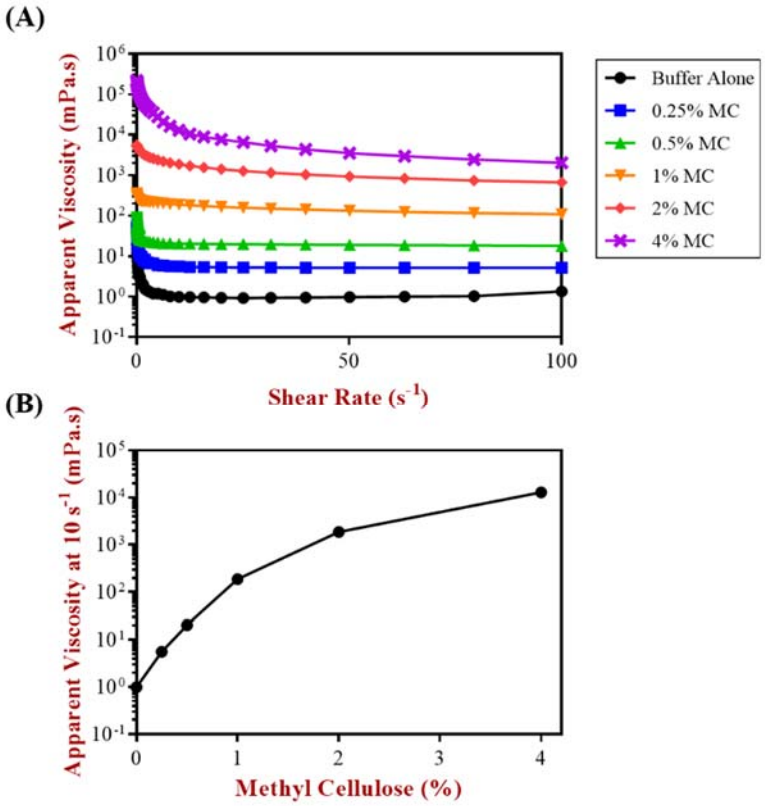

Figure 5. 3. (A) Flow profile and (B) apparent viscosity at 10 s^{-1} of aqueous buffered iron solutions (0.08 mM ferric iron in 50 mM sodium acetate/imidazole buffer, pH 5) thickened with methyl cellulose (MC). Error bars represent standard deviation (n=4) and are smaller than data points.

Hydroxamate chelation of ferric iron in an aqueous solution produces a characteristic red color complex that was first reported by Hestrin [129]. We have previously demonstrated that PP-*g*-PHA chelating active packaging materials develop such reddish-brown color upon chelation of ferric iron due to the formation of a PHA/Fe^{3+} complex.[85] The color change of PP-*g*-PHA iron chelating materials can therefore be quantified using colorimetry and correlated with iron chelating activity as characterized by ICP spectroscopy (**Figure 5.4**). Such correlation between iron chelating activity and PP-*g*-PHA color change was previously demonstrated in other work by our group.[130] For this study, color difference (ΔE^*) of PP-*g*-PHA iron chelating material before and after iron chelation was used to monitor iron chelating kinetics in aqueous buffered iron solutions of different viscosities during a 7 d storage study (**Figure 5.5a**). PP materials served as a control for this experiment and did not demonstrate significant color change during the course of the storage study, which indicates any iron precipitation that occurred during the course of the storage study did not significantly affect color change caused by hydroxamate-specific iron chelation. Furthermore, control PP materials incubated for 7 d in aqueous buffered iron solutions presented negligible iron content that was below the limit of detection of ICP-OES (< 2.80 nmol/cm^2 iron). The reddish-brown color of the PP-*g*-PHA iron chelating materials increased in intensity over the course of the storage study, at a rate dependent on the methyl cellulose content of the aqueous buffered iron solution. An example of the observed color change over time for the 1% methyl cellulose treatment is shown in **Figure 5.5b**. PP-*g*-PHA iron chelating active packaging materials incubated in aqueous buffered iron solutions with increasing methyl cellulose content (and increasing viscosity) exhibited a more gradual color change over time.

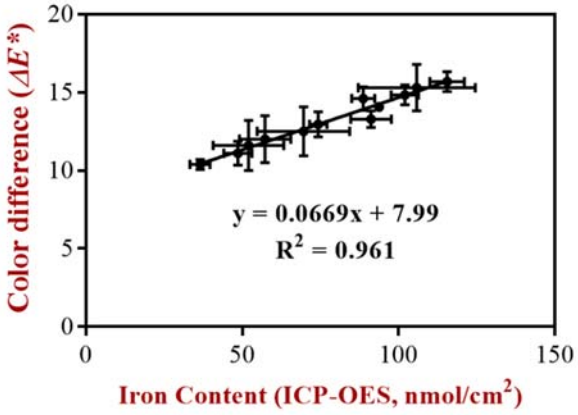

Figure 5.4. Correlation between color difference (*ΔE**) measured by colorimetry and iron content measured by ICP-OES of PP-*g*-PHA chelating packaging materials. Data represents iron chelating materials incubated under varying experimental conditions (ie: incubation time, viscosity, hydrocolloid chemistry). Error bars represent standard deviation (n=4).

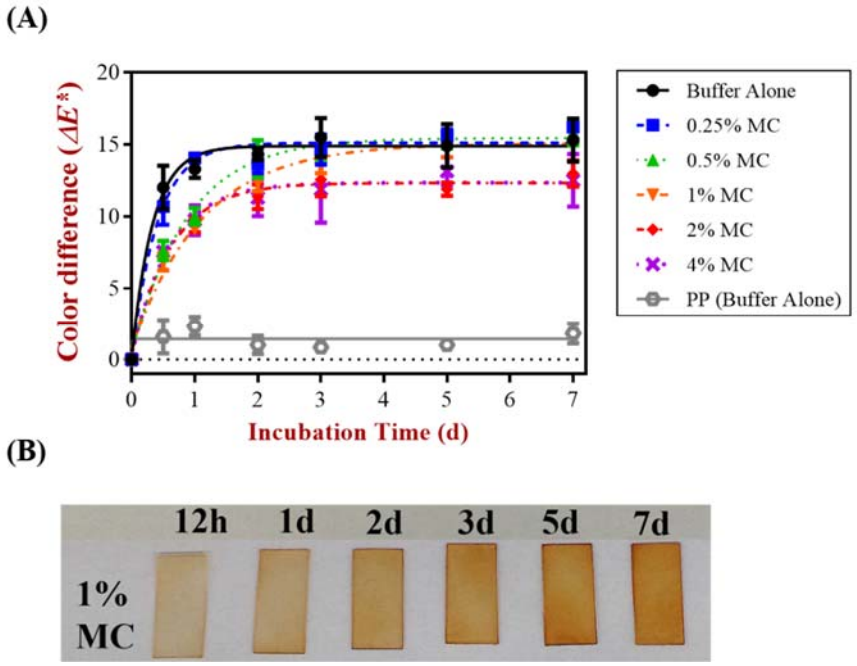

Figure 5.5. (A) Color change of PP-*g*-PHA chelating packaging material and control PP incubated in aqueous buffered iron solutions (0.08 mM ferric iron in 50 mM sodium acetate/imidazole buffer, pH 5) thickened with methyl cellulose (MC) and (B) PP-*g*-PHA chelating packaging material after incubation in iron solution modified with 1% methyl cellulose. Error bars represent standard deviation (n=4) and, in some instances, are smaller than data points.

To compare PP-*g*-PHA iron chelation kinetics as a function of food viscosity, data for each treatment were fitted to a one-phase association exponential model (**Figure 5.5a**):

$$\Delta E^* = (\Delta E^*_{max})(1-e^{-kt}) \quad (2)$$

where ΔE^* is the change in color, ΔE^*_{max} is the maximum color change achieved during the storage study, k is the color change rate constant (d^{-1}), and t is the incubation time (d). The measured data fit the one-phase association exponential model well (R^2>0.920), and calculated parameters are reported in **Table 5.2**. PHA iron chelating materials incubated in all of the aqueous buffered iron solutions demonstrated a color change half-time of less than 1 d, suggesting that these metal chelating active packaging materials would perform at a commercially relevant rate, even at increasing viscosities. A maximum color change of ΔE^*_{max} >14.9 was reached during the 7 d storage study for materials incubated in iron solutions with methyl cellulose concentrations of 0 to 1% (viscosity range ~1 to ~10^2 mPa·s). A semi-log correlation was observed between viscosity and color change rate constants for materials incubated under these viscosity conditions (R^2=0.875), suggesting that viscosity has a similar correlation with iron diffusion rate through model food systems. Materials incubated in iron solutions with methyl cellulose concentrations of 2% and 4% (viscosity ~10^3 and~10^4 mPa·s) reached a plateau in color change below the maximum material color change capacity (ΔE^*_{max} =12.3), indicating inhibition of iron chelation under these viscosity conditions. ICP-OES was performed on select samples from each viscosity treatment after having reached ΔE^*_{max} for direct characterization of material-bound iron content (**Table 5.3**). Results from ICP-OES supported those obtained via colorimetry. ICP-OES characterized iron chelating activity of PP-*g*-PHA chelating materials that reached the material maximum color change capacity (ΔE^*_{max}) ranged from 88.7-102 nmol/cm^2 iron (values found not to be statistically different) when incubated in iron solutions of methyl cellulose concentrations at or below

1%. At higher methyl cellulose concentrations (2% and 4%), there was a statistically significant drop in iron chelating capacity. Nevertheless, ICP-OES characterization demonstrated that even at high viscosities, at least 76% iron chelating capacity can be achieved within 2-3 days.

Table 5.2. One-phase association model parameters for iron chelating kinetics (measured via colorimetry) of chelating packaging materials incubated in aqueous buffered iron solutions thickened with methyl cellulose (MC). ΔE^*_{max} is the maximum material color change achieved during the storage study, k is the material color change rate constant (d^{-1}), and half-time is the incubation time (d) required for the material to achieve 50% of its maximum chelating capacity. Values represent means ± standard deviation (n=4). Significant differences are denoted with letters ($p<0.05$).

Model Parameters	Buffer alone	0.25% MC	0.5% MC	1% MC	2% MC	4% MC
ΔE^*_{max}	14.9 ± 0.28^a	15.1 ± 0.25^a	15.4 ± 0.26^a	15.0 ± 0.25^a	12.3 ± 0.22^b	12.3 ± 0.35^b
k	3.03 ± 0.36	2.46 ± 0.22	1.18 ± 0.075	0.983 ± 0.060	1.64 ± 0.13	1.69 ± 0.22
Half-life	0.229	0.282	0.590	0.705	0.424	0.411
R^2	0.955	0.968	0.977	0.979	0.967	0.920

Table 5.3. Iron content (nmol cm^{-2}) of chelating packaging materials as characterized by ICP-OES at maximum chelating capacity (ΔE^*_{max}). Values represent means ± standard deviation (n=4). Significant differences are denoted with letters ($p<0.05$).

Aqueous Buffered Iron Solution	Material Iron Content at ΔE^*_{max} (nmol cm^{-2})
Buffer alone	91.2 ± 6.5^a
0.25% MC	93.8 ± 0.4^a
0.5% MC	88.7 ± 3.7^a
1% MC	102 ± 4.4^a
2% MC	74.3 ± 2.8^b
4% MC	69.6 ± 15^b

At the methyl cellulose concentrations necessary to create high viscosity model food systems (2 and 4%), there are large fractions of methyl cellulose polymer chains in suspension that may result in significant chain overlap. The observed decrease in the activity of iron chelating materials incubated in high viscosity solutions (viscosity ~10^3 and~10^4 mPa.s) may be due to (1) iron diffusion limitations at high viscosity due to methyl cellulose polymer chain overlap and/or (2) obstruction of the surface-immobilized PHA chelator by overlapping methyl cellulose polymer chains. Considering that the half-time of metal chelating material color change was relatively short for both high viscosity solutions (less than half a day), it is unlikely that iron diffusion from the solution to the surface of the active packaging material was the major cause of reduced iron chelating capacity. Kaşgöz, et al. [131] suggested that polymers may form dense complexes on the surface of metal binding materials to inhibit diffusion of metals to metal chelating ligands and reduce observed metal chelating activity. These formation of dense polymer chain complexes on the material surface, which may be caused by hydrogen bonding and/or van der Waals interactions, could prevent the formation of potential chelating complexes. In the case of our study where a color development plateau was reached very quickly during storage, this may be the most probable explanation.

It is important to note that while iron chelating capacity and kinetics were found to be dependent on solution viscosities, even at the lowest maximum iron chelating capacity, values were well within commercially relevant parameters for EDTA usage. Current FDA limits for calcium disodium EDTA are 75 ppm (183 μM) in salad dressing, sauces and mayonnaise and 33 ppm (80 μM) in beverages.[20] Further research has demonstrated that iron bound in a 1:1 molar ratio with EDTA remains prooxidative and that higher molar

ratios (e.g. 2:1 EDTA:iron) are necessary to prevent iron from promoting lipid oxidation.[132, 133] We can therefore calculate a range of approximate EDTA equivalents of the non-migratory iron active chelating packaging material by assuming a food contact surface area to food volume ratio of 600 cm^2 packaging material/L food (as specified by current European Union legislation) and an EDTA:iron molar ratio range of 2:1 to 1:1. [134, 135] At the lowest maximum iron chelating capacity reported in this study (69.6 nmol iron/cm^2 in ~10^4 mPa·s model food system), the estimated EDTA equivalent of the iron chelating active packaging material is 17 to 35 ppm (42 to 84 μM), which is in the range of the legal limit for beverages. Although this is well below the legal limit for salad dressings, sauces and mayonnaise, as little as 16 μM EDTA (equivalent to 13.3 nmol iron/cm^2 active packaging material) is necessary to delay lipid oxidation in mayonnaise, a food that is very susceptible to iron promoted oxidation due to the iron content of egg yolk protein phosvitin.[136, 137] Therefore, the non-migratory iron chelating active packaging material reported here is higher than the minimum concentration necessary to inhibit lipid oxidation.

5.4.3 Influence of Food Hydrocolloid Chemistry on the Activity of Iron Chelating Material

Four representative food grade hydrocolloids were selected to characterize the influence of hydrocolloid chemistry on material iron chelation, including carrageenan, xanthan, locust bean, and guar gum. These hydrocolloids are commonly used in the food industry to thicken foods, such as salad dressings and sauces, that are susceptible to iron promoted oxidative degradation.[138] Carageenan is an anionic polysaccharide composed of sulfated galactans extracted from seaweed. Xanthan is an anionic microbial-produced

pyruvated polysaccharide composed of D- glucose, D-mannose, and D-glucuronic acid. Locust bean and guar gum are non-ionic galactomannans extracted from seeds. In this experiment, 1% methyl cellulose served as the control, since, as previously stated, methyl cellulose is non-ionic and has no specific affinity for iron. Hydrocolloids were added to aqueous buffered iron solutions at concentrations to yield viscosities similar to that of 1% methyl cellulose solution so that the only independent variable in the experiment was hydrocolloid chemistry (**Table 5.4**). PP-*g*-PHA chelating packaging materials were submerged in iron solutions for 7 d to ensure that maximum iron chelation capacity was achieved.

Table 5.4. Influence of hydrocolloid chemistry on iron chelation by chelating packaging materials as characterized by colorimetry (ΔE^*) and ICP-OES determined iron content (nmol cm^{-2}). Values represent means ± standard deviation (n=4). Significant differences are denoted with letters ($p<0.05$).

Aqueous Buffered Iron Solution	Hydrocolloid Chemistry	Apparent Viscosity at 10 s^{-1} (mPa·s)	ΔE^*	Iron Content (nmol cm^{-2})
1% methyl cellulose	Non-ionic methylated cellulose	181 ± 10	15.7 ± 0.65[a]	116 ± 5.5[a]
1% carrageenan	Anionic sulfated galactans	173± 3.9	15.3 ± 1.5[a]	106 ± 19[a]
0.3% xanthan	Anionic pyruvated polysaccharide of glucose, mannose, and glucoronic acid	187 ± 4.1	11.6 ± 1.6[b]	52.0 ± 11[b]
0.5% locust bean	Non-ionic galactomannans	169 ± 18	11.1 ± 0.77[b]	48.6 ± 4.5[b]
0.5% guar	Non-ionic galactomannans	179 ± 2.9	10.4 ± 0.32[b]	36.5 ± 3.2[b]

As before, colorimetry and direct ICP-OES analysis were performed to quantify iron chelation. Iron chelating materials exhibited a color change that correlated well with ICP-OES characterized iron content (**Table 5.4** and **Figure 5.6**). Materials incubated in

iron solutions thickened by carrageenan achieved similar iron chelation as those incubated in solutions thickened by methyl cellulose (**Table 5.4**). However, materials incubated in iron solutions thickened by guar gum, locust bean gum and xanthan achieved only 32-45% of the maximum iron chelating capacity of materials incubated in 1% methyl celluose (**Table 5.4**). While xanthan (an anionic hydrocolloid) significantly inhibited iron chelation by chelating packaging materials, the other anionic hydrocolloid tested here (carageenan) had no influence on chelation. These results suggest that charge of the hydrocolloid alone is not an indicator for competitive chelation for hydroxamate-functionalized chelating packaging materials, but rather metal-ligand specific interactions. The pyruvate group of xanthan gum has been hypothesized as a possible specific metal chelating ligand of xanthan gum based on a demonstrated high affinity for ferrous iron.[139] Since guar and locust bean gum are non-ionic hydrocolloids, competition for iron chelation by these food hydrocolloids occurred by metal-ligand specific interactions. Galactomannans may complex metals by two *cis*-hydroxyl groups of each monomeric unit.[140] Obstruction of surface-bound PHA chelating ligands by these hydrocolloids, as hypothesized for high viscosity methyl cellulose solutions, may have also occurred if they have a high affinity for the surface (e.g. hydrogen bonds, van der Waals interaction). However, further study is necessary to support such hypothesis.

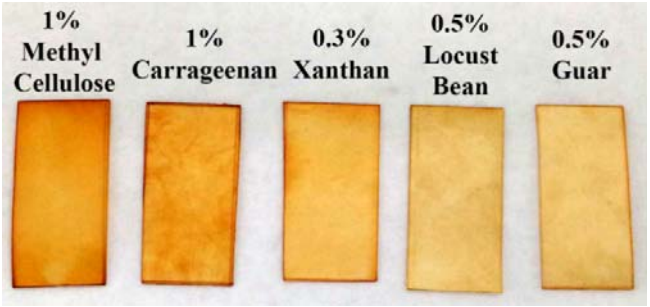

Figure 5.6.Color change of PP-*g*-PHA chelating packaging material after 7 d incubation in aqueous buffered iron reaction solutions modified with different food hydrocolloids.

To our knowledge, there has not been a formal study of hydrocolloid affinity for *ferric* iron. However, our observations are in agreement with reports on iron bioavailability studies which characterized the binding of *ferrous* iron by hydrocolloids. Platt and Clydesdale [127] examined binding of ferrous iron by guar gum (0.67%) under simulated duodenal pH conditions (pH 5) and found that guar gum exhibited specific binding for ferrous iron (K_{eff}= 6.27 x 10^6). Bosscher, et al. [141] determined that locust bean gum (0.42%) reduced iron bioavailibility 99.55% when incorporated into infant formula. Shimada, et al. [139] observed that xanthan (0.05%) had a pH independent affinity for ferrous iron. Despite the well established competitive iron chelation by certain hydrocolloids, it is important to consider the intended application of non-migratory metal chelating active packaging such as that reported here. As the goal of such active packaging is to inhibit metal-promoted oxidative degradation reactions such as lipid oxidation, competitive chelation by food hydrocolloids may support the overall antioxidant systems in food products. Previous research has demonstrated that food hydrocolloids that chelate iron can inhibit lipid oxidation of oil-in-water emulsions.[7, 139, 142]

5.5 Conclusion

Non-migratory active packaging enables a potential regulatory benefit over migratory technologies, as the active agent is covalently bound to the material. Yet, questions about activity in solutions of increasing viscosities (and corresponding diffusional limitations) have largely been unanswered. The overall aim of this study was to demonstrate the ability of surface-bound active agents to retain activity in liquid and semi-liquid food systems of increasing viscosities. Iron chelating active packaging materials were used to study the influence of food matrix viscosity on iron chelating

kinetics and capacity. A maximum iron chelating capacity of >88 nmol/cm^2 iron was achieved within the 7 d storage study for materials incubated in iron solutions up to ~10^2 mPa·s. At high viscosity iron solutions (~10^3 and~10^4 mPa·s, similar to sauce and mayonnaise viscosity), films retained at least 76% of their maximum iron chelating capacity. Under all viscosity conditions tested, PP-*g*-PHA chelating materials exhibited and iron chelating activity equivalent to at least 17 ppm EDTA. In addition, a study was performed to determine the influence of hydrocolloid chemistry on chelating capacity of the chelating packaging materials. Compared to the methyl cellulose control, guar, locust bean and xanthan gums demonstrated affinity for ferric iron that reduced iron chelation capacity of PP-*g*-PHA, whereas carrageenan did not inhibit iron chelation by PP-*g*-PHA iron chelating materials. Since food hydrocolloids can contribute to antioxidant systems in food products, it is unlikely that these interactions would significantly affect the performance of non-migratory iron chelating active packaging as an antioxidant. Understanding the impact of food matrix physical and chemical properties on the performance of non-migratory active packaging is essential to consider for commercial applications. This work demonstrates the potential application of non-migratory iron chelating active packaging in liquid and semi-liquid foods (viscosity range ~1 to 10^5 mPa·s) to allow for the removal of synthetic additives, while maintaining food quality.

CHAPTER 6

BIOMIMETIC POLYPHENOL COATING FOR ANTIOXIDANT ACTIVE PACKAGING APPLICATIONS[5]

6.1 Abstract

Oxidative instability of food, pharmaceutical, and consumer products can be promoted by trace metals, especially iron and copper, with subsequent propagation of free radicals. Plant-derived phenolic compounds that contain catechols are reported to have free radical scavenging, metal chelating and surface adhesion properties upon polymerization. The objective of this study was to synthesize biomimetic polyphenol coatings for development of antioxidant active packaging materials. Two synthetic routes were explored to apply polyphenol coatings to the surface of polypropylene by *in situ* polymerization of a mixture of catechol and catechin and oxidative polymerization with laccase and in alkaline saline. Both polyphenol coatings demonstrated potent metal chelating and radical scavenging capacity, which suggest potential antioxidant capacity. Dual functionality of polyphenol coatings as potent antioxidants and anchors makes them a promising candidate for active packaging coatings that can inhibit metal-promoted oxidative degradation.

6.2 Introduction

A major challenge to food, consumer products, and pharmaceutical industries is retaining stability of oxidation-sensitive bioactive compounds, such as unsaturated fatty acids, carotenoids, flavonoids, vitamins, and drugs. Oxidative stability of such compounds

[5] The contents of this chapter have been submitted for publication: Roman, M. J.; Decker, E. A.; Goddard, J. M. Biomimetic polyphenol coatings for antioxidant active packaging applications. **2016**. *Submitted.*

is determined by the propagation of free radicals. In dispersions containing bioactive compounds, trace amounts of metals, especially iron and copper, are key prooxidants that contribute to product instability as they promote hydroperoxide decomposition that catalyzes free radical chain reactions.[6] Since it is difficult to fully remove trace metals from raw materials and the processing environment, metal chelators, such as ethylenediaminetetraacetic acid (EDTA), and free radical scavengers, such as butylated hydroxytoluene (BHT), are often added to formulations as antioxidants to stabilize these products. In an effort to reduce use of synthetic additives due to consumer perception of toxicity risk, there has been increasing interest in alternative methods of product preservation using antioxidants obtained from natural sources. Directly substituting natural antioxidants into product formulations is challenging because they tend to be less potent than synthetic additives and therefore must be added in larger amounts that may change a product's organoleptic properties (i.e. color, flavor, viscosity). In order to overcome this challenge, researchers have explored incorporation of natural antioxidants into active packaging coatings. Antioxidant active packaging coatings may be applied to the product contact surface of common packaging materials by non-covalent or covalent attachment of antioxidants that are applied with or without a carrier polymeric resin.[143] These coatings are designed to either scavenge prooxidants from the product or slowly release antioxidants from the packaging material.

The majority of research on antioxidant active packaging coatings has been focused on application of free radical scavengers on the surface of packaging materials. Contini, et al. [144] spray deposited citrus extract on plasma pretreated polyethylene terephthalate trays that inhibited oxidative degradation of cooked meats. Garces, et al. [110] patented an

antioxidant active varnish for use on packaging materials composed of polymeric resin blended with plant extracts that is designed to scavenge free radicals in packaging headspace.[145] Arrua, et al. [113] covalently attached a polymer containing caffeic acid to the surface of polypropylene and demonstrated its ability to scavenge free radicals and inhibit degradation of vitamin C in orange juice. Recently, antioxidant active packaging coatings by graft polymerization of metal chelating polymers, such as poly(acrylic acid) and poly(hydroxamic acid), have been developed that exhibit functionality across a broad range of pH values and viscosity conditions and in the presence of competing ions.[76, 85, 130, 146, 147] Metal chelating active packaging coatings extended the lag phase of lipid oxidation in soybean oil-in-water emulsions and demonstrated improved performance for metal chelating polymers with high iron affinity.[43, 44]

Among free radical scavenging antioxidants derived from natural sources, plant-derived phenolic compounds that contain catechols are reported to have high affinity for iron (e.g. catechol log $\beta^{Fe(III)}$ =43.76, catechin log $\beta^{Fe(III)}$ =47.4).[148] In addition to their antioxidant capacity, phenolic compound that contain catechols have been researched as biomimetic of mussel adhesive proteins making them ideal candidates for coating technologies. With this in mind, the reported work seeks to design biomimetic catechol-based polyphenol surface coatings for the development of antioxidant active packaging materials that provide dual antioxidant functionality, both by scavenging free radicals directly and by removing trace transition metals from the system.

A facile method of coating plant phenols onto material surfaces is through oxidative polymerization. Polymerized plant phenols have been noted to have adhesive properties on many materials relevant to packaging due to their structural similarities to the widely

researched mussel adhesive proteins. Jeon, et al. [149] demonstrated that plant phenols can be polymerized onto a variety of material surfaces, including aluminum, glass, polyethylene terephthalate, and polypropylene, with the assistance of the oxidase enzyme, laccase. Barrett, et al. [150] prepared polyphenol coatings from plant phenols by polymerization in an alkaline aqueous buffer, similar to reported methods for the preparation of polydopamine coatings.[151] However, there has yet to be an investigation of the ability of such polyphenol coatings to function as both free radical scavengers and metal chelators for antioxidant applications. The objective of this study was to synthesize a biomimetic polyphenol coating for development of antioxidant packaging materials with both metal chelating and free radical scavenging character. Polyphenol coatings were applied to the surface of polypropylene by *in situ* polymerization of a mixture of catechol and catechin (2.5 mg/ml catechol; 2.5 mg/ml catechin) via enzymatic polymerization with laccase (1 mg/ml in 100 mM sodium acetate buffer, pH 5 and methanol (9:1)) or oxidative polymerization in alkaline saline (100 mM bicine, 600 mM sodium chloride, pH 8). Ability of the polyphenol coatings to chelate copper and iron ions and scavenge free radicals was demonstrated.

6.3 Materials and Methods

6.3.1 Materials

Polypropylene (isotactic, pellets) was purchased from Scientific Polymer Products (Ontario, NY). Hydroxylamine hydrochloride, ferrous sulfate heptahydrate (99+%), imidazole (99%), and 3-(2-pyridyl)-5,6-diphenyl-1,2,4-triazine-*p,p'*-disulfonic acid disodium salt hydrate (ferrozine, 98+%) were purchased from Acros Organics (Morris Plains, NJ). 1-2-Dihydroxybenzene (catechol, ≥99%), (+)-catechin hydrate (≥98%), zincon monosodium salt, 2,2-Azobis(2-methylpropionamidine) dihydrochloride (AAPH, 97%),

fluorescein sodium salt, and (±)-6-Hydroxy-2,5,7,8-tetramethylchromane-2-carboxylic acid (Trolox, 97%) were purchase from Sigma Aldrich (St. Louis, MO). Laccase M120 (from *Trametes versicolor*, EC 1.10.3.2, 1.19 x 10^5 U g^{-1}) was generously donated by Amano Enzymes (Nagoya, Japan). All other chemicals were purchased from Fisher Scientific (Fair Lawn, NJ).

6.3.2 Polypropylene Film Preparation

Polypropylene (PP) films were prepared as previously reported [43]. PP pellets were cleaned by sequentially sonicating in the following solvents twice for 10 min each rinse: isopropanol, acetone, and deionized water, and then dried over anhydrous calcium sulfate. Clean PP film was prepared on a Carver Laboratory Press (Carver, Inc., NJ). The press was set to 170°C, PP pellets were heated on the press at for 1 min, and then 9000 lbs of pressure was applied. PP films, average thickness of 257 ± 25 μm, were cut into 8 x 8 cm^2 pieces and washed using the same method as the PP pellets.

6.3.3 Surface Modification

Polyphenol coatings were applied to the surface of PP by *in situ* polymerization of a mixture of catechol and catechin via enzymatic polymerization with laccase [149] or oxidative polymerization in buffered saline.[150] Enzymatic polymerization reaction solution was as follows: 2.5 mg ml^{-1} catechol, 2.5 mg ml^{-1} catechin, and 1 mg ml^{-1} laccase in 100 mM sodium acetate buffer, pH 5:methanol (9:1). Alkaline oxidative polymerization reaction solution was as follows: 2.5 mg ml^{-1} catechol and 2.5 mg ml^{-1} catechin in 100 mM bicine, 600 mM sodium chloride, pH 8. All polymerization reactions were conducted at 20 ± 2°C with stirring for 24 h. After application of the coating, PP films were rinsed with DI

water, dried overnight over anhydrous calcium sulfate, and the cut into 1 x 2 cm^2 pieces for analysis.

6.3.4 Surface Chemistry

Attenuated total reflectance Fourier transform infrared spectroscopy (ATR-FTIR) was used to confirm the application of polyphenols on the surface of PP. An IRPrestige FTIR Spectrometer (Shimadzu Scientific Instruments, Inc., Kyoto, Japan) with a diamond ATR crystal was used to measure the spectrum under the following parameters: Happ-Genzel function, 32 scans, and 4 cm^{-1} resolution. Spectrum analysis was performed on KnowItAll(R) Informatics System 9.5 (Bio-Rad Laboratories, Inc., Informatics Division, Philadelphia, PA).

Total phenol content was quantified using an adapted Folin-Ciocalteu colorimetric assay, in which phenolic groups react with Folin-Ciocalteu reagent and form a blue chromaphore under alkaline conditions.[152] Each 1 x 2 cm^2 film was submerged in 1 ml Folin-Ciocalteu (0.2 N Folin-Ciocalteu phenol reagent) and 0.2 ml 0.05 N HCl and incubated while shaking at room temperature for 5 min. Then, 0.8 ml 7.5% sodium carbonate was added to the reaction and incubated for 2 h shaking in the dark at room temperature. The absorbance of the reaction solution was measured at 760 nm to quantify total phenol content by comparison to a standard curve of catechol in 0.5 N HCl.

6.3.5 Surface Morphology

Surface images of materials were taken with JCM-6000 NeoScope (JEOL, Japan) at 10 kV. Prior to imaging, samples was mounted on a small aluminum platform with double sided carbon tape and then sputter coated with gold under argon for 30 s. Images were taken twice on three independently prepared samples. Coating thickness was

determined by surface profilometry (Dektak 150 Stylus Profilometer, Veeco, NY). Prior to analysis, portions of coated materials were removed by absolute ethanol to determine coating thickness by step height. Measurements were taken on four independently prepared samples.

6.3.6 Iron and Copper Chelating Capacity

The ferric iron (Fe^{3+}) chelating activity of polyphenol coated films was determined using a method adapted from Tian, et al. [85] Each 1 x 2 cm^2 film was submerged in buffered iron solution (0.08 mM ferric chloride in 0.05M sodium acetate/imidazole buffer, pH 5) and allowed to chelate in the dark for 24 h at room temperature with shaking. The Fe^{3+} chelating activity of films was calculated by the difference of the Fe^{3+} concentration in buffered iron solution with films against the control (buffered iron solution without film). A modification of the ferrozine assay was performed to quantify the Fe^{3+} concentration of buffered iron solutions, in which a colorimetric complex is formed between Fe^{2+} and ferrozine reagent and read at 562 nm. The ferrous iron (Fe^{2+}) and cupric ion chelating activity of polyphenol coated films was determined using the same method as Fe^{3+} chelating activity. Buffered iron solution was made with ferrous sulfate instead of ferric chloride and iron was quantified by ferrozine assay. Buffered copper solution was made with cupric sulfate instead of ferric chloride and copper was quantified by colorimetric reaction with zincon. Additional chelating studies were conducted at different pH values (pH 3,4) in order to evaluate the coated material performance stability.

6.3.7 Radical Scavenging Activity

Free radical scavenging activity of the polyphenol coated PP films was evaluated using the oxygen radical absorbance capacity (ORAC).[153] ORAC uses hydrogen atom

transfer (HAT) reaction to quantify the antioxidant capacity of water-soluble antioxidants. For this method, AAPH is used to generate peroxyl radicals that oxidize fluorescein (probe), which results in a loss of fluorescence over time. The efficacy of an antioxidant is quantified by its ability to protect fluorescein from oxidative degradation by scavenging peroxyl radicals. An ORAC assay method was adapted for use with active packaging films.[153] To conduct ORAC on polyphenol coated films, a microtiter assay was developed using a 96 well microarray microtiter plate (AHC4x24, ArrayIt Corporation, Sunnyvale, CA), in which swatches of film are assembled at the bottom of the plate and function as the bottom of each well. Working solutions of fluorescein (93.5 nM), AAPH (221mM) and Trolox (standard, 100 µM) were prepared fresh daily. To each well, 50 µl of fluorescein and 50 µl of phosphate buffer or standard (100 µM Trolox) was added. The microarray microtiter plate was preheated for 5 min at 37°C prior to the addition of 50 µl AAPH. Immediately after the addition of AAPH, fluorescence was read on a Synergy 2 microplate reader (BioTek Instruments, Winooski, VT) at an excitation wavelength of 485/20 nm and an emission wavelength of 528/20 nm. The microarray microtiter plate was kept in the microplate reader at 37°C under constant shaking with measurements taken every 5 min for 2 h to generate a fluorescence decay curve. ORAC values were expressed as Trolox equivalents using the following equation:

$$ORAC\ \left(\frac{nmol\ TE}{cm^2}\right) = \frac{\frac{nmol_{Trolox} \times (AUC_{sample} - AUC_{Blank})}{(AUC_{Trolox} - AUC_{Blank})}}{A_{well}} \quad (1)$$

Where $nmol_{Trolox}$ is the molar amount of Trolox per well in standard (5 nmol), AUC is the area under the fluorescence decay curve, and A_{well} is the area of the well exposed to polyphenol coated film (0.4875 cm^2). AUC calculations and all statistical

analyses were conducted using GraphPad Prism 6.0 (La Jolla, CA). Reported results are representative of two independent experiments performed in triplicate.

6.4 Results and Discussion

Polymerization of the catechol and catechin by laccase (pH 5) and in alkaline saline (pH 8) was immediately observed by a change in the color of the reaction solution to a dark brown color, characteristic of polyphenol formation. Deposition of the polymerized phenolic coating onto the surface of polypropylene was identified by similar generation of a dark brown color on the polypropylene film after 24 h in the reaction solution. It is important to note, that for the oxidative polymerization reaction conducted at pH 8 without laccase, preliminary experiments revealed that a minimum of 200 mM sodium chloride was necessary for the polyphenol to be deposited on the surface, with optimum surface deposition at 600 mM sodium chloride (data not shown). Salt ions may shield charges on polyphenols formed under alkaline conditions to allow for better interactions with the hydrophobic polypropylene surface. Previous work in agreement with our findings was conducted by Sileika [154] who found that alkaline saline enabled improved surface deposition of polymerized phenolic compounds compared to pure water.

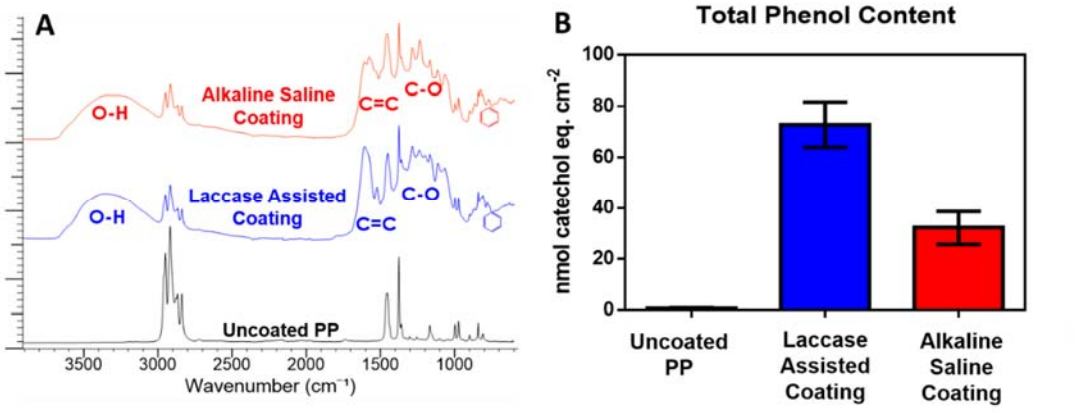

Figure 6.1. (a) Representative ATR-FTIR spectra and (b) total phenol content (n=4) of native PP and polyphenol coated PP.

Surface chemistry of the polyphenol coated materials was characterized by ATR-FTIR spectroscopy (**Figure 6.1**). Laccase assisted polyphenol coatings exhibited a strong O-H absorbance band (3000-3680 cm^{-1}), two C=C absorbance bands (1590, 1518 cm^{-1}) attributed to benzene rings on catechol and catechin, and several C-O absorbance bands that may be attributed to crosslinks of catechol and catechin or catechol ligands (1050-1290 cm^{-1}). These results are in agreement with reported spectra collected from laccase-assisted polymerization of catechol, catechin, and their combination.[149] The polyphenol coating produced by alkaline saline polymerization of catechol and catechin exhibited a similar ATR-FTIR spectrum, with slight differences in the intensity and number of absorbance bands for C=C (1606, 1575, 1537 cm^{-1}) and C-O bonds (1050-1290 cm^{-1}), which suggests that this polyphenol coating has a different structure than the polyphenol coating formed by laccase assisted polymerization. Oxidation of a phenol by laccase typically involves loss of a single electron that results in the formation of a cationic radical, whereas alkaline oxidation results in the formation of an anionic radical. Different reactive radicals may influence the structure of the polyphenol formed by subsequent polymerization reactions. The number of available catechol groups on the surface was assessed by Folin Ciocalteu assay (**Figure 6.1B**). Laccase assisted polyphenol coatings contained more than twice the number of available phenolic groups than alkaline saline polyphenol coatings (86.7 ± 12 nmol catechol eqv. cm^{-2} and 33.1 ± 7.3 nmol catechol eqv. cm^{-2}, respectively), while uncoated PP contained an insignificant amount of phenol groups (0.791 ± 0.14 nmol catechol eqv. cm^{-2}).

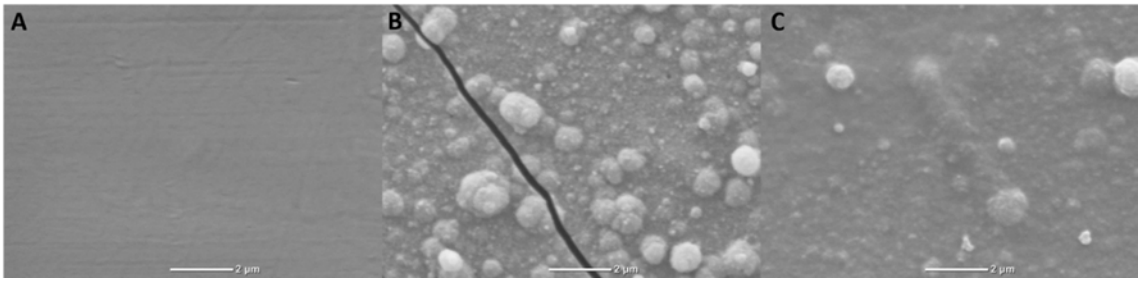

Figure 6.2. Representative SEM micrographs of (a) native PP, (b) laccase assisted polyphenol coated PP, and (c) alkaline saline polyphenol coated PP (10,000x magnification).

To determine the effect of coating preparation method on surface morphology, surface scanning electron microscopy (SEM) images of coated and uncoated materials were taken (**Figure 6.2**). Uncoated PP exhibited a smooth, uniform surface (**Figure 6.2A**). SEM micrographs confirmed the deposition of laccase assisted and alkaline saline polyphenol coatings onto the surface of polypropylene films. Laccase assisted polyphenol coatings significantly changed the surface morphology of the polypropylene to a rough surface with aggregates of polyphenols throughout the coating (**Figure 6.2B**). The coated surface also exhibited cracks throughout most likely caused by dehydration of the hydrophilic surface prior to imaging. The alkaline saline polyphenol coating was smoother than the laccase assisted polyphenol coating and did not have any visible cracking (**Figure 6.2C**). Compared to the uncoated PP material, both polyphenol coated surfaces were rougher with presence of polyphenol aggregates. These observations are consistent with previous research on *in situ* polymerization of dopamine on glass and aluminum,[155] which suggests that the hydrophobic surface properties of polypropylene did not significantly affect coating morphology. Changes in the surface morphology of coated PP materials were evident across the surface, demonstrating uniform application of the polyphenol coatings. Laccase assisted polyphenol coatings were approximately twice the thickness of alkaline polyphenol coatings (laccase assisted coating: 1087 ± 45.3 nm, alkaline coating: 506.5 ±

32.1 nm). This disparity between coating thickness corresponds with differences in the coatings available phenolic groups (**Figure 6.1B**).

The antioxidant efficacy of the polyphenol coated materials was characterized by screening both metal chelating and free radical scavenging capacity. The ability to chelate ferrous, ferric, and cupric ions was measured at pH 3-5 to reflect a pH range of relevant oxidation prone food and consumer products (**Figure 6.3**). Polyphenol coatings prepared by both synthetic routes exhibited significant ferrous ion chelating capacity that was pH dependent. Ferrous chelating capacity decreased with decreasing pH value, with optimum ferrous ion chelation at pH 5. In contrast, polyphenol coated materials exhibited optimum *ferric* ion chelating capacity at pH 4. The decline of ferric ion chelating capacity at pH 5 may be attributed to loss of ferric ion solubility at increasing pH values and/or oxidation of catechol hydroxyl groups by ferric ion that would result in the formation of quinones that have a low affinity for iron.[156] Lack of the ability of ferrous ions to convert hydroxyls to quinones could also help explain why chelating capacity of ferrous ions at pH 4 and 5 were higher than ferric ion chelating capacity. There was no significant difference in ferric and ferrous ion chelating capacity at pH 3. Despite significant differences in total phenol content (**Figure 6.1B**) and coating thickness, there was no significant difference in iron chelating capacity of the laccase assisted polyphenol coating and alkaline saline polyphenol coating. Similarities in iron chelating capacity suggests that chelating ligands of the polyphenolic coatings may be most active at the surface. Both polyphenol coated materials demonstrated lower copper chelating capacity than iron chelating capacity. Optimum copper chelation was demonstrated at pH 5 and decreased with decreasing pH values, with no significant difference between uncoated material and polyphenol coated material at pH

3. Similar to ferric ion, cupric ion may oxidize the catechol ligands to hinder effective chelation of metal ions. Ability to chelate ferrous ion, ferric ion, and cupric ion suggests that the reported polyphenol coated films may inhibit oxidative degradation reactions.

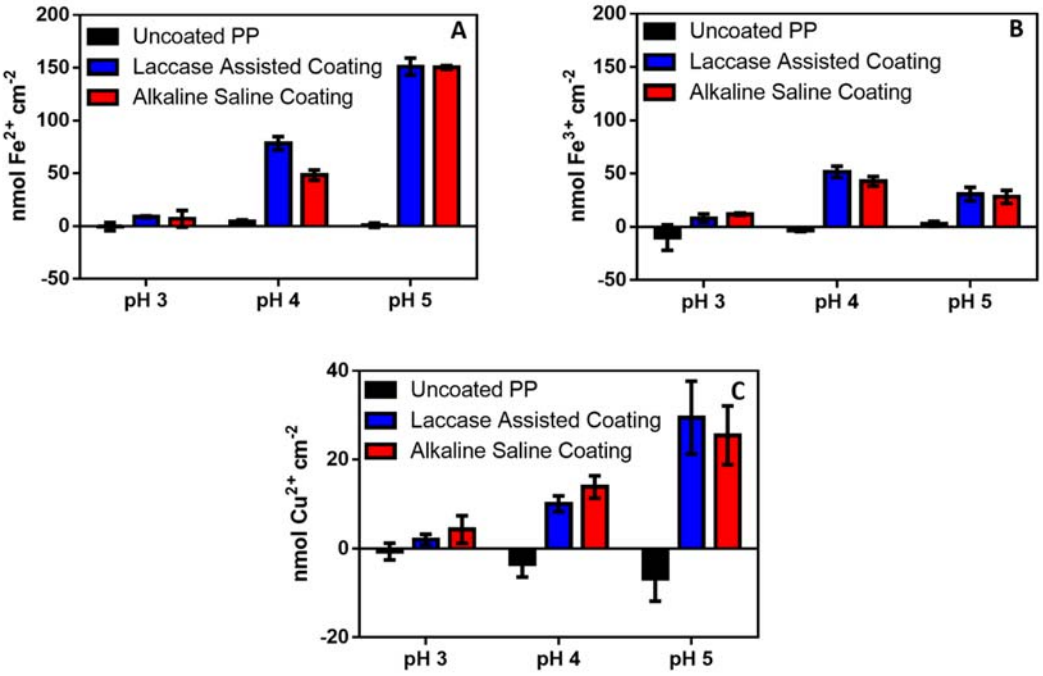

Figure 6.3. (a) Ferrous ion, (b) ferric ion, and (c) cupric ion chelating capacity (n=4) of native PP and polyphenol coated PP at different pH values (3.0, 4.0, and 5.0).

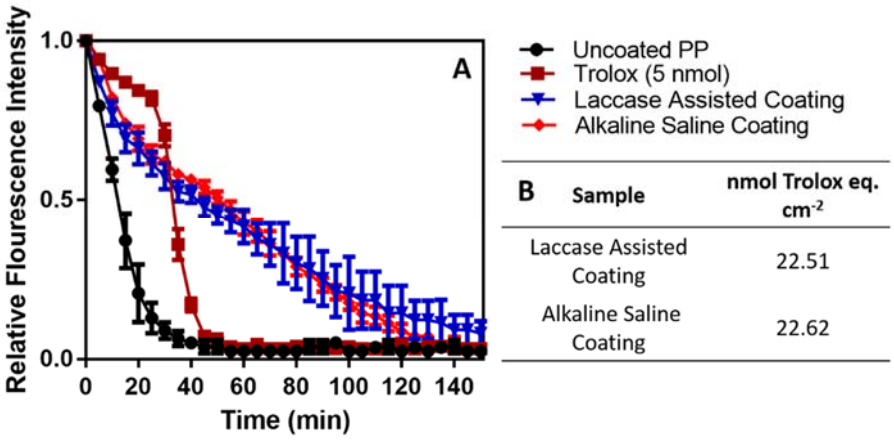

B

Sample	nmol Trolox eq. cm^{-2}
Laccase Assisted Coating	22.51
Alkaline Saline Coating	22.62

Figure 6.4. (a) Radical scavenging capacity of polyphenol coated PP (n=4) demonstrated by delayed decay of fluorescent probe in oxygen radical scavenging capacity (ORAC) assay. (b) Approximate radical scavenging capacity (Trolox eqv.) estimated by area under the curve.

Free radical scavenging capacity of polyphenol coated films was assessed by oxygen radical absorbance capacity (ORAC, **Figure 6.4**). For this assay, the efficacy of an antioxidant is quantified by its ability to protect fluorescein from oxidative degradation by scavenging peroxyl radicals generated by AAPH.[157] Polyphenol coated films were able to decrease the overall rate of fluorescein degradation, which is indicative of radical scavenging capacity. Based on area under the curve, laccase assisted polyphenol coating was estimated to have 22.51 nmol Trolox eq cm^{-2} and alkaline saline polyphenol coating was estimated to have 22.62 nmol Trolox eq cm^{-2}. As observed in the metal chelating capacity measurements, total phenol content did not appear to influence the free radical scavenging capacity of the coated films. Compared to the Trolox positive control, which demonstrates free radical scavenging behavior typical of soluble antioxidants, neither polyphenol coated materials exhibited a distinct lag phase for the induction of fluorescein oxidation (**Figure 6.4**). The lack of lag phase may be due to diffusion limitations of surface immobilized antioxidants to quench peroxyl radicals or possible higher redox potential of surface immobilized polyphenols compared to Trolox (E°' = 480 mV).[157] Nevertheless, both coatings demonstrated potent free radical scavenging capacity, which may contribute to their overall antioxidant capacity when applied to packaging materials.

6.5 Conclusions

Phenolic compounds that are derived from plants represent a promising source for antioxidants that may be used to hinder degradation of oxidation-sensitive bioactive compounds. Application of such phenolic compounds in active packaging coatings may prevent their interference with the organoleptic properties of food and consumer products, while still delivering antioxidant protection of bioactive compounds. Recent research has

demonstrated that compounds that bear structural similarities to mussel adhesive proteins, such as catechol-based plant phenols, have functional adhesive properties useful for the development of coating technologies. This proof of principle study demonstrated that polyphenol coatings can be applied by *in situ* laccase assisted polymerization or alkaline saline polymerization of catechol and catechin possess dual antioxidant capacity, exhibiting both metal chelating and radical scavenging properties. These findings warrant further investigation for the development of antioxidant polyphenol coatings for active packaging applications in food, consumer products, and pharmaceutical industries.

CHAPTER 7

NONMIGRATORY POLYPHENOL COATED ACTIVE PACKAGING MATERIAL: CHARACTERIZATION AND ANTIOXIDANT EFFICACY

7.1 Abstract

Oxidative degradation causes lipid rancidity, natural color loss, and nutrient degradation that decreases quality and shelf life of packaged foods. Synthetic food additives are effective inhibitors of oxidation, but are undesirable to consumers who prefer 'clean' label products. The aim of this study was to develop a polyphenol coated active packaging material and demonstrate its ability to inhibit lipid oxidation and lycopene degradation in oil-in-water emulsions. Polyphenol coatings were applied to chitosan functionalized polypropylene by laccase assisted polymerization of catechol and catechin. Polyphenol coated packaging material exhibited both metal chelating (39.3 ± 2.5 nmol Fe^{3+} cm^{-2}, pH 4.0) and free radical scavenging (3.51 ± 0.77 nmol Trolox eq. cm^{-2}, ORAC) capacity, resulting in *dual* antioxidant functionality. Lipid oxidation and lycopene degradation in oil-in-water emulsions (pH 4.0) were inhibited by polyphenol coated materials. This study suggests that polyphenol coatings can be used to prepare antioxidant active packaging materials for foods.

7.2 Introduction

In order to meet consumer demands for 'clean' label products, many food and beverage manufacturers have committed to removing synthetic additives from their product formulations.[158] This commitment is challenging as many synthetic additives play a key role in product preservation that is integral to food safety, quality and shelf life. One of the key limiting factors in the shelf life of food and beverages is oxidative degradation

that can lead to lipid rancidity, natural color loss, and nutrient degradation. Conventionally, oxidative degradation is inhibited by addition of synthetic antioxidants, such as ethylenediaminetetraacetic acid (EDTA) and butylated hydroxytoluene (BHT), which bind pro-oxidant metals and scavenge free radicals, respectively. An alternative preservation strategy that is being explored to allow for removal of artificial ingredients from food and beverages is antioxidant active packaging.[29, 30, 38, 109, 143] Currently, the most widely used antioxidant active packaging technologies are oxygen scavenging sachets and labels.[28, 159] Although these oxygen scavengers are effective in low moisture foods, they are not suitable for use in liquid and semi-liquid foods.

Recently, our group has developed nonmigratory active packaging materials for application in liquid and semi-liquid foods.[35, 41-44, 47, 76, 85, 160, 161] Such nonmigratory active packaging materials are synthesized by direct immobilization or tethering of active compounds to the packaging surface to allow for interaction with food to improve safety and quality without becoming a direct food additive. Muriel-Galet, et al. [42] developed antimicrobial packaging film by immobilization of lysozyme on the surface of ethylene vinyl alcohol and demonstrated its efficacy against *Listeria monocytogenes*. Wong, et al. [41] synthesized a nonmigratory lactase active packaging film for in-package processing of lactose-free products by layer-by-layer assembly of polyethyleneimine, glutaraldehyde, and lactase onto low density polyethylene. Since the active compound of such active packaging material is unlikely to migrate to the food, it is less likely to have adverse effects on product sensory properties (ie: color, flavor, viscosity) and would be classified as a food contact material rather than direct additive, which has a potential 'clean' label regulatory benefit.[38] As the primary prooxidants in liquid and semi-liquid foods are trace transition

metals, previous generations of non-migratory antioxidant active packaging materials have been designed to chelate prooxidant metals, such as iron. Tian, et al. [43] have demonstrated that nonmigratory metal chelating active packaging materials can significantly extend the shelf life of oil-in-water emulsions during accelerated lipid oxidation studies. The efficacy of such metal chelating active packaging materials was improved for surface modifications that contained metal chelating ligands with a high iron affinity, such as hydroxamic acid.[44, 114, 160] Among metal chelators, compounds that contain catechols have the highest affinity for iron (e.g. enterobactin log $\beta^{Fe(III)}$=52)[162] and therefore may be good candidates for design of such active packaging materials.

Catechols are found throughout nature, most notably in siderophores,[163] mussel adhesive proteins,[164] and plant phenols.[165] Phenols derived from edible plants have been widely researched as direct additives for antioxidant applications in foods due to their metal chelating and radical scavenging capacity.[166] Depending on the conditions of the oxidation study (food type, temperature, pH) and phenol chemistry (hydroxyl group location, solubility) that may influence partitioning and thus reactivity, plant phenols have demonstrated both prooxidant and antioxidant effects.[166-169] Škerget, et al. [166] found that quercetin *enhanced* heat-induced oxidation in bulk oil, but *inhibited* heat-induced oxidation in emulsified oil. Polymeric phenols, such as procyanidins, have demonstrated stronger antioxidant activity than their monomeric counterparts in emulsified oil.[167] However, polymeric phenols are not widely used as direct additives due to their undesirable sensory properties (astringent flavor, dark color). Herein, we propose the application of polymeric phenols in non-migratory active packaging to circumvent the challenges of direct addition of polymeric phenols as food antioxidants. We hypothesize that

nonmigratory polyphenol coated active packaging could provide dual antioxidant functionality by both chelating prooxidant trace metals and directly scavenging free radicals.

The objective of this study was to develop a nonmigratory catechol-based polyphenol active packaging material and demonstrate its antioxidant applications. Polyphenol coatings were applied to chitosan functionalized polypropylene (PP) by laccase assisted oxidative polymerization of catechol and catechin. Polyphenol coated materials were characterized for surface chemistry and morphology, iron chelating capacity, and radical scavenging capacity. In addition, antioxidant application of polyphenol coated materials was demonstrated in emulsified oils to inhibit lipid oxidation and lycopene degradation.

7.3 Materials and Methods

7.3.1 Materials

Polypropylene (PP) pellets (isotactic, Scientific Polymer Products, Ontario, NY) were pressed under 9000 lbs of pressure at 170°C on a Carver Laboratory Press (Carver Inc., NJ) to prepare PP films (average thickness 257 ± 25 μm). N-hydroxysuccinimide (NHS), hydroxylamine hydrochloride, ferrous sulfate heptahydrate (99+%), imidazole (99%), 3-(2-pyridyl)-5,6-diphenyl-1,2,4-triazine-*p,p'*-disulfonic acid disodium salt hydrate (ferrozine, 98+%), citric acid monohydrate, EDTA, and Tween 20 were purchased from Acros Organics (Morris Plains, NJ). Chitosan, 1-2-Dihydroxybenzene (catechol, ≥99%), (+)-catechin hydrate (≥98%), zincon monosodium salt, 2,2-Azobis(2-methylpropionamidine) dihydrochloride (AAPH, 97%), fluorescein sodium salt, (±)-6-Hydroxy-2,5,7,8-tetramethylchromane-2-carboxylic acid (Trolox, 97%), deferoxamine

mesylate salt (≥92.5%, DFO), nitrilotriacetic acid trisodium salt (≥98%, NTA), barium chloride dihydrate, ammonium thiocyanate, cumene hydroperoxide (80%), and hexanal (98%) were purchased from Sigma Aldrich (St. Louis, MO). 1-ethyl-3-(3-dimethylaminopropyl)carbodiimide hydrochloride (EDC) was purchased from ProteoChem (Denver, CO) . Medium chain triglycerides (MCT, Miglyol 812N) were purchased from Warner Graham Company (Cockeysville, MD). Soybean oil (Wesson, 100% natural vegetable oil) was purchased from a local grocery store. Laccase M120 (from *Trametes versicolor*, EC 1.10.3.2, 1.19 x 10^5 U g^{-1}) was generously donated by Amano Enzymes (Nagoya, Japan). Lycopene (11% in corn oil, redvivo) was generously donated by DSM Nutritional Products Ltd. (Basel, Switzerland). All other chemicals were purchased from Fisher Scientific and used without further purification (Fair Lawn, NJ).

7.3.2 Preparation of Polyphenol Coatings on PP Films

PP films were washed by sequential sonication in isopropanol, acetone, and DI water and then dried over anhydrous calcium sulfate. Clean PP films were treated in an UV/Ozone cleaner (15 min per side, Model 42, Jelight Company, Inc., Irvine, CA) to create active carboxylic acid groups for attachment of chitosan anchor for the polyphenol coating. Chitosan was covalently immobilized on the surface of UV/Ozone treated PP films by exposure to a conjugation solution (1 mg ml^{-1} chitosan, 50 mM EDC, 5 mM NHS, 17 mM sodium acetate pH 5) with stirring for 1 h, followed by rinsing in DI water for 5 min. Polyphenol coatings were immediately applied to the surface of chitosan functionalized PP films by *in situ* polymerization of a mixture of catechol and catechin via enzymatic polymerization with laccase as previously described.[149, 170] Enzymatic polymerization reaction solution was as follows: 2.5 mg ml^{-1} catechol, 2.5 mg ml^{-1} catechin, and 1 mg ml^{-}

[1] laccase in 100 mM sodium acetate buffer, pH 5:methanol (9:1). All polymerization reactions were conducted at 20±2°C with stirring for 24 h. After application of the coating, PP films were washed with DI water (30 min at 20±2°C, 60 min at 60°C, 30 min at 20±2°C) and dried overnight over anhydrous calcium sulfate.

7.3.3 Surface Chemistry

Attenuated total reflectance Fourier transform infrared spectroscopy (ATR-FTIR) was used to confirm the introduction of polyphenols to the surface of PP. Spectra were collected on an IRPrestige FTIR Spectrometer (Shimadzu Scientific Instruments, Inc., Kyoto, Japan) with a diamond ATR crystal under the following parameters: Happ-Genzel function, 32 scans, and 4 cm^{-1} resolution. Spectrum analysis was performed on KnowItAll(R) Informatics System 9.5 (Bio-Rad Laboratories, Inc., Informatics Division, Philadelphia, PA).

Surface phenol content was quantified using a Folin-Ciocalteu colorimetric assay adapted for active packaging film.[170] Each film (1 x 2 cm^2) was submerged in 1 ml 0.2 N Folin-Ciocalteu phenol reagent and 0.2 ml 0.05 N HCl and incubated with shaking for 5 min. Then, 0.8 ml 7.5% sodium carbonate was added to the reaction and incubated for 2 h shaking in the dark. The absorbance of the reaction solution was measured at 760 nm to quantify total phenol content by comparison to a standard curve of gallic acid in 0.5 N HCl to calculate gallic acid equivalents (GAE).

Residual polymer was recovered from the polymerization reaction solution for molecular weight characterization.[171] Polymer precipitates were collected by centrifugation, washed three times with methanol and then dried *in vacuo*. Polymer

molecular weight was measured by gel permeation chromatography (GPC) in DMF with 0.01 M LiCl at 50 °C and calibrated against poly(methyl methacrylate) (PMMA) standards.

7.3.4 Surface Morphology

Electron micrographs of control and coated PP films were acquired with JCM-6000 NeoScope (JEOL, Japan) at 10 kV. Prior to imaging, samples were mounted on a small aluminum platform with double sided carbon tape and then sputter coated with gold under argon for 30 s. Optical profilometry was used to quantify surface roughness of materials and coating thickness. Root mean square surface roughness (Sq) and step height measurements to characterize coating thickness were taken on a Zeta 20 Optimal Profilometer (Zeta Instruments, San Jose, CA) using 3D Zdot image analysis software (Zeta Instruments, San Jose, CA).

7.3.5 Coating Stability Study

The stability of polyphenol coated films was assessed using conditions of total immersion migration tests adapted from European Union regulations.[172, 173] Current EU legislation specifies a surface area to food volume ratio of 600 cm^2 packaging material per kg food. Therefore, all tests were conducted on 1 x 1 cm^2 polyphenol coated films (2 cm^2 surface area) immersed in 3.34 ml food simulants. Polyphenol coated films were incubated for 10 d at 40°C in the presence of the following food simulants: DI water (aqueous), 3% acetic acid (acidic), 10% ethanol (alcoholic), and MCT (fatty). Integrity of polyphenol coatings on PP after migration test was evaluated by ATR-FTIR and SEM to characterize the influence of exposure to food simulants on coating chemistry and morphology.

7.3.6 Iron Chelating Capacity

The ferric iron (Fe^{3+}) and ferrous iron (Fe^{2+}) chelating capacity of polyphenol coated films were determined using previously described method.[85] Each film (1 x 2 cm^2) was submerged in buffered iron solution (0.08 mM ferric chloride or ferrous sulfate in 0.05M sodium acetate/imidazole buffer, pH 5) and allowed to chelate in the dark for 24 h with shaking and then rinsed with copious amounts of DI water. Iron chelating capacity of each film was quantified ICP-MS analysis (PerkinElmer Elan 9000, Waltham, MA). Film was prepared for ICP-MS analysis by microwave acid digestion as previously described.[130, 147, 160] In order to evaluate the coated material performance stability and assess iron binding affinity, additional iron chelating studies were conducted at different pH values (pH 3, 3.5, 4, 4.5) and in the presence of competitive chelators at pH 4.0 at the following chelation ratios: 2:1 citric acid/Fe, 2:1 NTA/Fe, 1:1 EDTA/Fe, and 1:1 DFO/Fe.[44]

7.3.7 Radical Scavenging Capacity

Free radical scavenging capacity of the polyphenol coated PP films was evaluated using the oxygen radical absorbance capacity (ORAC) and trolox equivalent antioxidant capacity (TEAC).[153] An ORAC microtiter assay was adapted for use with active packaging films, wherein swatches of film are assemble at the bottom of a 96 well microarray microtiter plate (AHC4x24, ArrayIt Corporation, Sunnyvale, CA) and function as the bottom of each well.[21, 170] Native PP film was used for all control and standard treatments instead of polyphenol coated PP film. All reagents were prepared in 75 mM phosphate buffer, pH 7.0. To each well, 50 µl fluorescein (93.5 nM) and 50 µl phosphate buffer or standard (100 µM Trolox) was added. The microarray microtiter plate was preheated for 5 min at 37°C prior to the addition of 50 µl AAPH (221mM) to initiate the reaction. Loss of

fluorescence was measured every 5 min for 2 h on a Synergy 2 microplate reader (BioTek Instruments, Winooski, VT) at an excitation wavelength of 485/20 nm and an emission wavelength of 528/20 nm to generate a fluorescence decay curve. ORAC values were expressed as Trolox equivalents using the following equation:

$$ORAC\ \left(\frac{nmol\ TE}{cm^2}\right) = \frac{\frac{nmol_{Trolox} \times (AUC_{sample} - AUC_{Blank})}{(AUC_{Trolox} - AUC_{Blank})}}{A_{well}} \quad (1)$$

Where $nmol_{Trolox}$ is the molar amount of Trolox per well in standard (5 nmol), AUC is the area under the fluorescence decay curve, and A_{well} is the area of the well exposed to polyphenol coated film (0.4875 cm^2).

The TEAC assay reported by Zulueta, et al. [153] was modified for use with active packaging films. A stock ABTS solution (7 mM ABTS in 2.45 mM potassium persulfate) was prepared 16 h prior to the assay and stirred overnight in the dark. Stock ABTS was diluted in 75 mM phosphate buffer, pH 7 (hydrophilic antioxidant capacity) or ethanol (lipophilic antioxidant capacity) to an absorbance of 0.700 ± 0.05 at 734 nm. Each film (1 x 1 cm^2) was exposed to 5 ml ABTS solution for 1 h with shaking at room temperature. Percentage of absorbance inhibition at 734 nm was calculated and compared to a standard curve of Trolox to estimate TEAC (nmol Trolox eq. cm^{-2}) with native PP films serving as controls

7.3.8 Lipid Oxidation Study

Polyphenol coated PP films were characterized for their ability to control lipid oxidation in oil-in-water emulsions using an accelerated lipid oxidation study.[160] Briefly, 1 wt % soybean oil was mixed with 0.1 wt % Tween 20 in 50 mM sodium acetate/imidazole buffer, pH 4.0. The mixture was emulsified by homogenizing using a hand-held homogenizer (Biospec Products, Inc., Bartlesville, OK), followed by passing through a

microfluidizer (Microfluidics, Newton, MA) three times at 9000 bar. Polyphenol coated PP film (1 x 1 cm^2) was stored with 1 ml emulsion at 37°C in a sealed 10 ml gas chromatography (GC) vial, with emulsion (no film), emulsion with PP film, 0.08 mM catechin, or 0.08 mM EDTA as controls. The emulsions were sampled during storage for particle size, zeta potential, lipid hydroperoxides, and hexanal. Particle size and zeta potential of the emulsion were monitored using a ZetaSizer Nano (Malvern Instruments, Worcestershire, UK).

Lipid hydroperoxides were quantified using a modification of the method of Shantha and Decker.[174] Briefly, 0.30 ml emulsion was mixed with 1.5 ml iso-octane/iso-propanol (3:1 v/v) by vortex and then centrifuged at 3000 rpm for 3 min. An aliquot of 0.2 ml upper phase (containing the hydroperoxides) was pipetted into 2.8 ml methanol/butanol (2:1 v/v) and mixed with 30 µl thiocyanate/ferrous solution, which was made by mixing an equal volume of 3.94 M thiocyanate and 0.072 M ferrous chloride. The mixture was incubated for 20 min and then absorbances were read at 510 nm. Lipid hydroperoxide content was calculated by comparison to a standard curve of cumene hydroperoxide.

Hexanal formation was determined by headspace gas chromatography (GC-17A, Shimadzu, Tokyo, Japan) with a flame ionization detector (FID) and a fused-silica capillary column (30 m x 0.32 mm x 1 µm) with poly(dimethylsiloxane) coating (Equity 1, Supelco, Bellefonte, PA). Samples were pre-incubated at 55°C for 10 min and then extracted using a divinylbenzene/carboxen/polydimethylsiloxane solid-phase microextract (SPME) fiber (50/30 µm, Supelco, Bellefonte, PA) for 2 min. The SPME fiber was desorbed in the GC injector at 250°C for 3 min at a split ratio of 1:7, to release the absorbed volatile compounds. The injector, oven and detector temperatures were set at 250°C, 65°C and 250°C,

respectively. The integrated area of the hexanal peak was calculated and the hexanal concentration was determined by comparison to a standard curve of hexanal in an EDTA emulsion (1 wt % soybean oil, 0.1 wt % Tween 20, 0.08 mM EDTA, 50 mM sodium acetate/imidazole, pH 4.0).

7.3.9 Lycopene Degradation Study

Polyphenol coated PP films were characterized for their ability to control lycopene degradation in oil-in-water emulsions using an accelerated degradation study.[175-177] The oil phase of the emulsion was prepared immediately before use by dispersing the redvivo dispersion (11% lycopene + 1.5% α-tocopherol in corn oil) into medium chain triacylglycerols (MCT) at a final concentration of 0.30 mg of lycopene per gram MCT. Lycopene emulsions were formed by sonicating 5% w/w oil phase with 30 mM Tween 20 in 50 mM sodium acetate/imidazole buffer, pH 4.0 for 6 min, using 1 s pulses, at 70% amplitude (Fisher Scientific Sonic Dismembrator 500, Fairlawn, NJ) in an ice bath. Polyphenol coated PP film (7 cm^2) was stored with 7 mL emulsion at 37^oC in a capped 23-G-20 glass fluorometer cells (Starna Cells, Inc., Atascadero, CA), with emulsion (no film), emulsion with PP film, 0.08 mM catechin, or 0.08 mM EDTA as controls. Lycopene degradation was monitored by measuring absorbance at 470 nm using a Shimadzu UV-2101 PC UV–Vis scanning spectrophotometer equipped with an ISR integrating sphere assembly (Shimadzu, Kyoto, Japan). Lycopene concentration was determined by comparison to a standard curve of lycopene emulsion. Particle size and zeta potential of the emulsion was monitored by dynamic light scattering on a ZetaSizer Nano (Malvern Instruments, Worcestershire, UK).

Additional experiments were conducted to determine polyphenol coated film's ability to inhibit radical induced lycopene degradation. All lycopene emulsions were prepared as previously described with the addition of 0.08 mM EDTA to minimize ferric iron promoted lycopene degradation and treatments were as follows: emulsion (no film), emulsion with PP film, emulsion with polyphenol coated PP film, and emulsion with 0.08 mM catechin. Experiments were conducted at 37°C and a radical initiator, AAPH (10 mg/ml), was added to induce lycopene degradation.[178] Immediately after the addition of AAPH, lycopene degradation was monitored every 10 min for 2 h using a spectrophometer equipped with an ISR assembly as previously described.

7.3.10 Statistical Analysis

All measurements were conducted on samples prepared in at least two separate batches. Data are expressed at means ± standard deviation. AUC calculations and one way ANOVA with Tukey's post hoc test ($P<0.05$) were conducted using GraphPad Prism 6.0 (La Jolla, CA).

7.4 Results and Discussion

7.4.1 Surface Chemistry and Morphology

Polyphenol coatings were synthesized by laccase assisted oxidative polymerization of catechol and catechin. This substrate combination was chosen because of the individual substrates' high affinity for iron (ie: catechol log $\beta^{Fe(III)}$ =43.76, catechin log $\beta^{Fe(III)}$ =47.4)[148] and their reported high coating deposition efficiency.[149] The catechol/catechin polymers generated in reaction solution by laccase assisted oxidative degradation of catechol and catechin were relatively large with a molecular weight of 7.88×10^3 Da and a polydispersity index of 1.93. Polymer molecular weight was on the order of magnitude

(10^3 Da) reported for polymers produced by laccase assisted oxidative polymerization of catechin.[149] In the initial design of the surface modification, catechol and catechin were polymerized directly onto the surface of PP films.[170] Although the coatings adhered the PP film surface, adhesion was not robust enough to prevent delamination in aqueous and alcoholic food simulants during migration testing (data not shown). Therefore, the surface modification was redesigned to include a chitosan anchor that was applied by carbodiimide crosslinker chemistry to a UV/ozone pretreated PP film (**Figure 7.1a**). Phenolic compounds are hypothesized to covalently attach to chitosan via Michael addition or Schiff base reaction. After undergoing migration testing in food simulants, aqueous (DI water), acidic (3% acetic acid), alcoholic (10% ethanol) and fatty (MCT), as specified by European Union regulations, polyphenol coatings applied to chitosan functionalized PP films were retained morphology and surface chemistry similar to that of freshly prepared coatings, suggesting their resistance to delamination (**Figure 7.2, D1 and D2**).

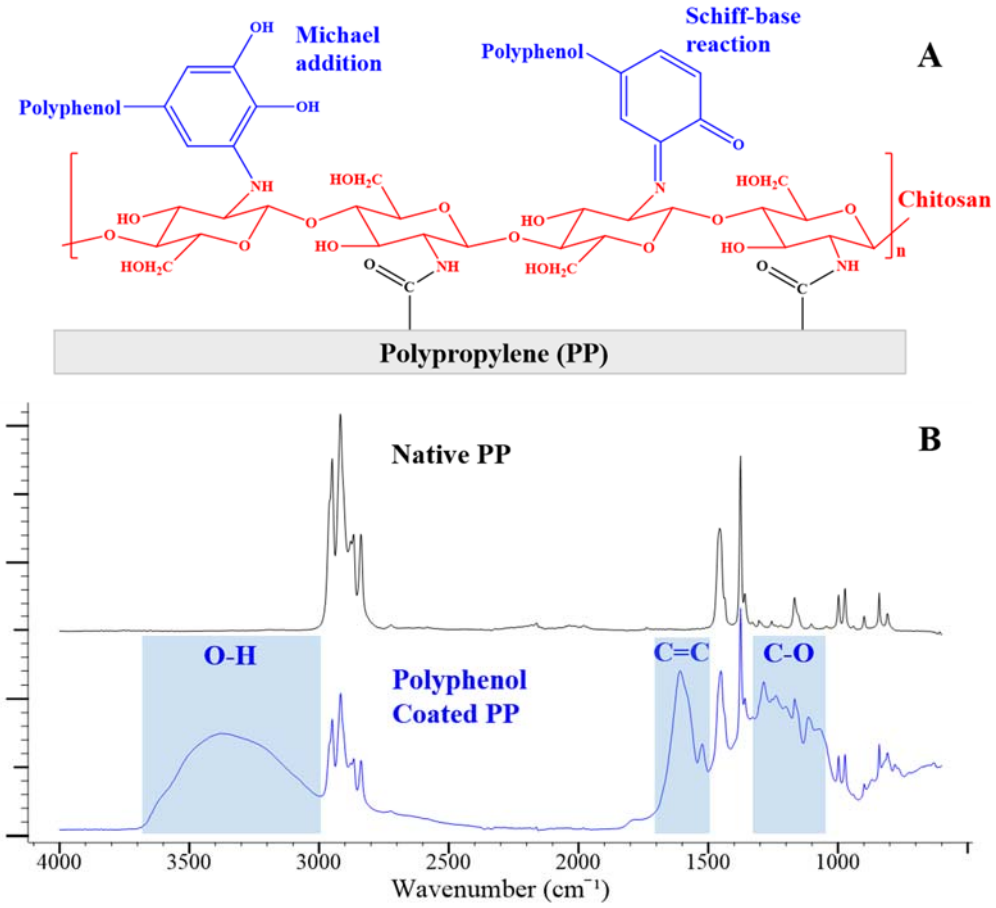

Figure 7.1. (a) Proposed surface chemistry of polyphenol coated PP and (b) representative ATR-FTIR spectra for native PP and polyphenol coated PP. Spectra are representative of a total of eight spectra collected on quadruplicate samples.

Surface chemistry of the polyphenol coated film was characterized by ATR-FTIR spectroscopy (**Figure 1b**). After PP films were coated with catechol/catechin polyphenol, there was a strong O-H absorbance band (3000-3680 cm^{-1}), two C=C absorbance bands (1590, 1518 cm^{-1}) attributed to benzene rings on catechol and catechin, and several C-O absorbance bands that may be attributed to crosslinks of catechol and catechin or catechol phenols (1050-1290 cm^{-1}). These spectra are in agreement with spectra collected from laccase assisted polymerization of catechol, catechin, and their combination.[149] Surface phenol content of polyphenol coated PP was 15.7 ± 0.43 nmol GAE cm^{-2} and significantly higher than native PP and chitosan functionalized PP controls (**Table 2**).

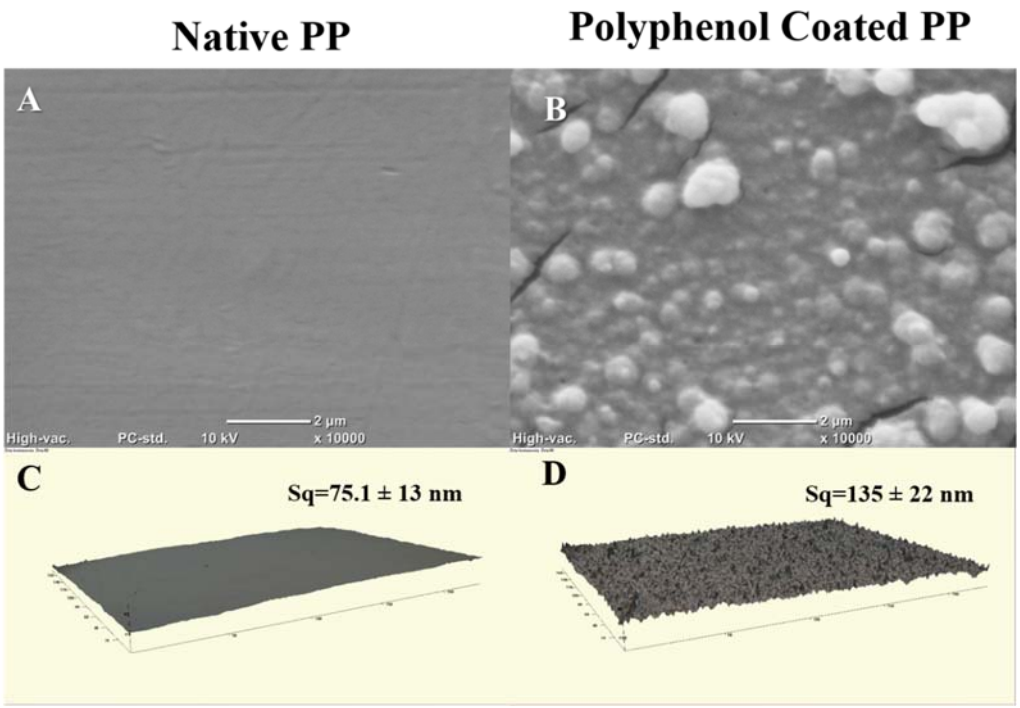

Figure 7.2. Representative SEM (10,000x) and optical profilometry images of (a,c) native PP and (b,d) polyphenol coated PP films. Average root mean square surface roughness (Sq) is noted on optical profilometry images. Images are representative of a total of nine images taken on triplicate samples.

Changes in the surface morphology of PP after application of the polyphenol coating was observed by SEM and optical profilometry (**Figure 7.2**). Native PP films exhibited a relatively smooth surface. Upon application of the polyphenol coating, surface exhibited a bumpy morphology with some cracking that resulted in an increase in root mean square surface roughness (Sq). Cracking may have occurred due to dehydration of the polyphenol coating prior to imaging. Polyphenol coating thickness was measured as 752 ± 130 nm by optical profilometry. Changes in surface morphology were evenly distributed across the surface of polyphenol coated PP.

7.4.2 Iron Chelating Capacity

Iron chelating capacity of polyphenol coated PP was characterized using ICP-MS from pH 3.0 to 5.0, which is a typical pH range for intended food and beverage applications. Native PP and chitosan functionalized PP had negligible iron content after incubation in

ferric or ferrous iron solution at all pH values (< 2 nmol iron cm^{-2}). Polyphenol coated PP retained chelating capacity for ferrous and ferric iron at all pH values except pH 3.0 (**Figure 7.3**). This loss of iron chelating capacity by polyphenol coated PP is in agreement with previous research on chelating capacity of phenolic compounds in solution, which demonstrated that catechol and phenol ligands are pH sensitive and lose activity at low pH values.[179] There was a significant difference the ferrous and ferric iron chelating capacity of the polyphenol coated PP across tested pH values. Ferric iron chelating capacity exhibited an optimum at pH 4.0, while ferrous iron chelating capacity increased exponentially with increasing pH value up to pH 5.0. Decline of ferric iron chelating capacity at pH > 4.0 may be attributed to autoxidation of the polyphenol coating in the presence of excess ferric iron. Previous research on flavonoid iron chelation has reported that pH dependent polyphenol autoxidation may occur in ferric iron solutions that have not been purged of oxygen.[180] Since polyphenol coated PP exhibited similar ferric and ferrous iron chelating activity at pH 4.0, this pH value was chosen for further testing in competitive chelation and oxidation studies.

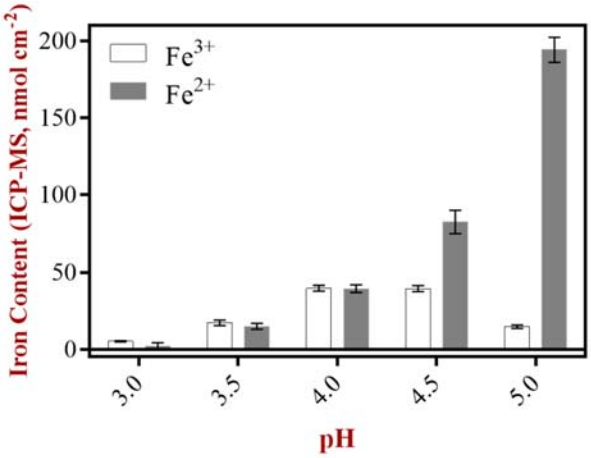

Figure 7.3. Iron chelating capacity of polyphenol coated PP at pH values 3.0 to 5.0 quantified by ICP-MS (n=2). Native PP and chitosan anchored PP exhibited minimal iron chelating capacity (<2.0 nmol cm-2).

Table 7.1. Iron chelating capacity of polyphenol coated PP reacted in pH 4.0 buffered iron solutions with metal chelators quantified by ICP-MS (n=2) and the corresponding chelator iron stability constant under optimum solution conditions.* Significant differences are denoted with letters ($P < 0.05$).

Treatment	Chelator Complex Stability Constant (log K1)[25]	Material Iron Content (nmol cm^{-2}, pH 4.0)
Fe^{2+}	N/A	39.3 ± 2.5^{a}
DFO/Fe^{2+}	7.2	15.8 ± 2.1^{b}
NTA/Fe^{2+}	8.84	14.1 ± 1.5^{b}
Citric acid/Fe^{2+}	3.2	8.45 ± 2.8^{c}
EDTA/Fe^{2+}	14.3	6.09 ± 1.7^{c}
Fe^{3+}	N/A	39.6 ± 1.9^{a}
DFO/Fe^{3+}	30.6	9.56 ± 0.00^{b}
NTA/Fe^{3+}	15.87	3.84 ± 0.46^{c}
Citric acid/Fe^{3+}	11.85	$4.37 \pm 0.87^{b,c}$
EDTA/Fe^{3+}	25.7	0.0817 ± 0.12^{c}

** Stability constants quantified in solution at 25°C, pH 7.0, 0.1 M ionic strength.*

Competitive chelation studies were conducted to assess the polyphenol coated PP film's affinity for ferric and ferrous iron at pH 4.0. Ferric or ferrous iron was chelated with the following chelators prior to exposure to polyphenol coated PP: citric acid, NTA, EDTA, and DFO. Iron binding constant of each chelator under optimum solution conditions and iron chelating capacity of polyphenol coated PP in the presence of chelate complexes at pH 4.0 are shown in **Table 7.1**. Polyphenol coated PP was able to sequester iron from all chelate complexes except in the case of EDTA/Fe^{3+} at pH 4.0. For both ferric and ferrous iron, relative iron chelating capacity of polyphenol coated PP in the presence chelator/iron complexes compared to iron alone was not correlated to chelator stability constant. A couple of possible explanations for this apparent discrepancy are (1) chelators may exhibit different iron affinity at pH 4.0 compared to optimum conditions and/or (2) polyphenol coating may form complexes with chelated iron for certain chelator chemistries (e.g. DFO).

The polyphenol coated PP film's ability to sequester iron from chelate complexes suggests the polyphenol coating had a specific affinity for both ferrous and ferric iron.

7.4.3 Radical Scavenging Capacity

Table 7.2. Surface phenol content (Folin-Ciocalteu) and radical scavenging capacities (ORAC and TEAC) of native PP, chitosan functionalized PP, and polyphenol coated PP (n = 4).

Sample	Surface phenol content (nmol gallic acid eq. cm^{-2})	ORAC (nmol Trolox eq. cm^{-2})	TEAC in phosphate buffer, pH 7 (nmol Trolox eq. cm^{-2})	TEAC in ethanol (nmol Trolox eq cm^{-2})
PP	0.0788 ± 0.085	0.000303 ± 0.063	0.795 ± 0.14	-2.01 ± 0.64
Chitosan Functionalized PP	0.128 ± 0.13	0.453 ± 0.47	0.795 ± 0.38	-2.29 ± 0.40
Polyphenol Coated PP	15.7 ± 0.43	3.51 ± 0.77	10.8 ± 1.7	52.9 ± 1.8

In addition to metal chelating properties, polyphenols are known to have radical scavenging capacity that contribute to their overall antioxidant capacity. Free radical scavenging capacity of the polyphenol coated PP films was evaluated using adaptations of the following assays: oxygen radical absorbance capacity (ORAC) and trolox equivalent antioxidant capacity (TEAC).[153] ORAC quantifies the ability of antioxidants to scavenge radicals by hydrogen atom transfer reaction, whereas TEAC quantifies an antioxidant's ability to stabilize radicals by electron transfer. Performing both free radical scavenging assays enables us to draw conclusions about which radical scavenging mechanism is favored by surface immobilized polyphenols. Polyphenol coated PP exhibited significantly higher radical scavenging capacity for both ORAC and TEAC assays than native PP and chitosan functionalized PP (**Table 7.2**). The radical scavenging capacities of polyphenol coated PP under conditions that favor hydrophilic antioxidants (ORAC and

TEAC in phosphate buffer) were less than the surface phenol content, which suggests that radical scavenging capacity may be limited to surface phenols. Higher radical scavenging capacity was observed by TEAC assay than ORAC assay. This finding suggests that radical scavenging by polyphenol coated materials may have proceeded more readily by electron transfer than hydrogen atom transfer reactions. The low ORAC value of polyphenol coated PP may also be due to diffusion limitations of surface immobilized antioxidants to quench active degradation induced by peroxyl radicals. TEAC assay was further conducted in ethanol to generate conditions that are favorable to lipophilic antioxidants. TEAC was significantly higher in ethanol than TEAC in neutral phosphate buffer and surface phenol content. These results suggest that lipophilic conditions improve accessibility of phenols entrapped within the polyphenol coating to enhance overall radical scavenging capacity. Arrua, et al. [113] quantified the radical scavenging capacity of caffeic acid polymers grafted onto PP and similarly observed higher radical scavenging capacity of surface grafted phenols in lipophilic media compared to hydrophilic media. Overall, ORAC, TEAC, and iron chelating assay of the polyphenol coated PP suggest that both radical scavenging and metal chelating potentially contribute to the overall antioxidant capacity of polyphenol coated PP.

7.4.4 Lipid Oxidation

An accelerated lipid oxidation study was performed at 37°C in soybean oil-in-water emulsions at pH 4.0 to assess the ability of polyphenol coated PP to inhibit lipid rancidity. Emulsion alone and emulsion with clean PP were negative controls, whereas emulsion with EDTA (0.08 mM, FDA maximum legal limit)[20] and catechin (0.08 mM, equivalent of iron chelating capacity of polyphenol coated PP) were positive controls. None of the treatments

had a significant effect on the physical stability of the emulsions as determined by comparing particle size and zeta potential on 0 d and 20 d (**Table D1**).

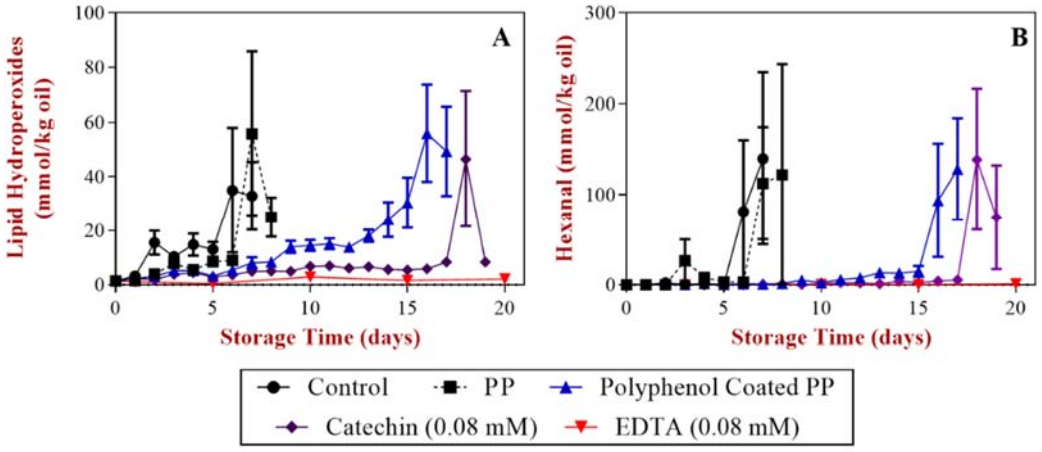

Figure 7.4. (a) Lipid hydroperoxide and (b) hexanal concentrations of soybean oil-in-water emulsions (pH 4.0) stored at 37 °C for 20 days (n=3).

The ability of polyphenol coated PP to inhibit lipid oxidation was determined by quantifying the lag phase of formation for lipid hydroperoxides (primary oxidation product) and hexanal (secondary oxidation product) (**Figure 7.4**). Lag phase was defined as the storage time before a statistically significant increase in concentration of oxidation products. The emulsion alone and emulsion with clean PP oxidized rapidly, with lag phases for oxidation product formation of 5 and 6 d, respectively. Polyphenol coated PP extended the lag phase of oxidation product formation to 15 d for both lipid hydroperoxides and hexanal. Emulsion with 0.08 mM catechin (concentration equivalent to the chelating capacity of polyphenol coated PP) exhibited an extended lag phase of 17 d for both lipid hydroperoxides and hexanal. One possible explanation for the longer lag phase of catechin compared to polyphenol coated PP is the diffusional limitations of a surface grafted antioxidant compared to a soluble antioxidant that may reduce overall efficacy. As expected, the emulsion with EDTA did not form oxidation products during the course of

the 20 d accelerated storage study. This lipid oxidation study confirmed that the polyphenol coated PP had antioxidant capacity to inhibit lipid rancidity in oil-in-water emulsions, but it was less reactive than soluble antioxidants (ie: catechin and EDTA).

7.4.5 Lycopene Degradation

The mode of action for polyphenol coated PP to inhibit oxidative degradation was further investigated using lycopene as a model oxidation-sensitive food component. Lycopene is a carotenoid pigment predominantly found in tomatoes that is used in the food industry as a natural color and bioactive in functional foods.[181] Previous research has demonstrated that the primary mechanism for oxidative degradation of lycopene in acidic emulsions is ferric iron promoted oxidation.[175-177] For this study, two models for lycopene degradation were tested: a ferric iron promoted oxidation model emulsion (lycopene emulsion alone) and a radical induced oxidation model (lycopene emulsion with EDTA and a radical initiator, AAPH) to elucidate the antioxidant mechanism of polyphenol coated PP. Lycopene was dispersed into medium chain triglycerides (MCT) rather than soybean oil to minimize co-oxidation reactions.

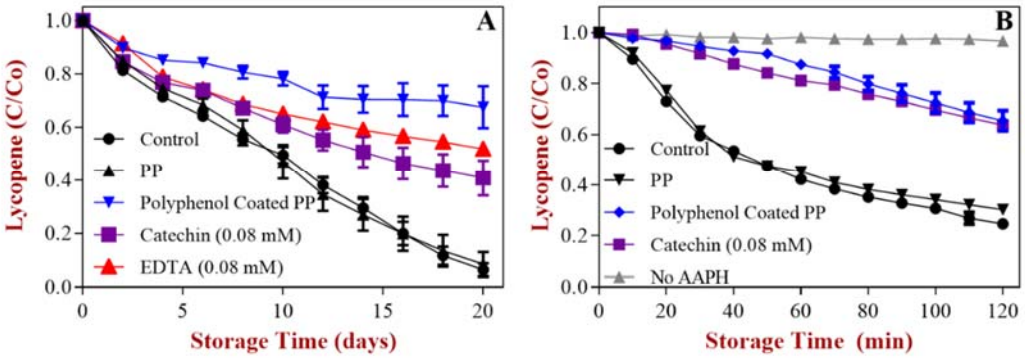

Figure 7.5. Lycopene degradation in oil-in-water emulsions, pH 4.0 at 37°C by (a) ferric iron promoted oxidation and (b) radical induced oxidation. Values represent means ± standard deviations (n=3).

Ferric iron promoted lycopene degradation was quantified by measuring loss of lycopene color in an emulsion (5% w/w oil phase (0.3 mg lycopene/g MCT), 30 mM Tween 20 in 50 mM sodium acetate/imidazole buffer, pH 4.0) during a 20 d storage study conducted at 37°C (**Figure 7.5a**). Similar to the lipid oxidation study, emulsion alone and emulsion with PP were negative controls, whereas emulsion with 0.08 mM EDTA and emulsion with 0.08 mM catechin were positive controls. None of the treatments had a significant effect on the physical stability of the emulsions as quantified by particle size and zeta potential (**Table D1**). As expected, emulsion alone and emulsion with PP film exhibited rapid lycopene degradation. Polyphenol coated PP was more effective than EDTA and catechin at inhibiting ferric iron promoted lycopene degradation during the storage study. After 20 d storage at 37°C, emulsion with polyphenol coated PP retained approximately 68 % lycopene, whereas emulsion with 0.08 mM EDTA retained approximately 52% lycopene and emulsion with catechin retained approximately 41% lycopene. Improved efficacy was hypothesized to be attributed to the partitioning of ferric iron from the emulsion droplet interface onto the polyphenol coated PP surface to impede iron reactivity. In contrast, EDTA/iron and catechin/iron chelate complexes may have some reactivity as soluble chelator complexes are dispersed throughout the emulsion and may interact with the emulsion droplet interface. In fact, it has been reported that at pH 3.0, EDTA can improve the solubility of iron to enhance lycopene degradation in emulsions.[175]

Radical induced lycopene degradation was quantified by measuring loss of lycopene in an emulsion (5% w/w oil phase (0.3mg lycopene/g MCT), 30 mM Tween 20, 0.08 mM EDTA in 50 mM sodium acetate/imidazole buffer, pH 4.0) at 37°C in the presence of a radical initiator, AAPH (10 mg/ml emulsion) (**Figure 7.5b**). The radical

initiator caused lycopene degradation to occur more rapidly than the ferric iron promoted oxidation lycopene model emulsion. Negative controls (emulsion, emulsion with PP film) had a higher initial rate of lycopene degradation compared to emulsion with polyphenol coated PP and emulsion with 0.08 mM catechin, which suggest both soluble and surface bound phenols can inhibit radical induced degradation. This finding is in agreement with previous research, in which tea catechins immobilized in methyl cellulose film protected β-carotene against radical induced degradation.[178] There was no significant difference in the lycopene degradation of emulsion with polyphenol coated PP and emulsion with 0.08 mM catechin. After 2 h at 37°C, both emulsion with polyphenol coated PP and emulsion with 0.08 mM catechin retained approximately 65 % lycopene. This finding is in contrast to what was observed in the ferric iron promoted lycopene degradation model, which further supports the hypothesis that partitioning of iron from emulsion droplets may have a key role in the enhanced inhibition of lycopene degradation by polyphenol coated PP.

7.5 Conclusions

In conclusion, a synthetic route to immobilize polyphenols onto PP film was developed by laccase assisted oxidative polymerization of catechol and catechin onto the surface of chitosan functionalized PP to create nonmigratory polyphenol coated active packaging material. This active packaging material demonstrated both iron chelating and radical scavenging capacity for dual antioxidant functionality. In lipid oxidation studies, polyphenol coated PP films were able to extend the lag phase of oxidation product formation in oil-in-water emulsions 10 d compared to emulsion alone. Polyphenol coated PP inhibited ferric iron promoted lycopene degradation better than soluble chelators, EDTA and catechin, potentially due to partitioning of ferric iron from the emulsion droplet

interface. The application of polyphenols in nonmigratory antioxidant active packaging may enable removal of synthetic preservatives from food and beverage product formulations while maintaining quality and shelf life.

CHAPTER 8

CONCLUSIONS

The overall goal of this work was to synthesize non-migratory metal chelating active packaging materials and demonstrate their ability to inhibit microbial growth and oxidation to extend the shelf life of packaged foods. Metal chelating active packaging materials were synthesized by grafting of metal chelating polymers from the surface of a common food packaging material, polypropylene (PP). Three metal chelating ligand chemistries were investigated for their known affinity for iron: carboxylic acids, hydroxamic acids, and catechols. Iron was chosen a target metal ion because it is a strong prooxidant and essential nutrient for spoilage and pathogenic bacteria. When utilizing the surface modification technique of photoinitiated graft polymerization, it was demonstrated metal chelating polymer chain length and density may be manipulated to tailor ferrous iron chelating capacity. In the case of carboxylic acid functionalized PP (PP-*g*-PAA), polymer chain length influenced overall metal chelating capacity, whereas polymer chain density influenced ligand to metal binding ratio.

Microbial growth is one of the key limiting factors in the shelf life and safety of packaged foods. Potential antimicrobial application of metal chelating active packaging was assessed by examining the ability of PP-*g*-PAA to enhance the antimicrobial activity of lysozyme against *Listeria monocytogenes*. The antimicrobial interaction of PP-*g*-PAA and lysozyme depended on growth media composition at neutral pH. At low ionic strength, PP-*g*-PAA hindered lysozyme activity (2.48 log increase at 64.4 mM total ionic strength), whereas lysozyme activity was enhanced by PP-*g*-PAA at high ionic strength (5.22 log reduction at 120 mM total ionic strength). It is hypothesized that, at neutral pH, carboxylic

acid functionalized PP films (PP-*g*-PAA, pKa^{bulk} 6.45) and lysozyme (pI 11.35) antimicrobial activity is optimal in moderate to high ionic strength environments to reduce undesirable charge interactions (e.g. protein fouling). Furthermore, these findings suggest that a metal chelating active packaging material with lower effective charge under neutral conditions, such as PP-*g*-PHA (pKa^{bulk} 9.65), may be more effective to enhance the activity of food antimicrobials.

Performance stability of metal chelating active packaging relies on the retained activity of the surface grafted chelator in complex food systems. The performance stability of PP-*g*-PHA was investigated by evaluating the influence of pH value (3.0 to 5.0), competing ions (Na^+, Mg^{2+}, Ca^{2+}), food viscosity (~1 to 10^5 mPa·s), and hydrocolloid chemistry on ferric iron chelating capacity. Maximum iron chelating capacity was observed at pH 5.0 (102 ± 9.7 nmol Fe^{3+} cm^{-2}) and reduced by 29% and 77% at pH 4.0 and 3.0, respectively. PP-*g*-PHA retained iron chelating capacity in the presence of sodium, magnesium and calcium competing ions, although at pH 5.0 the presence of calcium reduced iron chelation. Although maximum iron chelating capacity was reduced in viscous solutions (>10^2 mPa·s), PP-*g*-PHA retained at least 76% iron chelating capacity. When in contact with food hydrocolloids with specific affinity for iron, materials retained 32-45% iron chelating capacity. It is important to note that such competitively chelating food hydrocolloids may support antimicrobial and antioxidant systems in food products. These findings suggest that surface grafted hydroxamic acids may retain functionality in complex food products.

Polyphenols have been widely researched as direct additives to control oxidation in foods because they possess catechol metal chelating ligands and radical scavenging

phenolic ligands that provide dual antioxidant functionality. A synthetic route was explored to polymerize phenols (catechol and catechin) onto the surface of polypropylene films by oxidative polymerization to create a polyphenol coated active packaging material. Polyphenol coated active PP demonstrated both iron chelating (39.3 ± 2.5 nmol Fe^{3+} cm^{-2}, pH 4.0) and radical scavenging capacity (3.51 ± 0.77 nmol Trolox eq. cm^{-2}, ORAC). However, iron chelating capacity of polyphenol coated PP was not as stable at low pH value as PP-*g*-PHA (polyphenol coated PP: 13% maximum ferric iron chelating capacity at pH 3.0; PP-g-PHA: 23% maximum ferric iron chelating capacity at pH 3.0). Polyphenol coated PP tripled the lag phase of lipid oxidation in oil-in-water emulsions (pH 4.0) in accelerated storage studies. Lycopene degradation in oil-in-water emulsions (pH 4.0), where ferric iron is the primary prooxidant, was inhibited by polyphenol coated PP. Indeed, polyphenol coated PP inhibited lycopene degradation better than soluble chelators, EDTA and catechin, possibly due to partitioning of ferric iron from the emulsion droplet interface to the packaging surface.

In conclusion, this work demonstrates the synthesis and characterization of non-migratory metal chelating active packaging materials that contain carboxylic acid, hydroxamic acid and catechol ligands. Non-migratory metal chelating active packaging materials retained iron chelating capacity under conditions typically found in packaged food products (ie: pH, counter-ions, competitive chelating ingredients, viscosity) and exhibited antimicrobial and antioxidant efficacy. Such active packaging technology may be used to reduce synthetic additive use in packaged foods without loss of food quality and safety.

CHAPTER 9

FUTURE WORK

The non-migratory metal chelating active packaging materials that were developed and characterized in this dissertation research have demonstrated potential to preserve foods while reducing use of synthetic additives, such as EDTA. However, further research is recommended to optimize design and overcome practical challenges of commercialization of such active packaging technology.

9.1 Improving Material Chemistry

A variety of metal chelating polymers with different metal chelating ligand chemistries (ie: carboxylic acid, hydroxamic acid, catechol) were explored in this dissertation work. Each chelator chemistry exhibited drawbacks that warrant further investigation in improving material chemistry. For example, although carboxylic acid functionalized PP (PP-*g*-PAA) enhanced the antimicrobial activity of lysozyme, it could do so only under certain ionic strength conditions that minimized protein fouling onto the packaging food contact surface. Optimization of material chemistry may involve further characterization of metal chelating polymer chemistry, such as pKa, stability constants, and molecular weight, and relating those parameters to material functionality and performance. Additionally, exploring surface grafting of fouling resistant polymers, combinations of metal chelating polymers and antimicrobials (e.g. lysozyme, nisin, polylysine), and other metal chelating polymers may be useful in design of material chemistry for specific intended applications.

9.2 Efficacy in Real Food Matrices

Thus far, non-migratory metal chelating active packaging materials have only been evaluated in model food systems in order to identify specific factors that may limit applications and address those limitations in the improvement of material chemistry. However, it is important to demonstrate that non-migratory metal chelating active packaging materials can inhibit oxidation and microbial growth in real food matrices that currently use EDTA as a preservative, such as beverages, salad dressings, sauces and mayonnaise. Understanding in which real food matrices non-migratory metal chelating active packaging materials are effective may give further insight to improve chemistry and drive technology development.

9.3 Evaluating Chemical Food Safety

An important consideration for the development of active packaging materials that are intended for use with food and beverages is chemical food safety. Although metal chelating active packaging materials are designed to be non-migratory by covalent attachment of metal chelating polymers to the food contact surface, there is still potential for migration. For example, poly(hydroxamic acid) has the potential to hydrolyze and release hydroxylamine into the food matrix. Therefore, formal migration study using standard food simulants (water, 3% acetic acid, 15% ethanol, olive oil, iso-octane, and 95% ethanol) as per FDA and EU regulations should be performed to confirm metal chelating active packaging materials are indeed ‘non-migratory’ and does not pose a safety risk.

9.4 Scaling Up Packaging Production

The research presented in this dissertation is intended to guide in the development of metal chelating active packaging for commercial application in the food industry. As

such, fabrication methods should be improved to translate to commercial production of both flexible and rigid packaging materials. Incorporation of metal chelating polymers into an ink that can be applied to the packaging surface by gravure printing is a potential method that can be explored for roll-to-roll processing of flexible packaging. Functionalization of activated polymers with metal chelating ligands by melt functionalization can be explored to create metal chelating polymers that may be formed into a parison for blow molding of rigid packaging or as a component of multilayer packaging. Prior to scale up, the influence of metal chelating polymers on bulk material properties (thermostability, barrier) should be evaluated as any significant change in these properties would significantly influence material processability and permeability.

APPENDIX A: IRON CHELATING ACTIVE PACKAGING: INFLUENCE OF COMPETING IONS AND PH VALUE ON EFFECTIVENESS OF SOLUBLE AND IMMOBILIZED HYDROXAMATE CHELATORS[6]

The following work was conducted in collaboration with Yoshiko Ogiwara under the guidance of Julie M. Goddard and Eric A. Decker. The author of this dissertation outline made the following contributions: experimental design, ICP-MS sample preparation and data collection, data interpretation, and manuscript revision.

A.1 Abstract

Many packaged foods utilize synthetic chelators (e.g. ethylenediaminetetraacetic acid, EDTA) to inhibit iron-promoted oxidation or microbial growth which would result in quality loss. To address consumer demands for all natural products, we have previously developed a *non-migratory* iron chelating active packaging material by covalent immobilization of polyhydroxamate and demonstrated its efficacy in delaying lipid oxidation. Herein, we demonstrate the ability of this hydroxamate-functionalized iron chelating active packaging to retain iron chelating capacity; even in the presence of competing ions common in food. Both immobilized and soluble hydroxamate chelators retained iron chelating capacity in the presence of calcium, magnesium, and sodium competing ions, although at pH 5.0 the presence of calcium reduced immobilized hydroxamate iron chelation. A strong correlation was found between colorimetric and mass spectral analysis of iron chelation by the chelating packaging material. Such chelating active packaging may support reducing additive use in product formulations, while retaining quality and shelf life.

[6] The contents of this chapter have been published: Ogiwara, Y.; Roman, M. J.; Decker, E. A.; Goddard, J. M. Iron chelating active packaging: Influence of counter-ions and pH value on effectiveness of soluble and immobilized hydroxamate chelators. *Food Chem.* **2015**, *196,842-847*.

A.2 Introduction

In foods, beverages, and consumer products, the presence of even trace concentrations of transition metals (e.g. Fe, Cu) can cause degradative reactions and support microbial growth which leads to unacceptable changes in product quality. Lipid oxidation, natural color degradation, and nutrient loss are examples of such degradative reactions that ultimately lead to product loss.[182] To inhibit such metal promoted degradation reactions, synthetic chelators (e.g. ethylenediaminetetraacetic acid, EDTA) are commonly incorporated into products.[1] However, as consumers are increasingly demanding products free of synthetic additives in the food and consumer products industries, alternative technologies are needed. Active packaging, in which the packaging performs a role beyond containment, may offer a solution by performing the functional role of additives. Many reported technologies on antioxidant active packaging rely on migration of an active component from the package into the product. For example, common antioxidants, including butylated hydroxyanisole (BHA), butylated hydroxytoluene (BHT), rosemary extract, and δ-tocopherol, were added to low-density polyethylene (LDPE) to preserve color by migration from LDPE film to the surface of fresh beef.[183] In addition, a multilayer packaging, where the innermost layer composed of LDPE with either BHT, BHA, or α-tocopherol designed for antioxidant migration into the food product, demonstrated inhibition of lipid oxidation in whole milk powder [184]. While effective, such *migratory* active packaging technologies (as it pertains to food packaging regulations) would still fall under the classification of direct additive, as the functional agent is intended to become a part of the food product.[37] Recently, our and other groups have explored the concept of *non-migratory* active packaging, in which the active agent is covalently bound

to the packaging material such that it retains activity but is unlikely to migrate to the food product.[30, 113]

We have recently reported on the development of novel non-migratory active packaging materials capable of chelating iron ions at a capacity similar to that of the maximum legal limit of EDTA in beverages.[43, 44, 76, 85, 146] Such materials are designed for application in liquid and semi-liquid foods that are susceptible to oxidation, such as citrus beverages, salad dressing, sauces, and mayonnaise. First generation materials utilized carboxylic acid derived functional groups grafted from the surface of polymer films (ie: polyacrylic acid grafted from polypropylene). While effective in both chelating iron ions and significantly delaying the onset of lipid oxidation at pH values of 5.0 and above, these materials had reduced effectiveness at lower pH values.[146] This result was to be expected due to the pK_a of the chelating moiety (pK_a~6.45), as further explored in detailed studies on their dissociation behavior.[77] To expand the potential application of our non-migratory iron chelating active packaging materials, we then grafted polyhydroxamic acid from the surface of polypropylene films (noted PP-*g*-PHA) and demonstrated greatly improved performance at pH values down to 3.0.[44] What is unique about the hydroxamate chelating moiety compared to other chelating compounds is the well characterized high specificity to iron compared to other ions, as well as its low effective charge (**Figure A.1**).[77, 114] These characteristics suggest that a chelating active packaging material prepared using hydroxamic acid chelators would be effective even in the presence of complex matrix components (e.g. proteins, lipids, carbohydrates, and competing ions) typical of food and consumer products. The goal of the present work was to demonstrate the ability of our PP-*g*-PHA iron chelating non-migratory active packaging materials to perform in the presence

of competing ions (calcium, magnesium, and sodium) at a range of pH values typical of food and consumer products. Additionally, the performance of the PP-*g*-PHA iron chelating packaging material was compared to a soluble analog, deferoxamine (DFO).

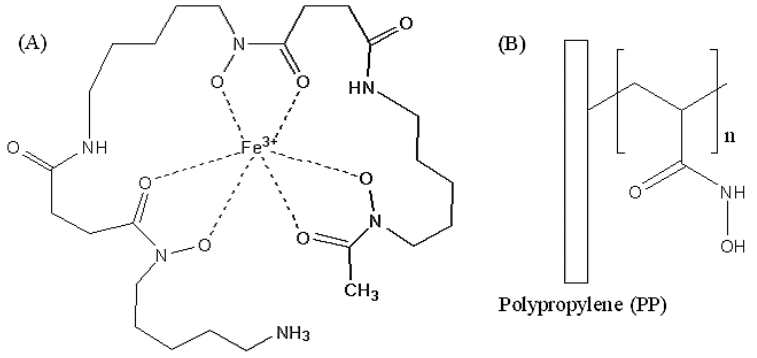

Figure A.1. Chemical structure of (A) soluble DFO/Fe^{3+} complex and (B) PP-*g*-PHA non-migratory iron chelating active packaging material.

A.3 Materials and Methods

A.3.1 Materials

Polypropylene (PP, isotactic, pellets) was purchased from Scientific Polymer Products (Ontario, NY). Isopropanol, acetone, heptane, methanol, sodium acetate trihydrate, ferric chloride hexahydrate, hydrochloric acid, nitric acid (trace metal grade), sodium hydroxide, calcium chloride, and sodium chloride were purchased from Fisher Scientific (Fair Lawn, NJ). Hydroxylamine hydrochloride, magnesium chloride hexahydrate (99%) and imidazole (99%) were purchased from Acros Organics (Morris Plains, NJ). Benzophenone (BP, 99%), deferoxamine mesylate salt (≥ 92.5%, DFO) and methyl acrylate (MA, 99%) were purchased from Sigma-Aldrich (St. Louis, MO). All the chemicals and reagents were used without further purification.

A.3.2 Preparation of Polyhydroxamic acid Grafted Polypropylene Iron Chelating Materials

Polyhydroxamic acid was grafted from the surface of polypropylene (resulting material denoted PP-*g*-PHA) using a method previously reported by Tian et al [85] (**Figure A.1b**), in which polymethyl acrylate (PMA) is grafted from PP via UV initiated graft polymerization, followed by conversion of methyl acrylate groups to hydroxamate chelating moieties by exposure to hydroxylamine. PP pellets were cleaned by sonication in isopropanol, acetone, and deionized water twice for each solvent. Cleaned PP pellets were then pressed into films using Carver Laboratory Press (Model B, Fred S. Carver Inc., NJ) at 170 ºC with a loaded force of 9000 lbs. PP were cut into 8 × 8 cm^2 squares and cleaned by same procedure as cleaned PP pellets. Cleaned PP were dried in a desiccator (25 ºC and 15 % relative humidity) until use.

A two-step photografting process was used to introduce PMA to the surface of PP. In the first step, the photoinitiator BP was covalently grafted to the PP surface. BP (5 wt% in heptane) was spin coated on both sides of the PP. BP coated PP were cut into 2 × 8 cm^2 pieces and placed in septum-fitted screw cap bottles. Nitrogen gas was purged into the bottles for 5 min to remove oxygen. Then, PP were exposed to ultraviolet (UV) irradiation (Dymax, Model 5000 flood, 320-395 nm, 200 mW/cm^2, Dymax Corporation, Torrington, CT) for 90 s. The BP-functionalized PP (PP-BP) were washed three times in acetone for 5 min for each time to remove non-covalently grafted BP. In the second step of the graft polymerization procedure, PP-BP were cut into 1 × 2 cm^2 and submerged in MA solution (70 wt% in acetone) in glass vials with septum-fitted screw caps. Vials were nitrogen purged for 5 min to remove oxygen, then PP-BP were exposed to UV irradiation for 3 min.

The resulting PP-*g*-PMA were extensively cleaned by Soxhlet extraction (150 mL acetone, 12 h) to remove any residual monomer and non-covalently grafted PMA homopolymers.[185]

Ester groups on the surface of PP-*g*-PMA were converted to hydroxamic acid by reaction with hydroxylamine, to produce the final PP-*g*-PHA iron chelating active packaging materials.[98, 99] Hydroxylamine reagent was prepared by neutralizing hydroxylamine hydrochloride solution (20 wt% in 5:1 methanol:water) to pH 13 by sodium hydroxide followed by removal of sodium chloride precipitate by Buchner filtration. PP-*g*-PMA were submerged in hydroxylamine solution in a flask equipped with a reflux condenser, and the hydroxyamidation reaction was conducted at 73 ºC for 4 h with stirring. After reaction, PHA-grafted PP materials (PP-*g*-PHA) were washed three times in methanol/water (5:1) for 30 min for each time, treated in hydrochloric acid solution [0.2 M in methanol/water (5:1)] for 5 min, washed three times in methanol/water (5:1), and finally washed three times in deionized water for 30 min for each time to remove residual compounds. PP-*g*-PHA were stored in a desiccator (25 ºC, 15% RH) until use.

A.3.3 Characterization of Material Surface Chemistry

The surface chemistry of PP, PP-*g*-PMA, and PP-*g*-PHA was analyzed by an attenuated total reflectance Fourier transform infrared (ATR-FTIR) spectrometer equipped with a diamond ATR crystal (IRPrestige-21, Shimadzu Scientific Instruments, Inc., Kyoto, Japan). Each spectrum was collected with 32 scans at a 4 cm^{-1} resolution. The representative spectrum of each sample reported in this work was replotted with SigmaPlot 12.0 (Systat Software, Inc., Chicago, IL).

A.3.4 Iron Chelating Capacity of Soluble Hydroxamate Chelators

Hydroxamic acids develop a characteristic reddish brown color when they chelate iron.[186-188] Therefore, the effect of pH value on ferric (Fe^{3+}) chelating activity of DFO was investigated by colorimetric quantification of the stability of the DFO/Fe^{3+} complex. DFO and ferric chloride were combined at the reported ligand:metal binding ratio of 1:1[189] at concentrations up to 1.0 mM in 0.05 M sodium acetate/imidazole at pH 3.0, 4.0, or 5.0. Experiments were not conducted above pH 5.0 due to precipitation of iron from the solution. The effect of competing ions on DFO ferric iron chelating activity was investigated by addition of the following salts to the DFO/Fe^{3+} reaction solutions (0.5 mM DFO and 0.5 mM ferric chloride in 0.05 M sodium acetate/imidazole, pH 3.0, 4.0, or 5.0): 35 mM $CaCl_2$, 10 mM $MgCl_2$, or 0.8 M NaCl. Competing ion concentration was determined based on the concentration of metal ion in milk, hard water, and salad dressing for calcium, magnesium, and sodium, respectively.[190-192] The reaction solutions were incubated for 48 h in the dark at room temperature, and the absorbances were quantified at 430 nm.

A.3.5 Iron Chelating Capacity of Polyhydroxamic acid Grafted Polypropylene Active Packaging Materials

Effect of pH on ferric (Fe^{3+}) chelating activity of PP-*g*-PHA active packaging material was investigated by quantifying the color difference (ΔE^*) of material color before and after Fe^{3+} chelate reaction. As with soluble hydroxamate moieties, immobilized hydroxamate groups turn a characteristic reddish-brown upon complexing with iron, which can be quantified using colorimetry (and confirmed by direct mass spectral quantification as noted below). The Fe^{3+} chelating reaction solution was prepared with 0.08 mM ferric chloride in 0.05 M sodium acetate/imidazole at pH values of 3.0, 4.0, or 5.0 to minimize

iron precipitation during the reaction time necessary to reach immobilized hydroxamate maximum iron chelating capacity. Effect of competing ion on Fe^{3+} chelating activity of PP-*g*-PHA was investigated by addition of the following salts to the Fe^{3+} chelating reaction solutions described above: 35 mM $CaCl_2$, 10 mM $MgCl_2$, or 0.8 M NaCl. Packaging materials (native PP, PP-*g*-PHA; 1 × 2 cm^2) were submerged in the appropriate Fe^{3+} solutions (10 mL) in the dark with shaking at room temperature for up to 48 hours. PP-*g*-PHA submerged in 0.05 M sodium acetate/imidazole (10 mL at pH 3.0, 4.0, or 5.0) without iron served as negative controls. After incubation, materials were washed three times in deionized water, and then dried in desiccator for 24 h at room temperature.

The color coordinates (L^*, a^*, and b^*) of packaging materials were measured by a colorimeter (ColorFlex EZ, HunterLab, Reston, VA) with a tristimulus absorption filter in which L^* represents the lightness (value ranging from 0-pure black to 100-pure white), a^* refers to the color change from greenness (negative values) to redness (positive values), and b^* value is a measure of the color from blueness (negative values) to yellowness (positive values).[193] Color difference (ΔE^*) between the material before (L_0^*, a_0^*, and b_0^*) and after chelating Fe^{3+} (L_t^*, a_t^*, and b_t^*) was calculated by eq 1.

$$\Delta E^* = [(L_0^* - L_t^*)^2 + (a_0^* - a_t^*)^2 + (b_0^* - b_t^*)^2]^{1/2} \quad (1)$$

Additionally, selected treatments of PP and PP-*g*-PHA were analyzed for iron chelating activity by inductively coupled plasma-mass spectroscopy (ICP-MS). PP samples were prepared for ICP-MS analysis using a standard method for analysis of lead in non-metal children's products.[126] Approximately 150 mg of the native PP or PP-*g*-PHA (1 x 2 cm^2 pieces) were weighed directly into microwave digestion vessels (Mars Xpress 75ml vessels, CEM, Matthews, NC) and nitric acid (5 ml) was added to each vessel. Calibration

standards were prepared with iron solution (1,000 ppm Iron ICP-MS Standard, Ricca Chemical Company, Arlington, TX) and clean PP. The microwave digestion was conducted in the Mars Xpress (CEM, Matthews, NC) and is as follows: ramp to 210°C for 20 min, hold at 210°C for 10 min, and cool for 10 min. Digested samples were transferred to 50 ml centrifuge tubes, diluted with deionized water, and held at 4°C until analysis. ICP-MS analysis was conducted on a Perkin Elmer Elan 9000 equipped with an autosampler (Waltham, MA).

A.4 Results and Discussion

A.4.1 ATR-FTIR Analysis of Material Surface Chemistry

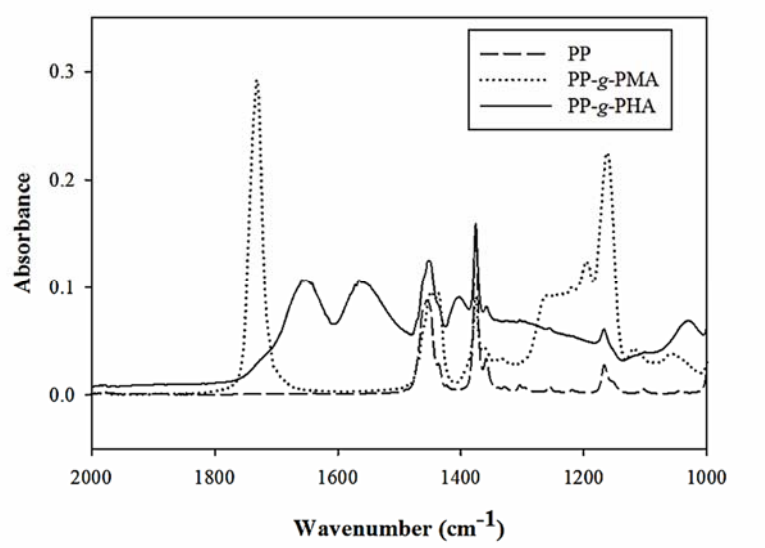

Figure A.2. ATR-FTIR spectra of PP, PP-*g*-PMA, and PP-*g*-PHA films from 1000-2000 cm^{-1}.

The surface chemistry of PP, PP-*g*-PMA, PP-*g*-PHA was analyzed by ATR-FTIR to confirm successful synthesis of PP-*g*-PHA iron chelating active packaging materials (**Figure A.2**). PP-*g*-PMA presented new absorption bands at 1735 and 1200 cm^{-1}, characteristic of the expected C=O and C-O of ester groups, respectively, confirming successful grafting of PMA from PP. After conversion to PP-*g*-PHA, the absorption band at 1735 cm^{-1} disappeared and new bands at 1649 and 1554 cm^{-1} appeared, corresponding

to C=O stretching vibrations and a combination of N-H bending vibration and C-N stretching vibration of amide groups, respectively. The introduction of absorbances characteristic of hydroxamate functionality in PP-*g*-PHA confirms successful conversion from PMA to PHA groups at the surface of the PP.

A.4.2 Influence of Competing ion and pH Value on Iron Chelating Capacity of Soluble Hydroxamate Chelators

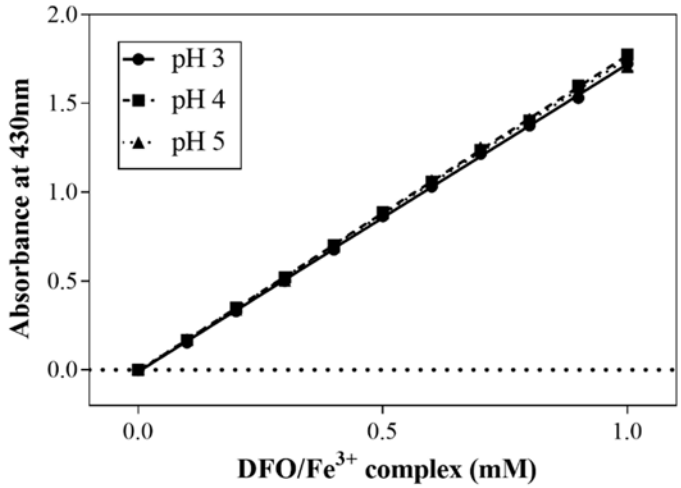

Figure A.3. Influence of increase concentration of DFO/Fe^{3+} complex in solution on absorbance at 430 nm. Error bars represent standard deviation (n=3). Error bars are smaller than data points.

As previously noted, the DFO/Fe^{3+} complex exhibits a characteristic reddish brown color (absorption maximum 430 nm) which enables its colorimetric quantification by spectrometry. The absorbance of the solution containing DFO and Fe^{3+} at concentrations ranging from 0 to 1.0 mM was measured to investigate the effect of pH on the stability of DFO/Fe^{3+} in solution (**Figure A.3**). A linear correlation was observed, with a slope of approximately 1.75 at each pH value tested. These results suggest that up to 1.0 mM concentration of both DFO and ferric iron, pH value does not influence the stability of the DFO/Fe^{3+}complex. In the absence of iron, absorbance of 1.0 mM DFO solutions were negligible.

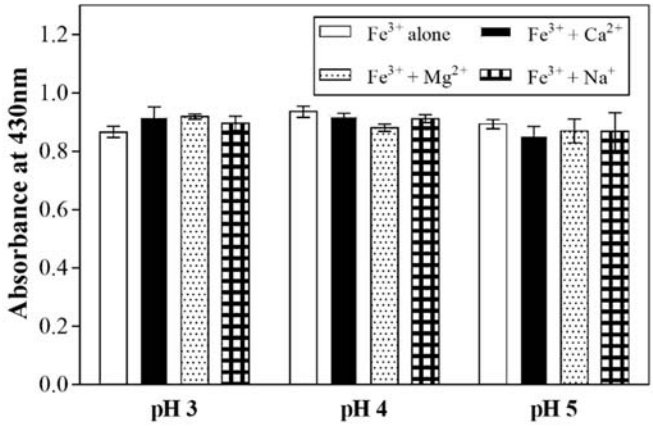

Figure A.4. Effect of competing ion and pH on DFO/Fe^{3+} complex in solution after 48 h incubation. Error bars represent standard deviation (n=3).

The effect of competing ion on the stability of DFO/Fe^{3+} complex in solution was demonstrated by quantifying the absorbance of 0.5 mM DFO and Fe^{3+} in 0.05 M sodium acetate/imidazole in the presence of competing ions (**Figure A.4**). There was no significant difference in solution absorbances among treatments, suggesting that the DFO/Fe^{3+} complex is highly stable in the solution regardless of the pH value and presence of competing ion. Our interest in hydroxamate chelators stems from the well characterized specificity of DFO to iron based on metal complex stability. Indeed the stability constant for the complexes formed between DFO and Fe^{3+} (30.4) is much higher than the stability constants for DFO/Ca^{2+} (3.03) and DFO/Mg^{2+} (2.8).[114] Our results correspond well to the reported stability constants of DFO.

A.4.3 Influence of Competing ion and pH Value on Iron Chelating Capacity of Polyhydroxamic acid Grafted PP Materials

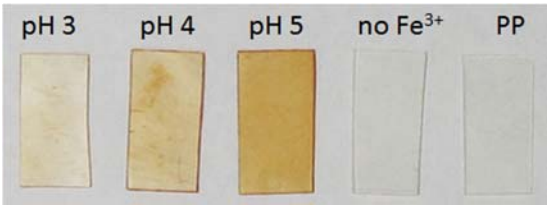

Figure A.5. PP-*g*-PHA film after 48 h incubation at pH 3, 4, and 5 in Fe^{3+} solution, PP-*g*-PHA film after 48 h incubation in buffer solution at pH 5, and PP film after 48 h incubation at pH 5 in Fe^{3+} solution.

The Fe^{3+} chelating activity of PP-*g*-PHA was quantified both by a colorimetric method and ICP-MS. As noted above, it is well characterized that hydroxamate chelators turn reddish brown after complexing with iron, and this color change was observed in our hydroxamate derived iron chelating PP-*g*-PHA materials as well (**Figure A.5**). This color change is specific to the hydroxamate/iron complex as PP-*g*-PHA incubated in buffer alone, and PP incubated in iron solution remain transparent. Prior work has shown that after 24 h incubation of PP-*g*-PHA with Fe^{3+} and presence or absence of competitive chelators, the material present a difference in color intensity that correspond with results of a colorimetric characterization of iron content in solution (ferrozine assay).[44] On the basis of these qualitative results, we developed a method to correlate color development (quantified by colorimetry) to iron chelation (directly quantified by ICP-MS). The color difference (ΔE^*) of native and PP-*g*-PHA before and after Fe^{3+} chelation was plotted against iron contents determined by inductively coupled plasma-mass spectroscopy (ICP-MS) (**Figure A.6**). A strong quadratic correlation between ΔE^* and iron content measured by ICP-MS was determined (R^2 of 0.903), confirming that colorimetric characterization can be used to effectively quantify iron chelation by PP-*g*-PHA.

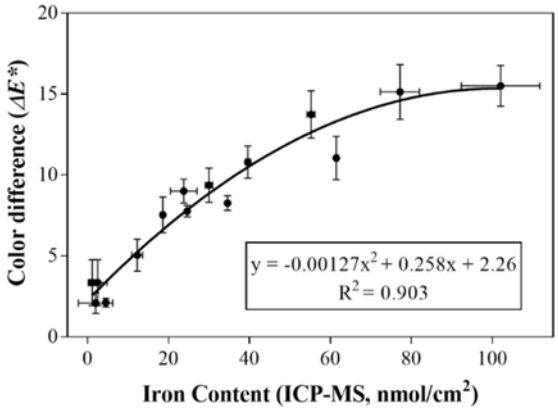

Figure A.6. Correlation between PP-*g*-PHA film color difference (ΔE^*) and iron content measured by ICP-MS. Error bars represent standard deviation (n=4). In some instances, error bars are smaller than data points.

PP-*g*-PHA incubated in Fe^{3+} chelating reaction solution exhibited a reddish brown color regardless of pH, with the color intensity of PP-*g*-PHA incubated in Fe^{3+} reaction solution increasing with increasing pH value (**Figure A.5**). The increasing chelating activity with pH value was further confirmed by ICP-MS quantification, supporting our colorimetric results (**Figure A.7**). At pH 3.0, PP-*g*-PHA exhibited approximately 23 % of the maximum chelating activity observed at pH 5.0 (102 ± 9.7 nmol/cm^2 iron), while PP-*g*-PHA at pH 4.0 exhibited approximately 61 % of the maximum observed chelating activity. Minimal iron was detected on control material (PP-*g*-PHA incubated in buffer without iron and native PP incubated with buffer with iron). The presence of slight iron on PP that increases with pH value is likely a result of pH induced precipitation of soluble iron from solution, but is orders of magnitude lower than the iron content observed in PP-*g*-PHA, suggesting that the iron quantified on PP-*g*-PHA is a result of hydroxamate specific iron chelation. These results are in support of other reports; for example, Haron, et al. [194] reported a maximum loading of PHA with Fe^{3+} attained at pH 4.75. Our results indicate the optimum pH value for Fe^{3+} chelating by PP-*g*-PHA to be 5.0 which is similar to previous reports.[85] At pH values greater than 5.0, iron precipitated from the reaction solution during the time it took for the immobilized hydroxamate to reach equilibrium, complicating data interpretation; we therefore limited our investigation to pH values at and below 5.0. This was not an issue for soluble hydroxamate since iron chelation reaction occurs rapidly in solution.

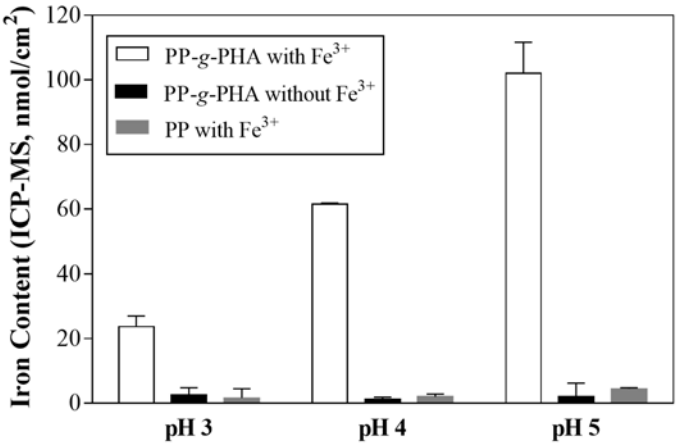

Figure A.7. Effect of pH on chelation of Fe^{3+} by PP-*g*-PHA films. Error bars represent standard deviation (n=4).

Colorimetry was utilized to further characterize the influence of time, pH value, and presence of competing ions (sodium, calcium, and magnesium) on chelating capacity of the PP-*g*-PHA (**Figure A.8**). For each pH value tested, material color difference (ΔE^*) fit a one-phase association exponential model (GraphPad Prism 6.0, La Jolla, CA), suggesting iron chelating reactions followed first order kinetics. Maximum chelation capacity was achieved within 24 hours of exposure to iron solutions. Saturation occurred more quickly at pH values 3.0 and 4.0, although total iron chelation capacity was greatest at pH 5.0, in agreement with ICP-MS results. As with the analysis of soluble hydroxamate chelators, the introduction of sodium and magnesium competing ions did not affect the chelating capacity of immobilized polyhydroxamate chelators of the PP-*g*-PHA. Likewise at pH values 3.0 and 4.0, introduction of calcium had no significant effect on the chelating capacity of PP-*g*-PHA. However, at pH 5.0, the presence of calcium ions reduced the maximum chelating capacity of the PP-*g*-PHA to approximately 22% (22.4 ± 1.3 nmol/cm^2 iron).

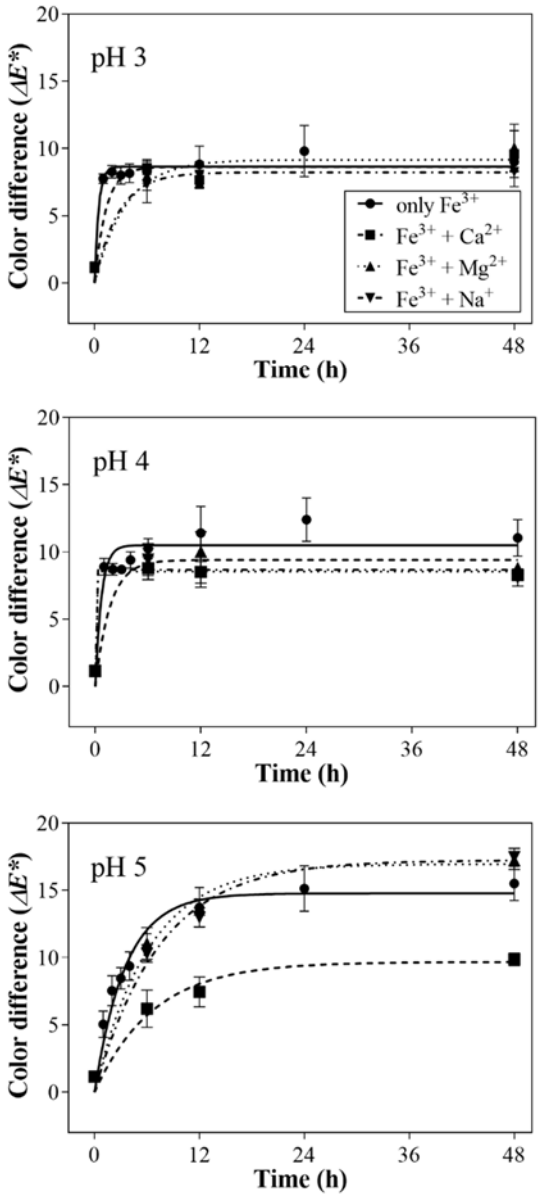

Figure A.8. Effect of competing ion on PP-*g*-PHA film Fe^{3+} chelating kinetics as measured by color difference (*ΔE**) at pH 3.0, 4.0, and 5.0. Error bars represent standard deviation (n=4). In some instances, error bars are smaller than data points.

These results are in contrast with those of soluble hydroxamate chelators as observed in this study (**Figure A.4**). However, these findings are in agreement with other reports on solid support bound chelators. Polomoscanik, et al. [195] evaluated the effect of competing ions on hydroxamic acid-containing hydrogels at pH 5.7 and found that when

calcium was in excess (89 times ferrous iron concentration), iron chelating capacity was reduced 74%. It is hypothesized that the observed discrepancy between soluble and solid support bound hydroxamate chelators may be structure related. The high binding constant and specificity of deferoxamine to iron is a result of its unique chemical structure. While the grafted polyhydroxamate chelating moieties are expected to have similar chemistry to soluble hydroxamate chelators,[77] there is inherent difference in graft chain length, degree of cross-linking, and local chain mobility which cause steric restrictions that may affect not only chelating kinetics and capacity, but also specificity.[196] Nevertheless, our results suggest that the PP-*g*-PHA chelating active packaging materials are effective in chelating iron specifically, even in the presence of competing ions commonly found in food and consumer products and the environment.

A.5 Conclusions

We have synthesized iron chelating active packaging materials by the UV initiated graft polymerization of polymethyl acrylate from polypropylene, followed by conversion to polyhydroxamate chelating grafts in aqueous hydroxylamine. The PP-*g*-PHA iron chelating materials were able to chelate iron at pH values down to 3.0, with maximum chelating capacity at pH 5.0, above which precipitation of iron from solution began to occur. Both immobilized and soluble hydroxamate chelators retained iron chelating capacity even in the presence of calcium, magnesium, and sodium competing ions, although at pH 5.0 the introduction of calcium ions reduced iron chelation by PP-*g*-PHA. A colorimetric method to quantify iron chelation in solid support bound hydroxamate chelators was developed with strong correlation to direct ICP-MS quantification of iron content. These results support the potential application of PP-*g*-PHA iron chelating non-

migratory active packaging materials for preventing iron promoted degradative reactions in packaged products. Such non-migratory active packaging technologies may offer an alternative strategy to using synthetic additives in food and consumer products, while retaining product quality and shelf life.

APPENDIX B: SUPPLEMENTARY MATERIAL FOR CHAPTER 2

Table B.1. Water contact angles of native polypropylene (PP), benzophenone activated polypropylene (PP-BP) and poly(acrylic acid) on polypropylene (PP-*g*-PAA) films. Values are means ± standard deviations (n=6). Letters denote significant differences ($p<0.05$).

Variable	Test Parameters	Advancing Angle	Receding Angle	Hysteresis
Native PP		101.5 ± 5.8[a]	75.1 ± 7.1[a]	26.4
PP-BP		103.5 ± 5.7[a]	83.3 ± 3.1[a]	20.2
Control Parameters		42.4 ± 2.1[d]	14.6 ± 1.2[f]	27.8
Benzophenone Concentration	3%	55.9 ± 3.3[c]	16.3 ± 3.2[e,f]	39.6
	1%	69.7 ± 4.3[b]	36.4 ± 2.9[b,c]	33.3
Benzophenone Graft Time	1 min	72.9 ± 6.2[b]	35.0 ± 7.4[b,c]	37.9
	0.5 min	39.9 ± 3.5[d,e]	16.5 ± 3.4[e,f]	23.4
Acrylic Acid Concentration	30%	56.4 ± 5.7[c]	29.0 ± 4.5[c,d]	27.4
	20%	32.0 ± 2.2[e]	14.0 ± 2.4[f]	18.0
	15%	64.7 ± 2.2[b]	26.8 ± 2.7[c,d]	37.9
	10%	71.7 ± 4.9[b]	42.6 ± 3.8[b]	29.1
Acrylic Acid Graft Time	4.5 min	43.3 ± 3.2[d]	12.5 ± 2.9[f]	30.8
	3 min	52.8 ± 4.6[c]	24.9 ± 9.0[d,e]	27.9
	1.5 min	63.9 ± 2.0[b]	24.9 ± 3.4[d,e]	39.0

APPENDIX C: SUPPLEMENTARY MATERIAL FOR CHAPTER 4

Table C.1. ATR-FTIR spectral band assignment for PP-*g*-PAA. All bands present in the FTIR spectra were attributed to PAA brushes and the base material, PP, except for a band at 700 cm^{-1}, which is attributed to the aromatic ring of the photoinitiator, benzophenone, used to active PP for surface polymerization.

Band	PP-*g*-PAA Protonated (pH 2.99)	PP-*g*-PAA Deprotonated (pH 8.87)	PP-*g*-PAA/Fe Complex (pH 5)
C=O	1710	1566 1411	1710 1589 1547
C-O	1255	1255	1255
O-H	1043		
Fe-O			631
C-C, C-H	1454 1375 1357 1166 997 972 898 840 808 750	1454 1375 1357 1166 997 972 898 840 808 750	1454 1375 1357 1166 997 972 898 840 808 750
Aromatic ring	700	700	700

Table C.2. ATR-FTIR spectral band assignment for PP-*g*-PHA. All bands present in the FTIR spectra were attributed to PHA brushes and the base material, PP.

Band	PP-*g*-PHA Protonated (pH 5.98)	PP-*g*-PHA Deprotonated (pH 12.8)	PP-*g*-PHA/Fe Complex (pH 5)
C=O	1649	1612	1720 1678
C-NH	1554 1318	1554 1318	1587 1531 1207
N-O	1031	1033	1049
Fe-O			631
C-C, C-H	1454 1375 1357 1166 997 972 898 840 808 750	1454 1375 1357 1166 997 972 898 840 808 750	1454 1375 1357 1166 997 972 898 840 808 750

APPENDIX D: SUPPLEMENTARY MATERIAL FOR CHAPTER 7

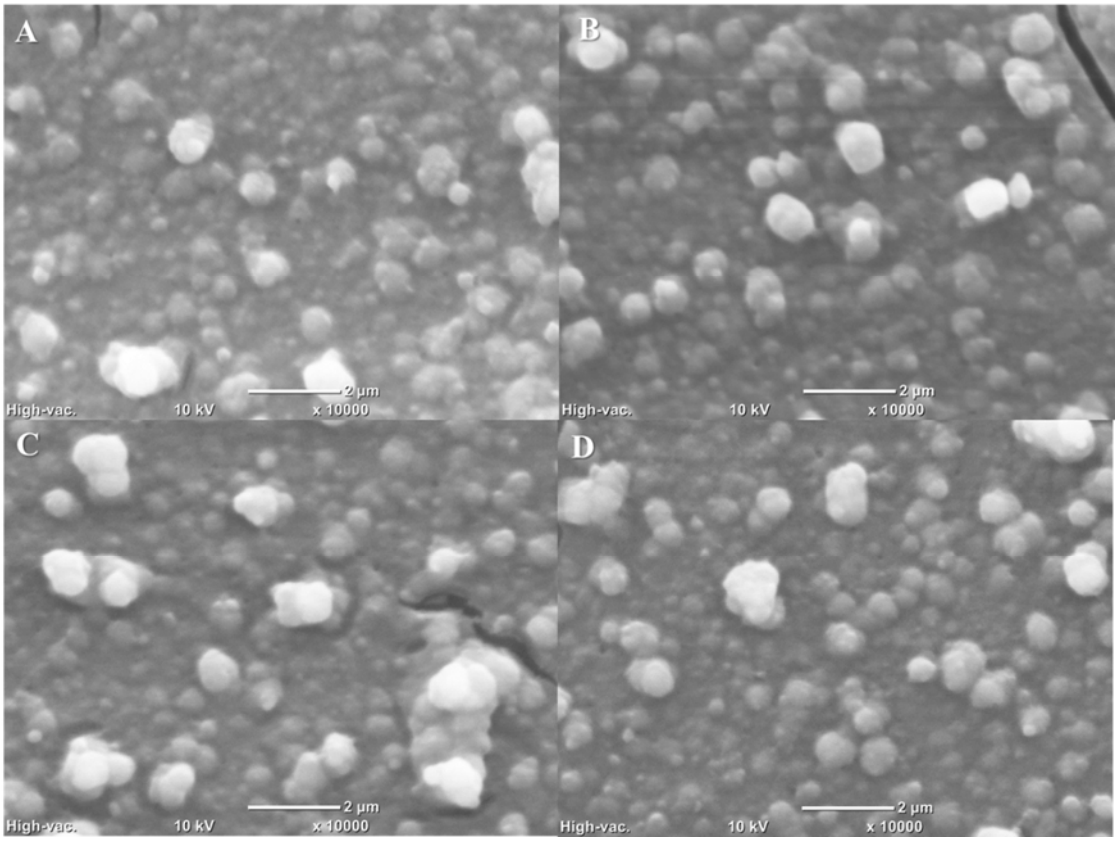

Figure D.1. Representative SEM micrographs of polyphenol coated PP films after incubation in (a) aqueous (DI water), (b) acidic (3% acetic acid), (c) alcoholic (10% ethanol), and (d) fatty (MCT) food simulants at 40°C for 10 d. Micrographs are representative of a total of eight images taken on quadruplicate samples at 10,000x (scale bar is 2 µm).

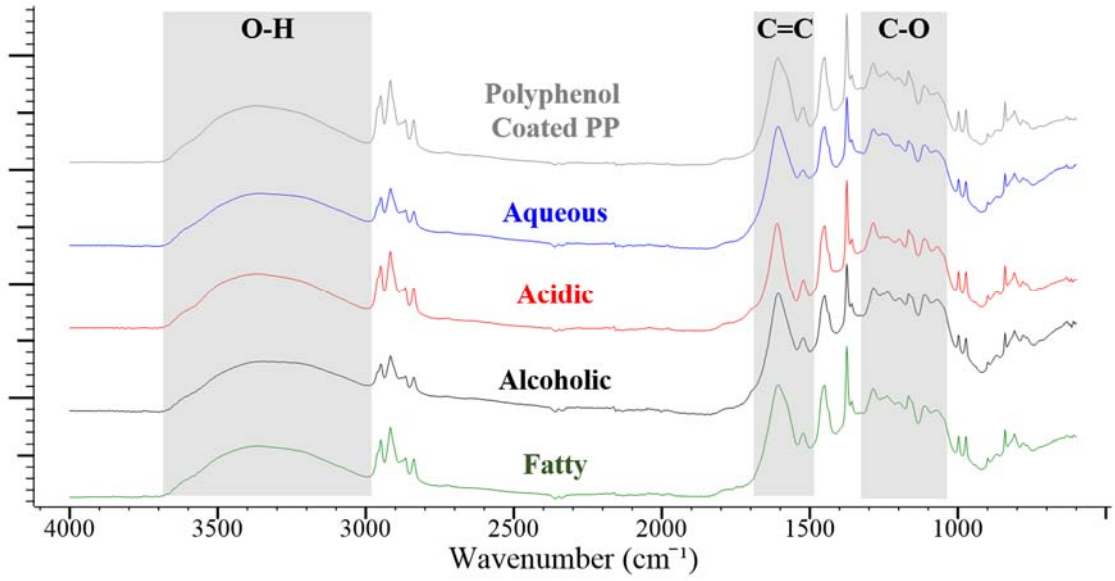

Figure D.2. Representative ATR-FTIR spectra of polyphenol coated PP films before and after incubation in aqueous (DI water), acidic (3% acetic acid), alcoholic (10% ethanol), and fatty (MCT) food simulants at 40°C for 10 d. Spectra are representative of a total of eight spectra collected on quadruplicate samples.

Table D.1. Particle size and zeta potential of oil-in-water emulsions stored for 20 days at 37°C for lipid oxidation and lycopene degradation studies. Values represent mean ± standard deviation (n=3). Significant differences for treatments of each oxidation study are denoted with letters ($p<0.05$).

Oxidation Study	Treatment	Particle Size (nm)	Zeta Potential (mV)
Lipid Oxidation	Original Emulsion (d=0)	202 ± 4.7[a]	-1.41 ± 0.40[a]
	No film	204 ± 7.0[a]	-2.52 ± 0.61[a]
	PP	210 ± 8.4[a]	-2.55 ± 0.65[a]
	Polyphenol Coated PP	192 ± 4.3[a,b]	-2.62 ± 1.8[a]
	Catechin	183 ± 2.4[b]	-1.60 ± 0.62[a]
	EDTA	208 ± 3.5[a]	-1.75 ± 0.48[a]
Lycopene Degradation	Original Emulsion (d=0)	188 ± 4.5[c]	-1.24 ± 0.88[a]
	No film	201 ± 3.3[b]	-1.88 ± 1.1[a]
	PP	215 ± 2.9[a]	-1.30 ± 0.97[a]
	Polyphenol Coated PP	214 ± 7.2[a]	-0.750 ± 0.64[a]
	Catechin	209 ± 2.2[a]	-1.62 ± 0.98[a]
	EDTA	212 ± 5.6[a]	-1.34 ± 0.78[a]

REFERENCES

(1) Hart, J. R. EDTA-type chelating agents in everyday consumer products: Some food, cleaning, and photographic applications. *J. Chem. Educ.* **1985**, *62*, 75.

(2) Sloan, A. E. Coming Clean. *Food Technol.* **2014**, *68*.

(3) Panera Bread. The No No List. https://www.panerabread.com/panerabread/documents/panera-no-no-list-05-2015.pdf (March 30, 2016).

(4) Whole Foods Market. Food Ingredient Quality Standards. http://www.wholefoodsmarket.com/about-our-products/quality-standards/food-ingredient (March 30, 2016).

(5) Frankel, E. N., *Lipid oxidation*. The Oily Press: 2005.

(6) Waraho, T.; McClements, D. J.; Decker, E. A. Mechanisms of lipid oxidation in food dispersions. *Trends Food Sci. Technol.* **2011**, *22*, 3-13.

(7) McClements, D. J.; Decker, E. A. Lipid oxidation in oil-in-water emulsions: Impact of molecular environment on chemical reactions in heterogeneous food systems. *J. Food Sci.* **2000**, *65*, 1270-1282.

(8) Decker, E. A.; McClements, D. J. Transition metal and hydroperoxide interactions: an important determinant in the oxidative stability of lipid dispersions. *Inform* **2001**, *12*, 251-255.

(9) Pasch, J.; Elbe, J. Betanine stability in buffered solutions containing organic acids, metal cations, antioxidants, or sequestrants. *J. Food Sci.* **1979**, *44*, 72-75.

(10) Xu, D.; Wang, X.; Jiang, J.; Yuan, F.; Decker, E. A.; Gao, Y. Influence of pH, EDTA, α-tocopherol, and WPI oxidation on the degradation of β-carotene in WPI-stabilized oil-in-water emulsions. *LWT-Food Sci. Technol.* **2013**, *54*, 236-241.

(11) Buescher, R.; Hamilton, C. Protection of cucumber quality by CaNa2EDTA1. *J. Food Qual.* **2000**, *23*, 429-441.

(12) Ball, G. F., *Vitamins in foods: analysis, bioavailability, and stability*. CRC Press: 2005.

(13) Madhavi, D.; Deshpande, S.; Salunkhe, D. K., *Food antioxidants: Technological: Toxicological and health perspectives*. CRC Press: 1995.

(14) Damodaran, S.; Parkin, K. L.; Fennema, O. R., *Fennema's food chemistry*. CRC press: 2007.

(15) Mei, L.; Decker, E. A.; McClements, D. J. Evidence of iron association with emulsion droplets and its impact on lipid oxidation. *J. Agric. Food Chem.* **1998**, *46*, 5072-5077.

(16) Mei, L.; McClements, D. J.; Wu, J.; Decker, E. A. Iron-catalyzed lipid oxidation in emulsion as affected by surfactant, pH and NaCl. *Food Chem.* **1998**, *61*, 307-312.

(17) Shimoni, E.; Armon, R.; Neeman, I. Antioxidant properties of deferoxamine. *J. Am. Oil Chem. Soc.* **1994**, *71*, 641-644.

(18) Jacobsen, C.; Hartvigsen, K.; Thomsen, M. K.; Hansen, L. F.; Lund, P.; Skibsted, L. H.; Hølmer, G.; Adler-Nissen, J.; Meyer, A. S. Lipid oxidation in fish oil enriched mayonnaise: calcium disodium ethylenediaminetetraacetate, but not gallic acid, strongly inhibited oxidative deterioration. *J. Agric. Food Chem.* **2001**, *49*, 1009-1019.

(19) Rufián-Henares, J. A.; de la Cueva, S. P. Antimicrobial activity of coffee melanoidins: A study of their metal-chelating properties. *J. Agric. Food Chem.* **2009**, *57*, 432-438.

(20) FDA. In *Food additives for direct addition to food for human consumption*, Code of Federal Regulations Title 21 Section 172.120, Washington D.C., 2013; US Government Printing Office: Washington D.C., 2013.

(21) Roman, M. J.; Decker, E. A.; Goddard, J. M. Metal-chelating active packaging film enhances lysozyme inhibition of Listeria monocytogenes. *J. Food. Prot.* **2014**, *77*, 1153-1160.

(22) Branen, J. K.; Davidson, P. M. Enhancement of nisin, lysozyme, and monolaurin antimicrobial activities by ethylenediaminetetraacetic acid and lactoferrin. *Int. J. Food Microbiol.* **2004**, *90*, 63-74.

(23) Boland, J.; Davidson, P.; Bruce, B.; Weiss, J. Cations reduce antimicrobial efficacy of lysozyme-chelator combinations. *J. Food. Prot.* **2004**, *67*, 285-294.

(24) Boland, J.; Davidson, P.; Weiss, J. Enhanced inhibition of Escherichia coli O157: H7 by lysozyme and chelators. *J. Food. Prot.* **2003**, *66*, 1783-1789.

(25) Martell, A. E.; Smith, R. M., *Critical stability constants*. Springer: 1974; Vol. 1.

(26) Pokorný, J. Are natural antioxidants better–and safer–than synthetic antioxidants? *Eur. J. Lipid Sci. Technol.* **2007**, *109*, 629-642.

(27) Mahoney, J. R.; Graf, E. Role of alpha-tocopherol, ascorbic acid, citric acid and EDTA as oxidants in model systems. *J. Food Sci.* **1986**, *51*, 1293-1296.

(28) Robertson, G. L., *Food packaging: principles and practice*. CRC press: 2012.

(29) Nerín, C.; Decker, E.; Elias, R.; McClements, D. Antioxidant active food packaging and antioxidant edible films. *Oxidation in foods and beverages and antioxidant applications. Volume 2: Management in different industry sectors* **2010**, 496-515.

(30) Tian, F.; Decker, E. A.; Goddard, J. M. Controlling lipid oxidation of food by active packaging technologies. *Food Funct.* **2013**, *4*, 669-80.

(31) Ünalan, İ. U.; Korel, F.; Yemenicioğlu, A. Active packaging of ground beef patties by edible zein films incorporated with partially purified lysozyme and Na2EDTA. *Int. J. Food Sci. Tech.* **2011**, *46*, 1289-1295.

(32) Güçbilmez, Ç. M.; Yemenicioğlu, A.; Arslanoğlu, A. Antimicrobial and antioxidant activity of edible zein films incorporated with lysozyme, albumin proteins and disodium EDTA. *Food Res. Int.* **2007**, *40*, 80-91.

(33) Hosseini, M. H.; Razavi, S. H.; Mousavi, S. M. A.; Yasaghi, S. A. S.; Hasansaraei, A. G. Improving antibacterial activity of edible films based on chitosan by incorporating thyme and clove essential oils and EDTA. *J. Appl. Sci.* **2008**, *8*, 2895-2900.

(34) Sivarooban, T.; Hettiarachchy, N.; Johnson, M. Physical and antimicrobial properties of grape seed extract, nisin, and EDTA incorporated soy protein edible films. *Food Res. Int.* **2008**, *41*, 781-785.

(35) Barish, J. A.; Goddard, J. M. Polyethylene glycol grafted polyethylene: A versatile platform for nonmigratory active packaging applications. *J. Food Sci.* **2011**, *76*, E586-E591.

(36) Goddard, J. M.; Hotchkiss, J. Polymer surface modification for the attachment of bioactive compounds. *Prog. Polym. Sci.* **2007**, *32*, 698-725.

(37) Koontz, J. Active packaging materials to inhibit lipid oxidation: US regulatory framework. *Inform* **2012**, *23*, 598-600.

(38) Koontz, J. L., Packaging technologies to control lipid oxidation. In *Oxidative Stability and Shelf Life of Foods Containing Oils and Fats*, Academic Press and AOCS Press: 2016; pp 479–517.

(39) Rånby, B. In *Surface modification of polymers by photoinitiated graft polymerization*, Makromol. Chem., Macromol. Symp., 1992; Wiley Online Library: 1992; pp 55-67.

(40) Soares, N.; Hotchkiss, J. Naringinase immobilization in packaging films for reducing naringin concentration in grapefruit juice. *J. Food Sci.* **1998**, *63*, 61-65.

(41) Wong, D. E.; Talbert, J. N.; Goddard, J. M. Layer by layer assembly of a biocatalytic packaging film: Lactase covalently bound to low-density polyethylene. *J. Food Sci.* **2013**, *78*, E853-E860.

(42) Muriel-Galet, V.; Talbert, J. N.; Hernandez-Munoz, P.; Gavara, R.; Goddard, J. Covalent immobilization of lysozyme on ethylene vinyl alcohol films for nonmigrating antimicrobial packaging applications. *J. Agric. Food Chem.* **2013**, *61*, 6720-6727.

(43) Tian, F.; Decker, E. A.; Goddard, J. M. Control of lipid oxidation by nonmigratory active packaging films prepared by photoinitiated graft polymerization. *J. Agric. Food Chem.* **2012**, *60*, 7710-8.

(44) Tian, F.; Decker, E. A.; Goddard, J. M. Controlling lipid oxidation via a biomimetic iron chelating active packaging material. *J. Agric. Food Chem.* **2013**, *61*, 12397–12404.

(45) Frankel, E. N. Review. Recent advances in lipid oxidation. *J. Sci. Food Agric.* **1991**, *54*, 495-511.

(46) Tian, F.; Decker, E. A.; Goddard, J. M. Development of an iron chelating polyethylene film for active packaging applications. *J. Agric. Food Chem.* **2012**, *60*, 2046-52.

(47) Mahoney, K. W.; Talbert, J. N.; Goddard, J. M. Effect of polyethylene glycol tether size and chemistry on the attachment of lactase to polyethylene films. *J. Appl. Polym. Sci.* **2013**, *127*, 1203-1210.

(48) Bastarrachea, L. J.; Peleg, M.; McLandsborough, L. A.; Goddard, J. M. Inactivation of Listeria monocytogenes on a polyethylene surface modified by layer-by-layer deposition of the antimicrobial N-halamine. *J. Food Eng.* **2013**, *117*, 52-58.

(49) Ozdemir, M.; Yurteri, C. U.; Sadikoglu, H. Physical polymer surface modification methods and applications in food packaging polymers. *Crit. Rev. Food Sci. Nutr.* **1999**, *39*, 457-477.

(50) Desmet, T.; Morent, R.; Geyter, N. D.; Leys, C.; Schacht, E.; Dubruel, P. Nonthermal plasma technology as a versatile strategy for polymeric biomaterials surface modification: a review. *Biomacromolecules* **2009**, *10*, 2351-2378.

(51) Deng, J.; Wang, L.; Liu, L.; Yang, W. Developments and new applications of UV-induced surface graft polymerizations. *Prog. Polym. Sci.* **2009**, *34*, 156-193.

(52) Chan, C.-M.; Ko, T.-M.; Hiraoka, H. Polymer surface modification by plasmas and photons. *Surf. Sci. Rep.* **1996**, *24*, 1-54.

(53) Ma, H.; Davis, R. H.; Bowman, C. N. A novel sequential photoinduced living graft polymerization. *Macromolecules* **2000**, *33*, 331-335.

(54) Rånby, B. Surface modification and lamination of polymers by photografting. *Int. J. Adhes. Adhes.* **1999**, *19*, 337-343.

(55) Mohd Yusof, A. H.; Ulbricht, M. Polypropylene-based membrane adsorbers via photo-initiated graft copolymerization: optimizing separation performance by preparation conditions. *J. Membr. Sci.* **2008**, *311*, 294-305.

(56) Ulbricht, M.; Yang, H. Porous polypropylene membranes with different carboxyl polymer brush layers for reversible protein binding via surface-initiated graft copolymerization. *Chem. Mater.* **2005**, *17*, 2622-2631.

(57) Yu, H.-Y.; Xu, Z.-K.; Yang, Q.; Hu, M.-X.; Wang, S.-Y. Improvement of the antifouling characteristics for polypropylene microporous membranes by the sequential photoinduced graft polymerization of acrylic acid. *J. Membr. Sci.* **2006**, *281*, 658-665.

(58) Ma, H.; Davis, R. H.; Bowman, C. N. Principal factors affecting sequential photoinduced graft polymerization. *Polymer* **2001**, *42*, 8333-8338.

(59) Ulbricht, M. Photograft-polymer-modified microporous membranes with environment-sensitive permeabilities. *React. Funct. Polym.* **1996**, *31*, 165-177.

(60) Himstedt, H. H.; Marshall, K. M.; Wickramasinghe, S. R. pH-responsive nanofiltration membranes by surface modification. *J. Membr. Sci.* **2011**, *366*, 373-381.

(61) Mansourpanah, Y.; Habili, E. M. Preparation and modification of thin film PA membranes with improved antifouling property using acrylic acid and UV irradiation. *J. Membr. Sci.* **2012**, *430*, 158-166.

(62) Seman, A.; Khayet, M.; Bin Ali, Z.; Hilal, N. Reduction of nanofiltration membrane fouling by UV-initiated graft polymerization technique. *J. Membr. Sci.* **2010**, *355*, 133-141.

(63) Costamagna, V.; Strumia, M.; López-González, M.; Riande, E. Gas transport in surface-modified low-density polyethylene films with acrylic acid as a grafting agent. *J. Polym. Sci., Part B: Polym. Phys.* **2006**, *44*, 2828-2840.

(64) Costamagna, V.; Strumia, M.; López-González, M.; Riande, E. Gas transport in surface grafted polypropylene films with poly (acrylic acid) chains. *J. Polym. Sci., Part B: Polym. Phys.* **2007**, *45*, 2421-2431.

(65) Fasce, L.; Costamagna, V.; Pettarin, V.; Strumia, M.; Frontini, P. Poly (acrylic acid) surface grafted polypropylene films: Near surface and bulk mechanical response. *eXpress Polym. Lett.* **2008**, *2*, 779-790.

(66) Uchida, E.; Uyama, Y.; Ikada, Y. Sorption of low-molecular-weight anions into thin polycation layers grafted onto a film. *Langmuir* **1993**, *9*, 1121-1124.

(67) Kang, E.; Tan, K.; Kato, K.; Uyama, Y.; Ikada, Y. Surface modification and functionalization of polytetrafluoroethylene films. *Macromolecules* **1996**, *29*, 6872-6879.

(68) Mirabella, F. M., *Internal reflection spectroscopy: Theory and applications*. CRC Press: 1993; Vol. 15.

(69) Davidson, P. M.; Taylor, T. M., Chemical preservatives and natural antimicrobial compounds. In *Food microbiology: fundamentals and frontiers*, 3rd ed.; Doyle, M. P.; Beuchat, L. R.; Montville, T. J., Eds. ASM Press: Washington D.C., 2007; pp 713-745.

(70) Phillips, D. C. The hen egg-white lysozyme molecule. *Proc. Natl. Acad. Sci. U. S. A.* **1967**, *57*, 483.

(71) Anonymous, Nonagricultural (nonorganic) substances allowed as ingredients in or on processed products labeled as “organic” or “made with organic (specified ingredients or food group(s))". In *7*, Regulations, C. o. F., Ed. US Government Printing Office: Washington D.C., 2012.

(72) Gill, A. O.; Holley, R. A. Interactive inhibition of meat spoilage and pathogenic bacteria by lysozyme, nisin and EDTA in the presence of nitrite and sodium chloride at 24 C. *Int. J. Food Microbiol.* **2003**, *80*, 251-259.

(73) Cannarsi, M.; Baiano, A.; Sinigaglia, M.; Ferrara, L.; Baculo, R.; Del Nobile, M. A. Use of nisin, lysozyme and EDTA for inhibiting microbial growth in chilled buffalo meat. *Int. J. Food Sci. Tech.* **2008**, *43*, 573-578.

(74) Gill, A. O.; Holley, R. A. Surface application of lysozyme, nisin, and EDTA to inhibit spoilage and pathogenic bacteria on ham and bologna. *J. Food. Prot.* **2000**, *63*, 1338-1346.

(75) Mastromatteo, M.; Lucera, A.; Sinigaglia, M.; Corbo, M. R. Synergic antimicrobial activity of lysozyme, nisin, and EDTA against Listeria Monocytogenes in Ostrich meat patties. *J. Food Sci.* **2010**, *75*, M422-M429.

(76) Roman, M. J.; Tian, F.; Decker, E. A.; Goddard, J. M. Iron chelating polypropylene films: Manipulating photoinitiated graft polymerization to tailor chelating activity. *J. Appl. Polym. Sci.* **2014**, *131*, 39948.

(77) Roman, M. J.; Decker, E. A.; Goddard, J. M. Fourier Transform Infrared studies on the dissociation behavior of metal-chelating polyelectrolyte brushes. *ACS Appl. Mater. Interfaces* **2014**, *6*, 5383-5387.

(78) Richter, A.; Paschew, G.; Klatt, S.; Lienig, J.; Arndt, K.-F.; Adler, H.-J. P. Review on hydrogel-based pH sensors and microsensors. *Sensors* **2008**, *8*, 561-581.

(79) Gong, P.; Wu, T.; Genzer, J.; Szleifer, I. Behavior of surface-anchored poly (acrylic acid) brushes with grafting density gradients on solid substrates: 2. Theory. *Macromolecules* **2007**, *40*, 8765-8773.

(80) Dong, R.; Lindau, M.; Ober, C. K. Dissociation behavior of weak polyelectrolyte brushes on a planar surface. *Langmuir* **2009**, *25*, 4774-4779.

(81) Min, S.; Harris, L. J.; Han, J. H.; Krochta, J. M. Listeria monocytogenes inhibition by whey protein films and coatings incorporating lysozyme. *J. Food. Prot.* **2005**, *68*, 2317-2325.

(82) Kihm, D. J.; Leyer, G. J.; An, G.-H.; Johnson, E. A. Sensitization of heat-treated Listeria monocytogenes to added lysozyme in milk. *Appl. Environ. Microbiol.* **1994**, *60*, 3854-3861.

(83) Seyrek, E.; Dubin, P. L.; Tribet, C.; Gamble, E. A. Ionic strength dependence of protein-polyelectrolyte interactions. *Biomacromolecules* **2003**, *4*, 273-282.

(84) Halperin, A. Polymer brushes that resist adsorption of model proteins: Design parameters. *Langmuir* **1999**, *15*, 2525-2533.

(85) Tian, F.; Roman, M. J.; Decker, E. A.; Goddard, J. M. Biomimetic design of chelating interfaces. *J. Appl. Polym. Sci.* **2015**, *132*, 41231.

(86) Pincus, P. Colloid stabilization with grafted polyelectrolytes. *Macromolecules* **1991**, *24*, 2912-2919.

(87) Delcroix, M.; Huet, G.; Conard, T.; Demoustier-Champagne, S.; Du Prez, F.; Landoulsi, J.; Dupont-Gillain, C. Design of mixed PEO/PAA brushes with switchable properties toward protein adsorption. *Biomacromolecules* **2012**, *14*, 215-225.

(88) Schmaljohann, D. Thermo- and pH-responsive polymers in drug delivery. *Adv. Drug Del. Rev.* **2006**, *58*, 1655-1670.

(89) Welch, M.; Rastogi, A.; Ober, C. Polymer brushes for electrochemical biosensors. *Soft Matter* **2011**, *7*, 297-302.

(90) Santonicola, M. G.; de Groot, G. W.; Memesa, M.; Meszyńska, A.; Vancso, G. J. Reversible pH-controlled switching of poly(methacrylic acid) grafts for functional biointerfaces. *Langmuir* **2010**, *26*, 17513-17519.

(91) Wang, H.; Lee, I. H.; Yan, M. A general method to determine ionization constants of responsive polymer thin films. *J. Colloid Interface Sci.* **2012**, *365*, 178-183.

(92) Currie, E.; Sieval, A.; Avena, M.; Zuilhof, H.; Sudhölter, E.; Cohen Stuart, M. Weak polyacid brushes: preparation by LB deposition and optically detected titrations. *Langmuir* **1999**, *15*, 7116-7118.

(93) Kilbey II, S. M.; Ankner, J. F. Neutron reflectivity as a tool to understand polyelectrolyte brushes. *Curr. Opin. Colloid Interface Sci.* **2012**, *17*, 83-89.

(94) Aulich, D.; Hoy, O.; Luzinov, I.; Brücher, M.; Hergenröder, R.; Bittrich, E.; Eichhorn, K.-J.; Uhlmann, P.; Stamm, M.; Esser, N. In situ studies on the switching behavior of ultrathin poly (acrylic acid) polyelectrolyte brushes in different aqueous environments. *Langmuir* **2010**, *26*, 12926-12932.

(95) Dunderdale, G.; Howse, J.; Fairclough, P. pH-dependent control of particle motion through surface interactions with patterned polymer brush surfaces. *Langmuir* **2012**, *28*, 12955-12961.

(96) Hinrichs, K.; Aulich, D.; Ionov, L.; Esser, N.; Eichhorn, K.-J.; Motornov, M.; Stamm, M.; Minko, S. Chemical and structural changes in a pH-responsive mixed polyelectrolyte brush studied by infrared ellipsometry. *Langmuir* **2009**, *25*, 10987-10991.

(97) Aureau, D.; Ozanam, F.; Allongue, P.; Chazalviel, J.-N. The titration of carboxyl-terminated monolayers revisited: In situ calibrated Fourier transform infrared study of well-defined monolayers on silicon. *Langmuir* **2008**, *24*, 9440-9448.

(98) Lutfor, M.; Sidik, S.; Wan Yunus, W.; Rahman, M.; Mansor, A.; Haron, M. Synthesis and characterization of poly (hydroxamic acid) chelating resin from poly (methyl acrylate) ‐ grafted sago starch. *J. Appl. Polym. Sci.* **2001**, *79*, 1256-1264.

(99) Wen, Y.; Siew, S.; Rahman, M. L.; Arshad, S. E.; Surugau, N.; Musta, B. Synthesis and characterization of poly (hydroxamic acid) ‐ poly (amidoxime) chelating ligands from polymer ‐ grafted acacia cellulose. *J. Appl. Polym. Sci.* **2012**, *124*, 4443-4451.

(100) Konradi, R.; Rühe, J. Interaction of poly (methacrylic acid) brushes with metal ions: swelling properties. *Macromolecules* **2005**, *38*, 4345-4354.

(101) Edwards, D. C.; Nielsen, S. B.; Jarzęcki, A. A.; Spiro, T. G.; Myneni, S. C. Experimental and theoretical vibrational spectroscopy studies of acetohydroxamic acid and desferrioxamine B in aqueous solution: Effects of pH and iron complexation. *Geochim. Cosmochim. Acta* **2005**, *69*, 3237-3248.

(102) Holmén, B. A.; Tejedor-Tejedor, M. I.; Casey, W. H. Hydroxamate complexes in solution and at the goethite-water interface: A cylindrical internal reflection Fourier transform infrared spectroscopy study. *Langmuir* **1997**, *13*, 2197-2206.

(103) Yang, J.; Bremer, P. J.; Lamont, I. L.; McQuillan, A. J. Infrared spectroscopic studies of siderophore-related hydroxamic acid ligands adsorbed on titanium dioxide. *Langmuir* **2006**, *22*, 10109-10117.

(104) Siebner-Freibach, H.; Hadar, Y.; Yariv, S.; Lapides, I.; Chen, Y. Thermospectroscopic study of the adsorption mechanism of the hydroxamic siderophore ferrioxamine B by calcium montmorillonite. *J. Agric. Food Chem.* **2006**, *54*, 1399-1408.

(105) Deacon, G.; Phillips, R. Relationships between the carbon-oxygen stretching frequencies of carboxylato complexes and the type of carboxylate coordination. *Coord. Chem. Rev.* **1980**, *33*, 227-250.

(106) Boukhalfa, H.; Reilly, S. D.; Neu, M. P. Complexation of Pu (IV) with the natural siderophore desferrioxamine B and the redox properties of Pu (IV)(siderophore) complexes. *Inorg. Chem.* **2007**, *46*, 1018-1026.

(107) Gotić, M.; Musić, S. Mössbauer, FT-IR and FE SEM investigation of iron oxides precipitated from FeSO4 solutions. *J. Mol. Struct.* **2007**, *834*, 445-453.

(108) Siebner-Freibach, H.; Yariv, S.; Lapides, Y.; Hadar, Y.; Chen, Y. Thermo-FTIR spectroscopic study of the siderophore ferrioxamine B: spectral analysis and stereochemical implications of iron chelation, pH, and temperature. *J. Agric. Food Chem.* **2005**, *53*, 3434-3443.

(109) Gómez-Estaca, J.; Lopez-de-Dicastillo, C.; Hernandez-Munoz, P.; Catala, R.; Gavara, R. Advances in antioxidant active food packaging. *Trends Food Sci. Technol.* **2014**, *35*, 42-51.

(110) Garces, O.; Nerin, C.; Beltran, J.; Roncales, P. Antioxidant active varnish. *European Patent EP1477159-A1* **2003**.

(111) Nerín, C.; Tovar, L.; Djenane, D.; Camo, J.; Salafranca, J.; Beltrán, J. A.; Roncalés, P. Stabilization of beef meat by a new active packaging containing natural antioxidants. *J. Agric. Food Chem.* **2006**, *54*, 7840-7846.

(112) Lopez de Dicastillo, C.; Nerin, C.; Alfaro, P.; Catala, R.; Gavara, R.; Hernandez-Munoz, P. Development of new antioxidant active packaging films based on ethylene vinyl alcohol copolymer (EVOH) and green tea extract. *J. Agric. Food Chem.* **2011**, *59*, 7832-7840.

(113) Arrua, D.; Strumia, M. C.; Nazareno, M. A. Immobilization of caffeic acid on a polypropylene film: Synthesis and antioxidant properties. *J. Agric. Food Chem.* **2010**, *58*, 9228-9234.

(114) Farkas, E.; Enyedy, É. A.; Csóka, H. A comparison between the chelating properties of some dihydroxamic acids, desferrioxamine B and acetohydroxamic acid. *Polyhedron* **1999**, *18*, 2391-2398.

(115) Roberts, D. D.; Elmore, J. S.; Langley, K. R.; Bakker, J. Effects of sucrose, guar gum, and carboxymethylcellulose on the release of volatile flavor compounds under dynamic conditions. *J. Agric. Food Chem.* **1996**, *44*, 1321-1326.

(116) Bylaite, E.; Adler-Nissen, J.; Meyer, A. S. Effect of xanthan on flavor release from thickened viscous food model systems. *J. Agric. Food Chem.* **2005**, *53*, 3577-3583.

(117) Lo, Y.; Robbins, K.; Argin ‐ Soysal, S.; Sadar, L. Viscoelastic effects on the diffusion properties of curdlan gels. *J. Food Sci.* **2003**, *68*, 2057-2065.

(118) Secouard, S.; Malhiac, C.; Grisel, M.; Decroix, B. Release of limonene from polysaccharide matrices: viscosity and synergy effect. *Food Chem.* **2003**, *82*, 227-234.

(119) Carr, J.; Baloga, D.; Guinard, J.-X.; Lawter, L.; Marty, C.; Squire, C., The effect of gelling agent type and concentration on flavor release in model systems. In *Flavor-Food Interactions*, McGorrin, R. J., Ed. American Chemical Society: 1996; pp 98-108.

(120) Landy, P.; Rogacheva, S.; Lorient, D.; Voilley, A. Thermodynamic and kinetic aspects of the transport of small molecules in dispersed systems. *Colloids Surf. B. Biointerfaces* **1998**, *12*, 57-65.

(121) Daubert, C. R.; Foegeding, E. A., Rheological Principles for Food Analysis. In *Food Analysis*, 3rd ed.; Nielsen, S. S., Ed. Plenum Publishers: New York, 2003; pp 503-516.

(122) Briggs, J. L.; Steffe, J. F. Using Brookfield data and the Mitschka method to evaluate power law foods. *J. Texture Stud.* **1997**, *28*, 517-522.

(123) Maruyama, K.; Sakashita, T.; Hagura, Y.; Suzuki, K. Relationship between rheology, particle size and texture of mayonnaise. *Food Sci. Technol. Res.* **2007**, *13*, 1-6.

(124) Bai, G.; Bee, J. S.; Biddlecombe, J. G.; Chen, Q.; Leach, W. T. Computational fluid dynamics (CFD) insights into agitation stress methods in biopharmaceutical development. *Int. J. Pharm.* **2012**, *423*, 264-280.

(125) Singh, S. P.; Burgess, G. J.; Rojnuckarin, P. Test protocol for simulating truck and rail vibration and rail impacts in shipments of automotive engine racks. *Packag. Technol. Sci.* **1995**, *8*, 33-41.

(126) Standard Operating Procedure for Determining Total Lead (Pb) in Nonmetal Children's Products. In *CPSC-CH-E1002-08.3*, Commission, U. S. C. P. S., Ed. Rockville, MD, 2012.

(127) Platt, S. R.; Clydesdale, F. M. Mineral binding characteristics of lignin, guar gum, cellulose, pectin and neutral detergent fiber under simulated duodenal pH conditions. *J. Food Sci.* **1987**, *52*, 1414-1419.

(128) Saravacos, G. D.; Maroulis, Z. B., Transport properties of foods. In CRC Press: 2001.

(129) Hestrin, S. The reaction of acetylcholine and other carboxylic acid derivatives with hydroxylamine, and its analytical application. *J. Biol. Chem.* **1949**, *180*, 249-261.

(130) Ogiwara, Y.; Roman, M. J.; Decker, E. A.; Goddard, J. M. Iron chelating active packaging: Influence of counter-ions and pH value on effectiveness of soluble and immobilized hydroxamate chelators *Food Chem.* **2015**, *196*, 842-847.

(131) Kaşgöz, H.; Özgümüş, S.; Orbay, M. Modified polyacrylamide hydrogels and their application in removal of heavy metal ions. *Polymer* **2003**, *44*, 1785-1793.

(132) Frankel, E. N.; Satué-Gracia, T.; Meyer, A. S.; German, J. B. Oxidative stability of fish and algae oils containing long-chain polyunsaturated fatty acids in bulk and in oil-in-water emulsions. *J. Agric. Food Chem.* **2002**, *50*, 2094-2099.

(133) Gutteridge, J.; Richmond, R.; Halliwell, B. Inhibition of the iron-catalysed formation of hydroxyl radicals from superoxide and of lipid peroxidation by desferrioxamine. *Biochem. J* **1979**, *184*, 469-472.

(134) Grob, K.; Pfenninger, S.; Pohl, W.; Laso, M.; Imhof, D.; Rieger, K. European legal limits for migration from food packaging materials: 1. Food should prevail over simulants; 2. More realistic conversion from concentrations to limits per surface area. PVC cling films in contact with cheese as an example. *Food Control* **2007**, *18*, 201-210.

(135) European Commision. In *Union Guidelines on Regulation (EU) No 10/2011 on plastic materials and articles intended to come into contact with food*, Report of European Commission, 21 February 2014, 2014; European Commission: 2014.

(136) Nielsen, N. S.; Petersen, A.; Meyer, A. S.; Timm-Heinrich, M.; Jacobsen, C. Effects of lactoferrin, phytic acid, and EDTA on oxidation in two food emulsions enriched with long-chain polyunsaturated fatty acids. *J. Agric. Food Chem.* **2004**, *52*, 7690-7699.

(137) Jacobsen, C.; Timm, M.; Meyer, A. S. Oxidation in fish oil enriched mayonnaise: Ascorbic acid and low pH increase oxidative deterioration. *J. Agric. Food Chem.* **2001**, *49*, 3947-3956.

(138) Saha, D.; Bhattacharya, S. Hydrocolloids as thickening and gelling agents in food: a critical review. *J. Food Sci. Technol.* **2010**, *47*, 587-597.

(139) Shimada, K.; Muta, H.; Nakamura, Y.; Okada, H.; Matsuo, K.; Yoshioka, S.; Matsudaira, T.; Nakamura, T. Iron-binding property and antioxidative activity of xanthan on the autoxidation of soybean oil in emulsion. *J. Agric. Food Chem.* **1994**, *42*, 1607-1611.

(140) Mercê, A. L.; Fernandes, E.; Mangrich, A. S.; Sierakowski, M.; Szpoganicz, B. Fe (III)-galactomannan solid and aqueous complexes: Potentiometric, EPR spectroscopy and thermal data. *J. Braz. Chem. Soc.* **2001**, *12*, 791-798.

(141) Bosscher, D.; Van Caillie-Bertrand, M.; Deelstra, H. Effect of thickening agents, based on soluble dietary fiber, on the availability of calcium, iron, and zinc from infant formulas. *Nutrition* **2001**, *17*, 614-618.

(142) Chen, B.; McClements, D. J.; Decker, E. A. Role of continuous phase anionic polysaccharides on the oxidative stability of menhaden oil-in-water emulsions. *J. Agric. Food Chem.* **2010**, *58*, 3779-3784.

(143) Bastarrachea, L. J.; Wong, D. E.; Roman, M. J.; Lin, Z.; Goddard, J. M. Active packaging coatings. *Coatings* **2015**, *5*, 771-791.

(144) Contini, C.; Katsikogianni, M.; O'Neill, F.; O'Sullivan, M.; Boland, F.; Dowling, D.; Monahan, F. Storage stability of an antioxidant active packaging coated with citrus extract following a plasma jet pretreatment. *Food Bioprocess Tech.* **2014**, *7*, 2228-2240.

(145) Pezo, D.; Salafranca, J.; Nerín, C. Determination of the antioxidant capacity of active food packagings by in situ gas-phase hydroxyl radical generation and high-performance liquid chromatography–fluorescence detection. *J. Chromatogr. A* **2008**, *1178*, 126-133.

(146) Tian, F.; Decker, E. A.; McClements, D. J.; Goddard, J. M. Influence of non-migratory metal-chelating active packaging film on food quality: Impact on physical and chemical stability of emulsions. *Food Chem.* **2014**, *151*, 257-265.

(147) Roman, M. J.; Decker, E. A.; Goddard, J. M. Performance of nonmigratory iron chelating active packaging materials in viscous model food systems. *J. Food Sci.* **2015**, *80*, 1965-1973.

(148) Perron, N. R.; Brumaghim, J. L. A review of the antioxidant mechanisms of polyphenol compounds related to iron binding. *Cell Biochem. Biophys.* **2009**, *53*, 75-100.

(149) Jeon, J.-R.; Kim, J.-H.; Chang, Y.-S. Enzymatic polymerization of plant-derived phenols for material-independent and multifunctional coating. *J. Mater. Chem. B* **2013**, *1*, 6501-6509.

(150) Barrett, D. G.; Sileika, T. S.; Messersmith, P. B. Molecular diversity in phenolic and polyphenolic precursors of tannin-inspired nanocoatings. *Chem. Commun.* **2014**, *50*, 7265-7268.

(151) Lee, H.; Dellatore, S. M.; Miller, W. M.; Messersmith, P. B. Mussel-inspired surface chemistry for multifunctional coatings. *Science* **2007**, *318*, 426-430.

(152) Singleton, V. L.; Orthofer, R.; Lamuela-Raventos, R. M. Analysis of total phenols and other oxidation substrates and antioxidants by means of folin-ciocalteu reagent. *Method Enzymol.* **1999**, *299*, 152-178.

(153) Zulueta, A.; Esteve, M. J.; Frígola, A. ORAC and TEAC assays comparison to measure the antioxidant capacity of food products. *Food Chem.* **2009**, *114*, 310-316.

(154) Sileika, T. S. Functional Biomaterials Inspired by Natural Polyphenols. NORTHWESTERN UNIVERSITY, 2014.

(155) He, L.; So, V. L. L.; Xin, J. H. Dopamine polymerization-induced surface colouration of various materials. *RSC Advances* **2014**, *4*, 20317-20322.

(156) Nkhili, E.; Loonis, M.; Mihai, S.; El Hajji, H.; Dangles, O. Reactivity of food phenols with iron and copper ions: binding, dioxygen activation and oxidation mechanisms. *Food Funct.* **2014**, *5*, 1186-1202.

(157) Bisby, R. H.; Brooke, R.; Navaratnam, S. Effect of antioxidant oxidation potential in the oxygen radical absorption capacity (ORAC) assay. *Food Chem.* **2008**, *108*, 1002-1007.

(158) Cheatham, R. Wellness Newsletter: November 3, 2015, "Expert Insight-Transparency: Buzz word or new way of doing business?". http://www.ift.org/food-technology/newsletters/wellness-newsletter/2015/november/110315.aspx (March 15, 2016).

(159) Lopez-Rubio, A.; Lagaron, J.; Ocio, M., Active polymer packaging of non-meat products. In *Smart Packaging Technologies for Fast Moving Consumer Goods*, Kerry, J.; Butler, P., Eds. John Wiley & Sons Ltd: West Sussex, England, 2008; pp 19-30.

(160) Johnson, D. R.; Tian, F.; Roman, M. J.; Decker, E. A.; Goddard, J. M. Development of Iron-Chelating Poly(ethylene terephthalate) Packaging for Inhibiting Lipid Oxidation in Oil-in-Water Emulsions. *Journal of agricultural and food chemistry* **2015**, *63*, 5055-5060.

(161) Goddard, J. M.; Talbert, J.; Hotchkiss, J. Covalent attachment of lactase to low-density polyethylene films. *J. Food Sci.* **2007**, *72*, E036-E041.

(162) Carrano, C. J.; Raymond, K. N. Ferric ion sequestering agents. 2. Kinetics and mechanism of iron removal from transferrin by enterobactin and synthetic tricatechols. *J. Am. Chem. Soc.* **1979**, *101*, 5401-5404.

(163) Upritchard, H. G.; Yang, J.; Bremer, P. J.; Lamont, I. L.; McQuillan, A. J. Adsorption of enterobactin to metal oxides and the role of siderophores in bacterial adhesion to metals. *Langmuir* **2011**, *27*, 10587-10596.

(164) Waite, J. H. Surface chemistry: Mussel power. *Nat. Mater.* **2008**, *7*, 8-9.

(165) Andjelković, M.; Van Camp, J.; De Meulenaer, B.; Depaemelaere, G.; Socaciu, C.; Verloo, M.; Verhe, R. Iron-chelation properties of phenolic acids bearing catechol and galloyl groups. *Food Chem.* **2006**, *98*, 23-31.

(166) Škerget, M.; Kotnik, P.; Hadolin, M.; Hraš, A. R.; Simonič, M.; Knez, Ž. Phenols, proanthocyanidins, flavones and flavonols in some plant materials and their antioxidant activities. *Food Chem.* **2005**, *89*, 191-198.

(167) Hu, M.; McClements, D. J.; Decker, E. A. Antioxidant activity of a proanthocyanidin-rich extract from grape seed in whey protein isolate stabilized algae oil-in-water emulsions. *J. Agric. Food Chem.* **2004**, *52*, 5272-5276.

(168) Kiokias, S.; Varzakas, T. Activity of flavonoids and β-carotene during the auto-oxidative deterioration of model food oil-in water emulsions. *Food Chem.* **2014**, *150*, 280-286.

(169) Decker, E. A. Phenolics: prooxidants or antioxidants? *Nutr. Rev.* **1997**, *55*, 396-398.

(170) Roman, M. J.; Decker, E. A.; Goddard, J. M. Biomimetic polyphenol coatings for antioxidant active packaging applications. **2016**, *Submitted*.

(171) Kurisawa, M.; Chung, J. E.; Uyama, H.; Kobayashi, S. Laccase‐catalyzed synthesis and antioxidant property of poly (catechin). *Macromol. Biosci.* **2003**, *3*, 758-764.

(172) Dopico-García, M.; Lopez-Vilarino, J.; González-Rodríguez, M. Antioxidant content of and migration from commercial polyethylene, polypropylene, and polyvinyl chloride packages. *J. Agric. Food Chem.* **2007**, *55*, 3225-3231.

(173) Tovar, L.; Salafranca, J.; Sánchez, C.; Nerín, C. Migration studies to assess the safety in use of a new antioxidant active packaging. *J. Agric. Food Chem.* **2005**, *53*, 5270-5275.

(174) Shantha, N. C.; Decker, E. A. Rapid, sensitive, iron-based spectrophotometric methods for determination of peroxide values of food lipids. *J. AOAC Int.* **1994**, *77*, 421-424.

(175) Bou, R.; Boon, C.; Kweku, A.; Hidalgo, D.; Decker, E. A. Effect of different antioxidants on lycopene degradation in oil‐in‐water emulsions. *Eur. J. Lipid Sci. Technol.* **2011**, *113*, 724-729.

(176) Boon, C. S.; Xu, Z.; Yue, X.; McClements, D. J.; Weiss, J.; Decker, E. A. Factors affecting lycopene oxidation in oil-in-water emulsions. *J. Agric. Food Chem.* **2008**, *56*, 1408-1414.

(177) Boon, C. S.; McClements, D. J.; Weiss, J.; Decker, E. A. Role of iron and hydroperoxides in the degradation of lycopene in oil-in-water emulsions. *J. Agric. Food Chem.* **2009**, *57*, 2993-2998.

(178) Yu, S.-H.; Tsai, M.-L.; Lin, B.-X.; Lin, C.-W.; Mi, F.-L. Tea catechins-cross-linked methylcellulose active films for inhibition of light irradiation and lipid peroxidation induced β-carotene degradation. *Food Hydrocolloids* **2015**, *44*, 491-505.

(179) Hider, R. C.; Mohd-Nor, A. R.; Silver, J.; Morrison, I. E.; Rees, L. V. Model compounds for microbial iron-transport compounds. Part 1. Solution chemistry and Mössbauer study of iron (II) and iron (III) complexes from phenolic and catecholic systems. *J. Chem. Soc., Dalton Trans.* **1981**, 609-622.

(180) Hider, R. C.; Liu, Z. D.; Khodr, H. H. Metal chelation of polyphenols. *Method Enzymol.* **2001**, *335*, 190-203.

(181) Nguyen, M. L.; Schwartz, S. J. Lycopene: Chemical and biological properties. *Food Technol.* **1999**, *53*, 38-45.

(182) Goddard, J. M.; McClements, D. J.; Decker, E. A. Innovative technologies in the control of lipid oxidation. *Lipid Technol.* **2012**, *24*, 275-277.

(183) Moore, M.; Han, I.; Acton, J.; Ogale, A.; Barmore, C.; Dawson, P. Effects of antioxidants in polyethylene film on fresh beef color. *J. Food Sci.* **2003**, *68*, 99-104.

(184) Soto V, H.; Peralta, E.; Cano H, D. M.; Martinez A, O. L.; Granda R, D. M. Antioxidant active packaging effect whole milk powder sensorial quality and production of volatile compounds. *Vitae* **2011**, *18*, 115-123.

(185) Abu‐Ilaiwi, F. A.; Ahmad, M. B.; Ibrahim, N. A.; Ab Rahman, M. Z.; Dahlan, K. Z. M.; Yunus, Z. W.; Md, W. Optimized conditions for the grafting reaction of poly (methyl acrylate) onto rubberwood fiber. *Polym. Int.* **2004**, *53*, 386-391.

(186) Bartos, J. Colorimetric determination of organic compounds by formation of hydroxamic acids. *Talanta* **1980**, *27*, 583-590.

(187) Maguire, J. H.; Dudley, K. H. Colorimetric hydroxylamine-iron (III) methods for studies of the enzymic hydrolyses of cyclic imides and of amic acids. *Anal. Chem.* **1977**, *49*, 292-297.

(188) Ramua, B. K.; Raghubabua, K.; Syambabub, M. Development of a spectrophotometric method based on ferric hydroxamate reaction for determination of ramipril in formulations. *Indo. Global J. Pharm. Sci.* **2011**, *1*.

(189) Liu, Z. D.; Hider, R. C. Design of iron chelators with therapeutic application. *Coord. Chem. Rev.* **2002**, *232*, 151-171.

(190) Hallberg, L.; Rossander-Hultén, L.; Brune, M.; Gleerup, A. Bioavailability in man of iron in human milk and cow's milk in relation to their calcium contents. *Pediatr. Res.* **1992**, *31*, 524-527.

(191) Garzon, P.; Eisenberg, M. J. Variation in the mineral content of commercially available bottled waters: implications for health and disease. *Am. J. Med.* **1998**, *105*, 125-130.

(192) Grimes, C. A.; Nowson, C. A.; Lawrence, M. An evaluation of the reported sodium content of Australian food products. *Int. J. Food Sci. Tech.* **2008**, *43*, 2219-2229.

(193) HunterLab Application Note AN 1005.00: Hunter L, a, b versus CIE 1976 L*a*b*. www.hunterlab.com/an-1005b.pdf (12-1-2014).

(194) Haron, M.; Wan Yunus, W.; Yong, N.; Tokunaga, S. Sorption of arsenate and arsenate anions by iron (III)-poly (hydroxamic acid) complex. *Chemosphere* **1999**, *39*, 2459-2466.

(195) Polomoscanik, S. C.; Cannon, C. P.; Neenan, T. X.; Holmes-Farley, S. R.; Mandeville, W. H.; Dhal, P. K. Hydroxamic acid-containing hydrogels for nonabsorbed iron chelation therapy: synthesis, characterization, and biological evaluation. *Biomacromolecules* **2005**, *6*, 2946-2953.

(196) Winston, A.; Kirchner, D. Hydroxamic acid polymers. Effect of structure on the selective chelation of iron in water. *Macromolecules* **1978**, *11*, 597-603.